JAERI-M
82-118

DATA ON TRAPPING AND RE-EMISSION OF ENERGETIC HYDROGEN ISOTOPES AND HELIUM IN MATERIALS

August 1982

Sadae YAMAGUCHI,* Kunio OZAWA, Yohta NAKAI and Yasuaki SUGIZAKI*

日本原子力研究所
Japan Atomic Energy Research Institute

JAERI-Mレポートは，日本原子力研究所が不定期に公刊している研究報告書です。
入手の問合わせは，日本原子力研究所技術情報部情報資料課（〒319-11茨城県那珂郡東海村）あて，お申しこしください。なお，このほかに財団法人原子力弘済会資料センター（〒319-11 茨城県那珂郡東海村日本原子力研究所内）で複写による実費頒布をおこなっております。

JAERI-M reports are issued irregularly.
Inquiries about availability of the reports should be addressed to Information Section, Division of Technical Information, Japan Atomic Energy Research Institute, Tokai-mura, Naka-gun, Ibaraki-ken 319-11, Japan.

編集兼発行　日本原子力研究所
印　　刷　いばらき印刷㈱

JAERI-M 82-118

Data on Trapping and Re-emission of Energetic Hydrogen Isotopes and Helium in Materials

Sadae YAMAGUCHI*, Kunio OZAWA, Yohta NAKAI
and Yasuaki SUGIZAKI*

Division of Physics, Tokai Research Establishment,
JAERI

(Received August 6, 1982)

This report presents a compilation of the experimental data on trapping and re-emission of energetic hydrogen isotopes and helium in materials.

A survey has been made of the literatures up to end of 1980, by dividing it into following seven sections : 1) Dose Dependence, 2) Target Material Dependence, 3) Time Dependence, 4) Target Temperature Dependence, 5) Incident Energy Dependence, 6) Damage Effects, 7) Ion-Induced Release. The experimental data for helium, however, is cited only in limited cases, because of the lack of experiments.

Keywords: Trapping, Re-emission, Ion Implantation, Hydrogen Isotopes, Helium, Recycling, Plasma-surface Interactions, Data

---

* Department of Nuclear Engineering, Tohoku University, Sendai 980, Japan.

One of the authors(S.Y.) was supported by a research contract of Japan Atomic Energy Research Institute with Tohoku University in 1980 fiscal year.

JAERI－M　82－118

固体材料中に注入された水素同位体及びヘリウムの保持・放出に関するデータ集

日本原子力研究所東海研究所物理部
山口　貞衛*・小沢　国夫・中井　洋太
杉崎　康昭*

（1982年8月6日受理）

ステンレス・スチール，Mo,Tiなど固体材料中にイオン注入された水素，重水素，トリチウムの水素同位体及びヘリウム原子の保持及び放出に関する実験データは核融合炉のプラズマ・壁相互作用における水素リサイクリング過程のモデリングにとり重要な原子分子データを提供する。

本報告は1966～1980年迄の関連文献76を調査収集し，AMSTORシステムによる計算機作図化を行って，46図のデータ集として収録した。

構成は次の7章に分類整理した。

1）イオン照射量依存性　2）試料物質依存性　3）注入後時間依存性　4）標的温度依存性
5）入射イオンのエネルギー依存性　6）照射損傷の影響　及び　7）イオン誘起離脱

＊　東北大学

Contents

1. Introduction 1

2. SECTION A: HYDROGEN ISOTOPES 3

A - I Dose Dependence 3

A - II Target Material Dependence 8

A - III Time Dependence 11

A IV Target Temperature Dependence 15

A - V Incident Energy Dependence 29

A - VI Damage Effects 33

A - VII Ion-Induced Release 43

3. SECTION B: HELIUM 47

B - I Target Temperature Dependence 47

B - II Incident Energy Dependence 55

B - III Microstructure Dependence 57

4. Table of Trapping and Re-emission Data 60

References 66

目　　次

1. 序 …… 1
2. A：水素同位体 …… 3
A－Ⅰ 照射量依存性 …… 3
A－Ⅱ 試料物質依存性 …… 8
A－Ⅲ 時間依存性 …… 11
A－Ⅳ 温度依存性 …… 15
A－Ⅴ 入射エネルギー依存性 …… 29
A－Ⅵ 損傷の影響 …… 33
A－Ⅶ イオン誘起離脱 …… 43
3. B：ヘリウム …… 47
B－Ⅰ 温度依存性 …… 47
B－Ⅱ 入射エネルギー依存性 …… 55
B－Ⅲ 試料の微細構造の影響 …… 57
4. 保持及び再放出データ表 …… 60
文　献 …… 66

1. Introduction

When energetic ions are incident on the solid, those ions not directly backscattered can penetrate a solid surface. They will slow down to thermal energy by elastic and inelastic stopping processes and eventually come to rest near the projected range as trapping impurity atoms. Depending on the solubility, the diffusivity and the barrier of the surface, they may diffuse into the bulk of the solid, they may partly leave the surface or they may be trapped in the implanted layer. Such behaviors of the thermalized impurity atoms are solid state problems: diffusion, evaporation, segregation, binding with defects etc. It is noted, however, that most of these properties are influenced by radiation. Thus, the basic processes of trapping(retention) and detrapping(re-emission) of implanted gas are complex mixture of the various thermal processes and radiation induced processes in solid. The detrapping(re-emission) play a role in the recycling of plasma at the wall of fusion research plasma device; the trapping(retention) of hydrogen has important economic and safety consequences with respect to the tritium inventory holdup.

The purpose of this present report is to compile the experimental data depending on the various parameters, which relate to the trapping and detrapping mechanism. A survey has been made of the literatures upto end of 1980, by dividing it into following seven sections: 1) Dose Dependence, 2) Target Material Dependence, 3) Time Dependence, 4) Target Temperature Dependence, 5) Incident Energy Dependence, 6) Damage Effects, 7) Ion-Induced Release. The experimental data for helium, however, is cited only in limited cases, because of the lack of experiments.

The experimental data compiled in the present report are stored in the AMSTOR system of JAERI, and further addition of new data is in progress. The references for each experimental data are shown in the

figures, and all the literatures concerning trapping and detrapping of hydrogen isotopes and helium are listed chronologically and alphabetically in each year at the end of the report.

The authors are grateful to Dr. T. Shirai for his cooperation on the AMSTOR system. They are also thankful to Miss N. Komatsu for typing the manuscript and preparing the tables.

2. SECTION A: HYDROGEN ISOTOPES

Hydrogen trapping and detrapping can be studied by gas re-emission(GR), thermal desorption spectroscopy(TDS), nuclear reaction analysis(NRA) and secondary ion mass spectroscopy(SIMS). The experimental data as a function of fluence is typically given as the re-emission rate(R), expressed as a fraction of the incident flux(J_i), or as trapping coefficient(η), where $\eta \equiv 1-R$, or as total retention(n), where $n = \int \eta(J_i) dJ_i$. In the following, we review the existing data and examine the characteristic features of the trapping and detrapping processes.

A - I Dose Dependence

Retention studies in several materials exposed to energetic hydrogen ions are shown Figs. A-1, A-2, A-3 and A-4. In these figures, retention of deuterium in the samples are plotted as function of incident fluences. At low fluences ($<10^{16}$ ions/cm^2), all the incident deuteron is retained in the sample apart from a small fraction (typically 5∿10 %) which is kinematically reflected. As the incident fluence is increased, the trapping efficiency gradually decreases and a maximum hydrogen concentration(saturation) is reached in each of these materials. The saturation concentration depends not only on the surface material and temperature but also on the energy of the incident particles, the damage history and the concentration of the gas left in the lattice as shown in the later sections.

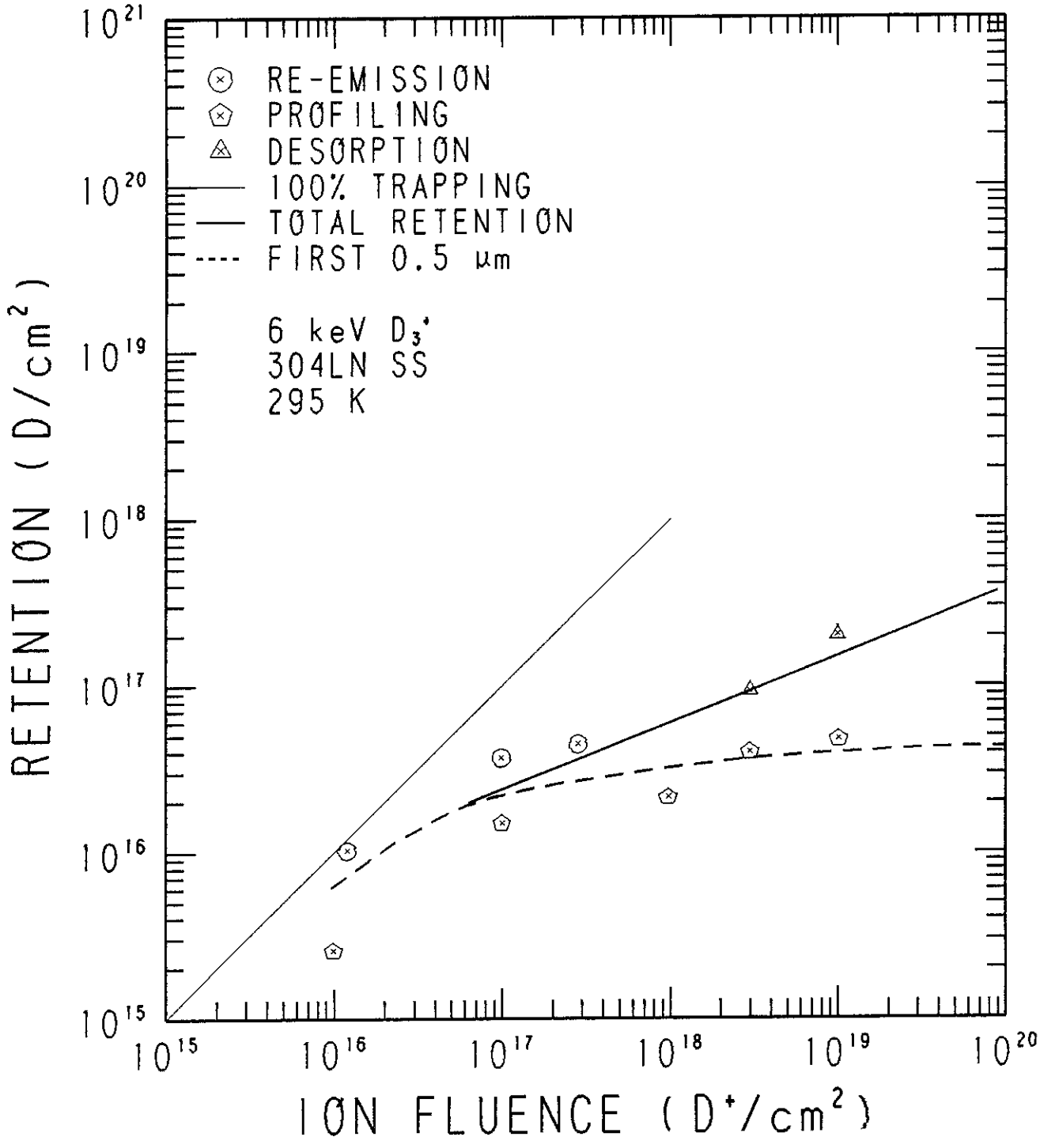

Fig. A-1 Retention of 6 keV D_3^+ in 304LN SS as a function of fluence at 295 K. The ion flux was 5×10^{14} $D^+/cm^2 \cdot sec$. Total retention in the sample was determined from gas re-emission or thermal desorption, while retention in the first 0.5 μm depth was obtained from $D(^3He, \alpha)H$ nuclear reaction profiling. Desorption and profiling samples were quenched after implantation at ≃ 0.25 K/sec. (ref. 55)

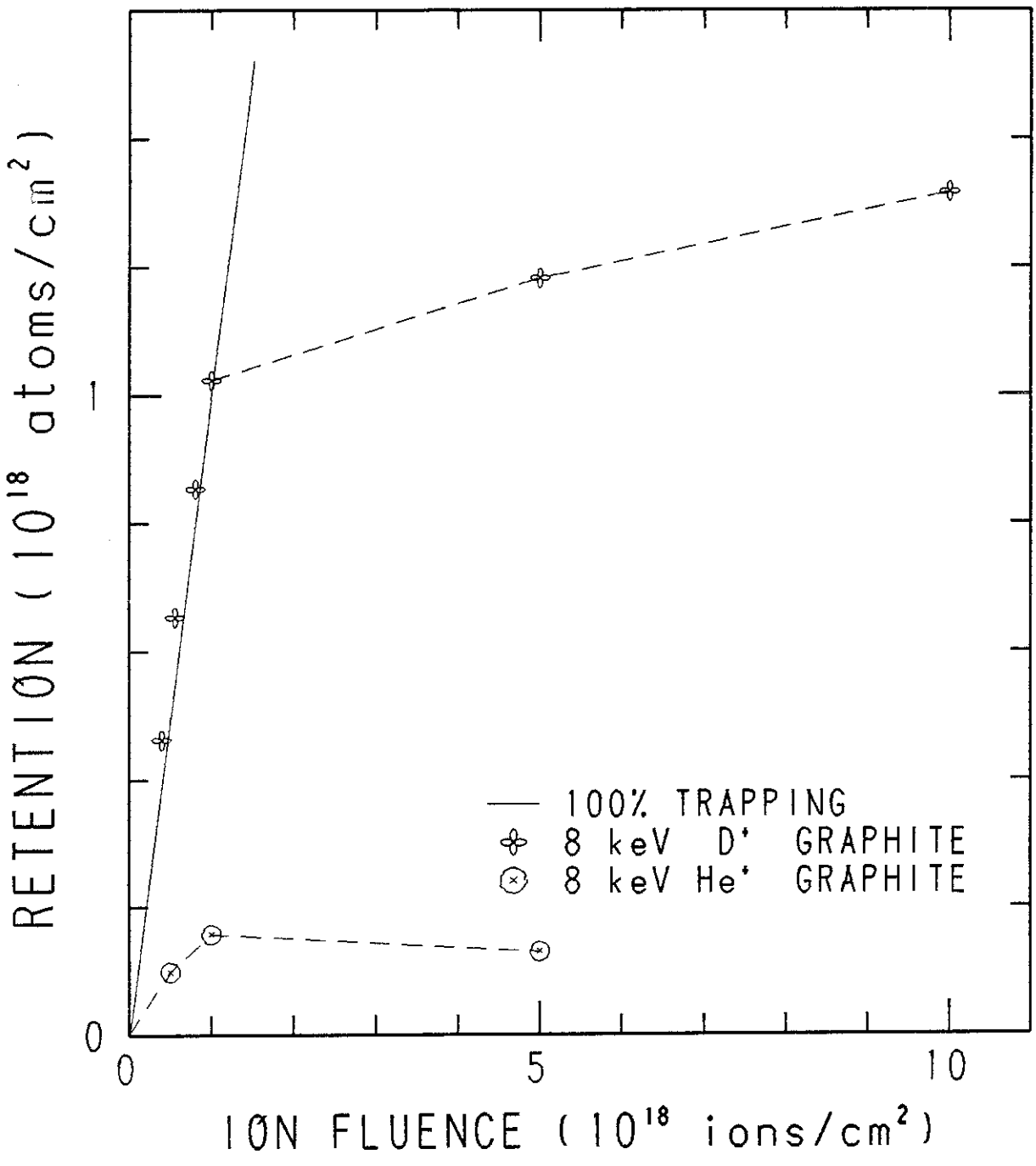

Fig. A-2 Implant (8 keV D^+ and He^+) trapped in graphite as a function of ion fluence at room temperature. Dashed lines are included to guide the eye. (ref. 37)

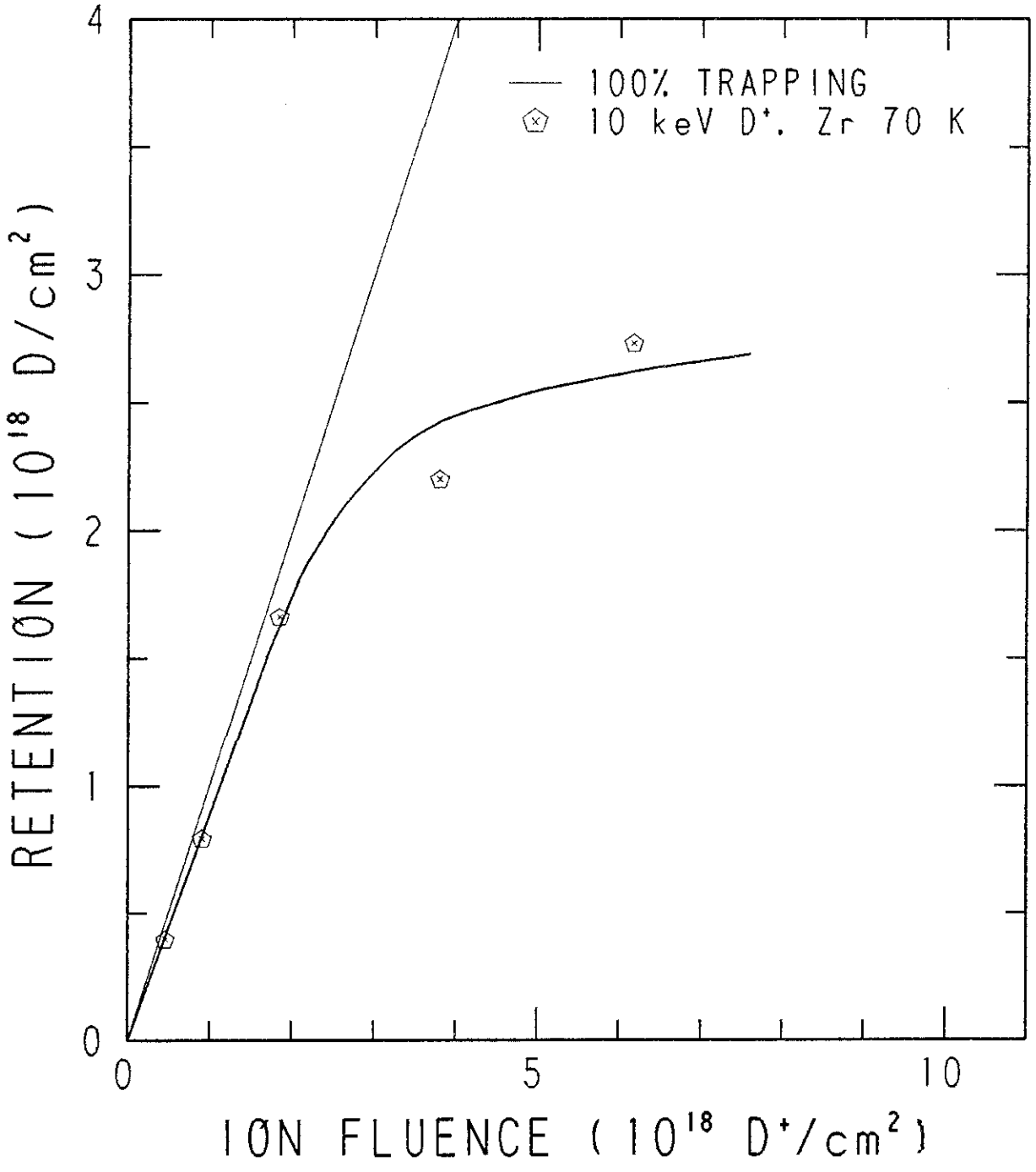

Fig. A-3 Retention curve for 10 keV D^+ implanted into Zr at 70 K. The particle flux was 2×10^{14} atoms/cm^2·sec. (ref. 64)

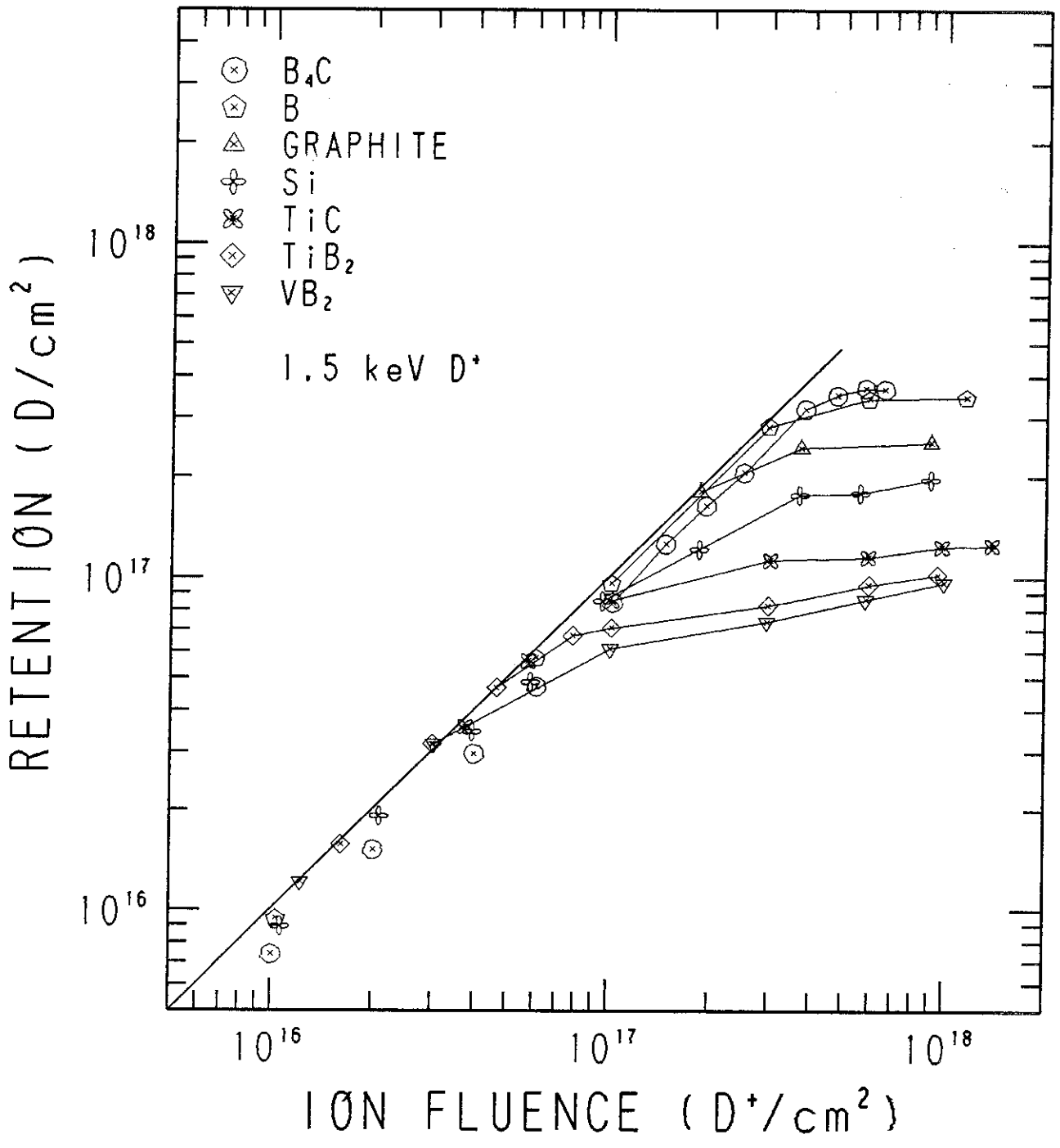

Fig. A-4 D saturation curves for 1.5 keV D^+ implanted into various low-Z materials. (ref. 57)

A - II Target Material Dependence

The trapping efficiencies for energetic hydrogen ions in molybdenum, titanium, zirconium and tantalum are shown in Figs. A-5 and A-6 as functions of ion dose and energy, respectively. It will be seen that Mo has initially a high trapping efficiency, but that the trapping efficiency rapidly decreases with dose and saturation is reached at about 10^{17} ions/cm^2 at room temperature. In Mo which do not react exothermically with hydrogen, the surface will act as a sink for diffusing atoms. Since the ion range will be very much less than the thickness of the target, the concentration gradient will be much steeper towards the surface than into the bulk. Thus the gas flow will be predominantly toward the bombarded surface and an equilibrium gradually sets up between the incident ions and the outcoming gas.

On the other hand, Ti, Zr and Ta exhibit markedly different behavior. Trapping efficiencies as high as 0.92 are observed and these are maintained constant up to doses of at least 10^{19} ions/cm^2. This implies diffusion of the hydrogen into bulk without diffusion out of the surface. In certain metals such as Ti, Zr, V, Nb, Ta and the rare earths, hydrogen reacts chemically and has a large negative heat of solution. In addition, in many cases, in the group Va metals, hydrogen is known to have large diffusion coefficients with activation energies considerably less than heat of solution. Thus implanted hydrogen ions can diffuse in the bulk of the metal without being able to penetrate the potential barrier at the surface.

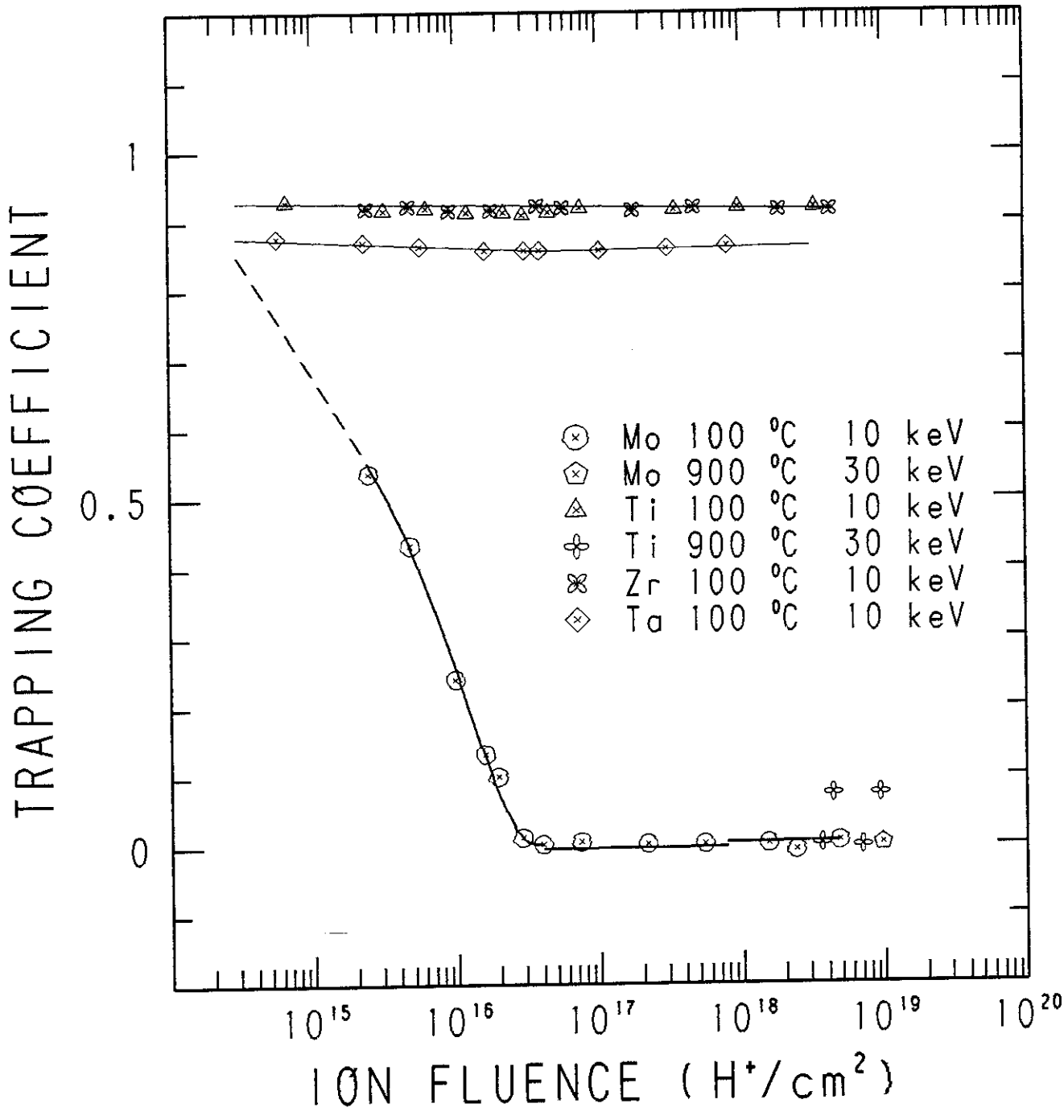

Fig. A-5 Variation of trapping coefficient of H^+ ions with fluence in Mo, Ti, Zr and Ta . Measurements were made with 10 and 30 keV H^+ ions at low (100°C) and high (900°C) temperatures, respectively. (ref. 2)

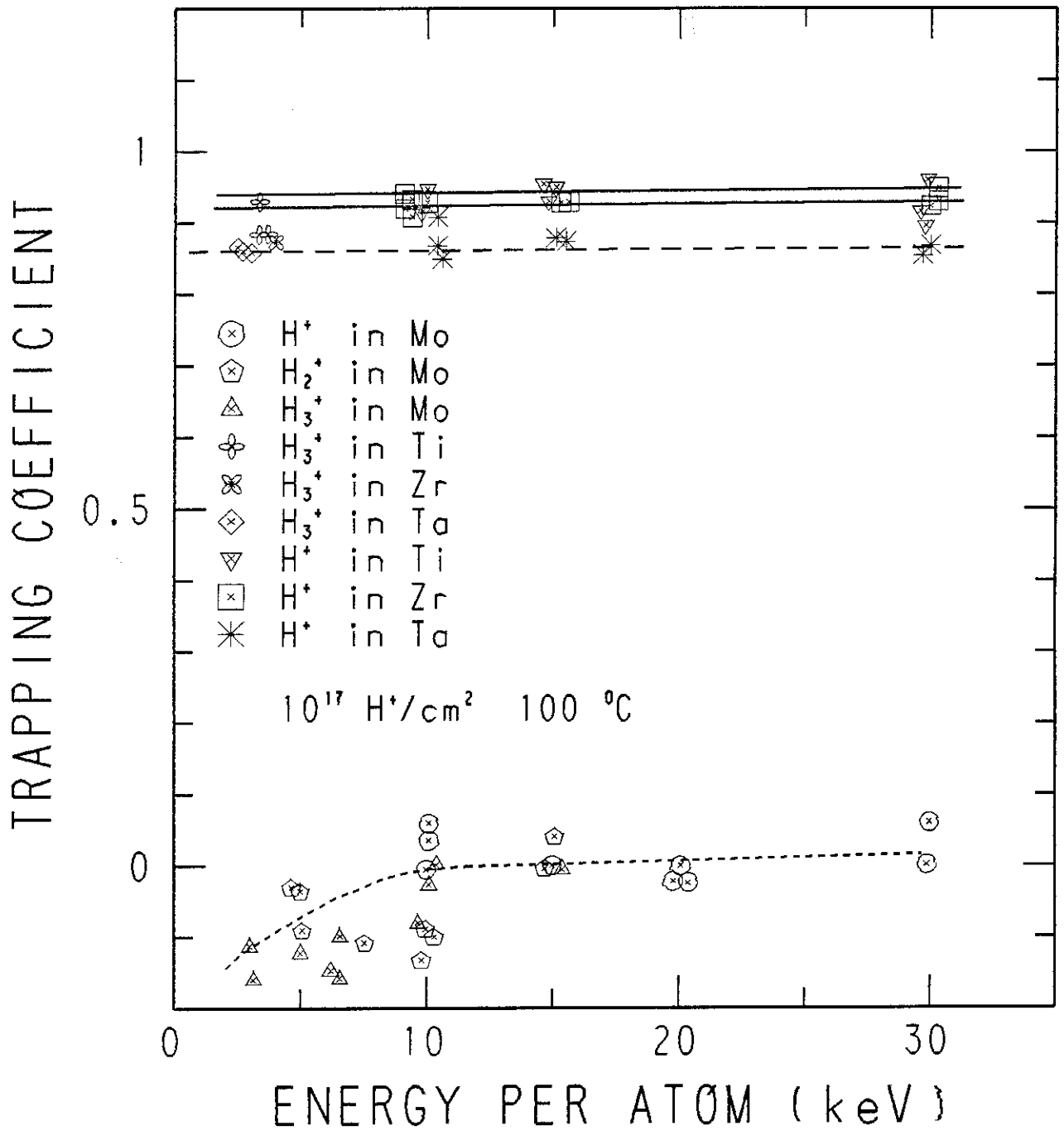

Fig. A-6 Variation of trapping coefficient of hydrogen ions with energy in Mo, Ti, Zr and Ta. Measurements were made at about 100°C at fluences greater than 10^{17} ions/cm^2. (ref. 2)

A - III Time Dependence

Time dependence of the deuterium retention after implantation for the various samples are given in Figs. A-7, A-8 and A-9. The decrease of the retained deuterium in 316 stainless steel shows that much of the deuterium rapidly moves out from the near-surface region either emerging at the surface or diffusing into the bulk. This behavior is expected as deuterium is mobile in stainless steel at room temperature.

For Ti and Ti alloy, the amount of deuterium retained in the near-surface region is found to vary significantly with alloy composition at any given time after implantation. Annealed pure titanium shows no significant decrease in the near surface deuterium concentration with time, while in the cold worked titanium retention decreases steadily. The Ti-6Al samples maintain nearly constant deuterium levels. But, for the Ti-6Al-4V alloys which are mixture of alpha and beta phases, nearly all of the deuterium leave the near-surface region within 10^5 sec. Severe cold-working and presence of the beta phase considerably reduce deuterium retention in the near-surface region.

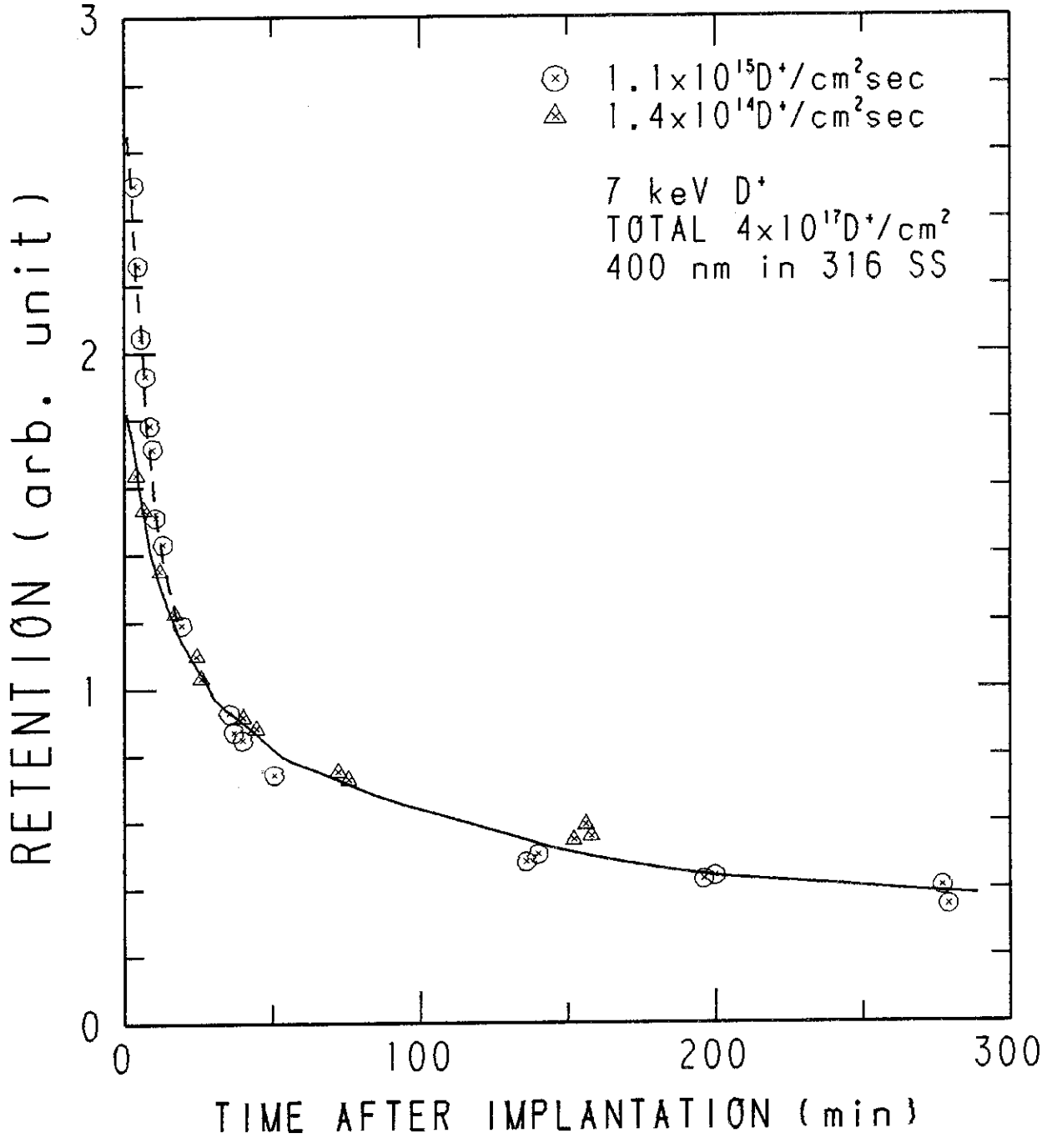

Fig. A-7 Retention of 7 keV D^+ in 316 SS in a surface layer of ∿400 nm as a function of time after 4×10^{17} D^+/cm^2 implantation for two different implantation rates. The $^3He^+$ beam of 0.79 MeV was used for nuclear reaction analysis. (ref. 30)

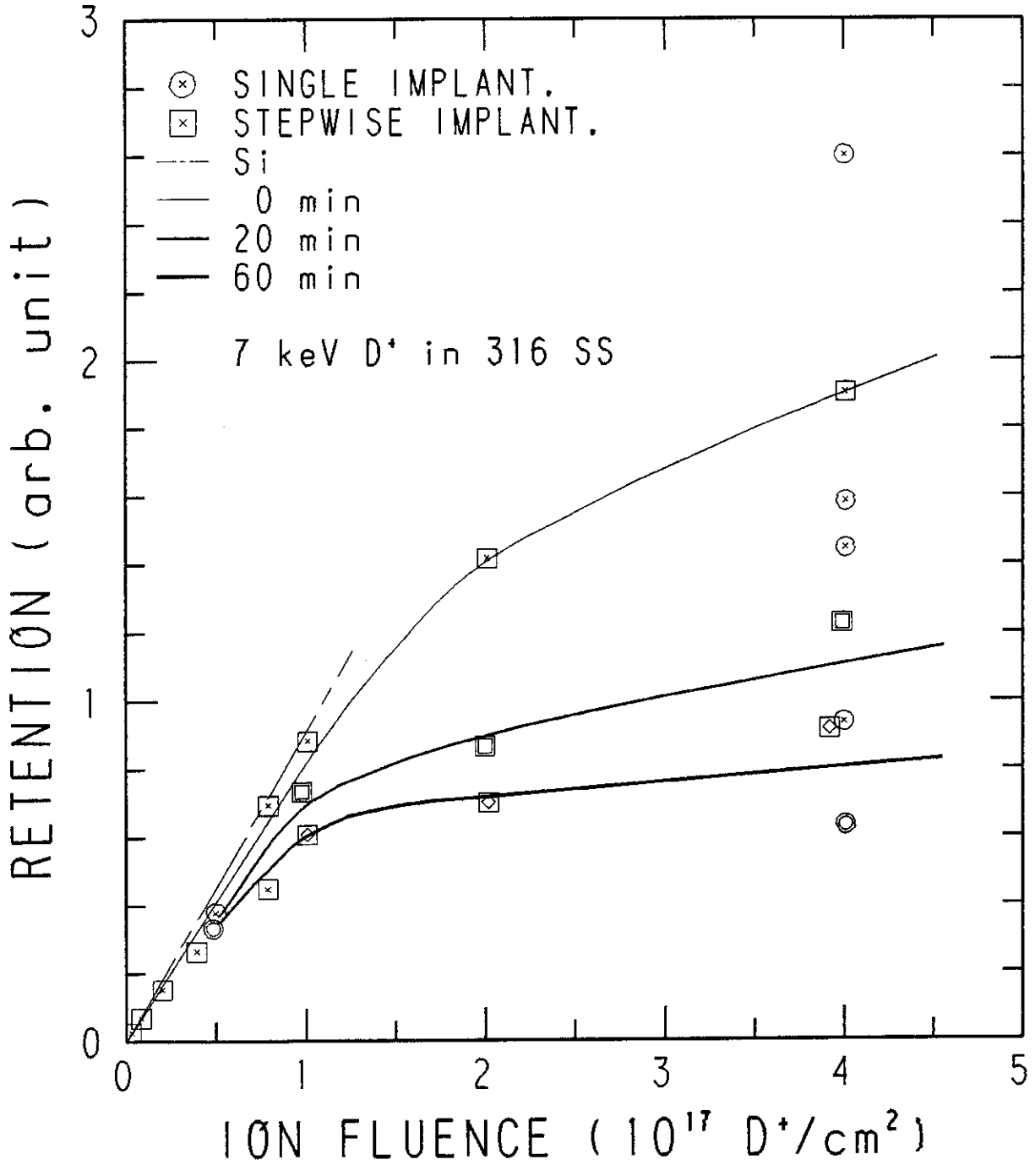

Fig. A-8 Retention of 7 keV D^+ in 316 SS as a function of ion fluence for three different holding times at room temperature after implantation. (ref. 30)

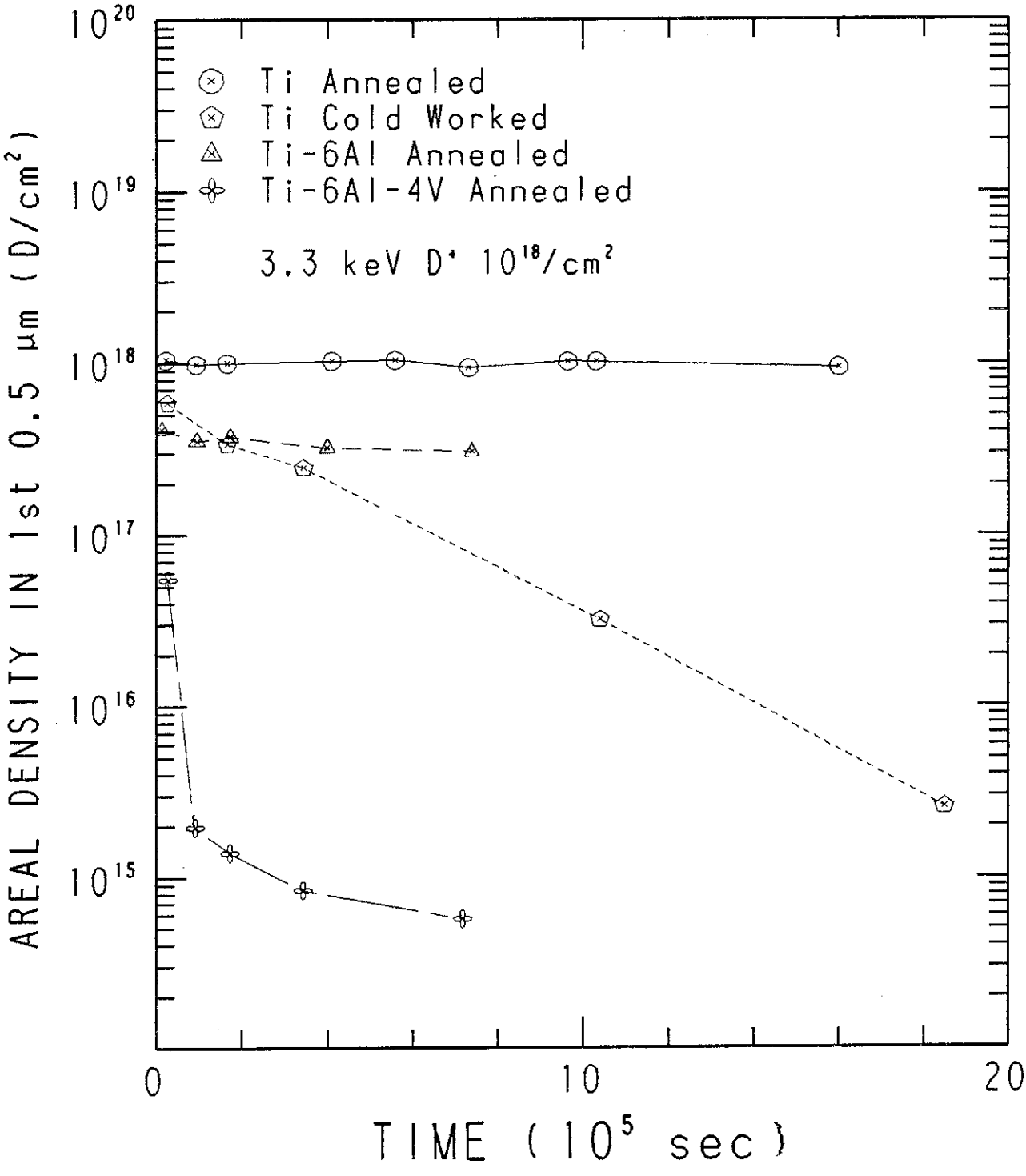

Fig. A-9 Deuterium retention vs. time for annealed Ti, cold-worked Ti, annealed Ti-6Al and annealed Ti-6Al-4V, fluence = 1×10^{18} D^+/cm^2. (ref. 49)

A - IV Target Temperature Dependence

Temperature dependence of re-emission rate during hydrogen bombardment have been measured on several unreactive targets such as nickel (Fig. A-10), molybdenum (Figs. A-11, A-12), stainless steel (Figs. A-13, A-14, A-15) and graphite (Fig. A-16). Below room temperature, hydrogen is unable to diffuse out of the implantation zone as fast as the arrival rate from the incident ion flux. The trapping coefficient is close to unity and hydrogen to metal ratio in the implanted surface layer exceeds 0.9. Above 300 K, trapping decreases rapidly with increasing fluence. The decrease in trapping is seen to be faster at high temperature. This temperature dependence suggests that hydrogen diffusion plays an important role in the re-emission phenomenon above room temperature.

Time dependence of the re-emitted gas flux is approximately described by diffusion model with the theoretical flux being given by:

$$J = J_o \mathrm{erf}[R/\sqrt{4Dt}]$$

where J_o is the incident flux, R the mean ion range, D the diffusion coefficient of the gas in the solid and t is time. Since diffusion coefficients vary with temperature in the well-known way,

$$D = D_o \exp(-Q/k_b T)$$

an increase of temperature results in an increase of D and hence the very much more rapid attainment of equilibrium. Qualitatively similar curves have been observed experimentally. In order to fit the theoretical curves to the experimental results, however, the values of diffusion coefficient required are about two orders of magnitude below those measured in conventional thermal diffusion experiments. The low diffusion coefficient observed will be attributed to the trapping of hydrogen atoms at the damage sites described in section A - VI. At higher temperatures (>400 K), hydrogen release may also be controlled by molecular recombination on the surface leading to thermal molecules being

re-emitted. Although it is difficult to know a reliable value for the surface recombination coefficient, the rate determing process may be determined by comparing the bulk concentration to the near surface concentration; a large ratio implies diffusion controlled release while a ratio near unity implies surface recombination controlled release. It is still to be determined experimentally whether the release take place as atoms, as molecules or as ions.

For reactive metals with hydrogen such as Ti, Zr and Ta, trapping efficiencies for keV hydrogen ions at room temperature is greater than 90 % up to doses of at least 10^{19} ions/cm^2 as seen in Figs. A-5, A-14 and A-17. However, the effective trapping efficiency decreases at higher temperature, where the atom has sufficient thermal energy to overcome the surface potential barrier. Trapping efficiencies measured after large doses as functions of temperature are shown in Figs. A-18, A-19 and A-20. It will be noted that the efficient trapping persists to higher temperatures, the higher the heat of solution of hydrogen in the metals.

At higher concentrations, hydrogen forms a hydride with the metal and the effective diffusion coefficient may drop, thus leading to a further increase in concentration. Profile measurements of deuterons implanted in Zr (Fig. A-21) show that high concentrations ($\sim$100 at.%) build up near the surface without significant release at temperatures in the range 300 - 400 K. At higher temperatures the deuterium atoms diffuse into the bulk, leaving a lower concentration at the surface. At lower temperatures the surface reaches saturation in a way similar to the behavior of unreactive metals.

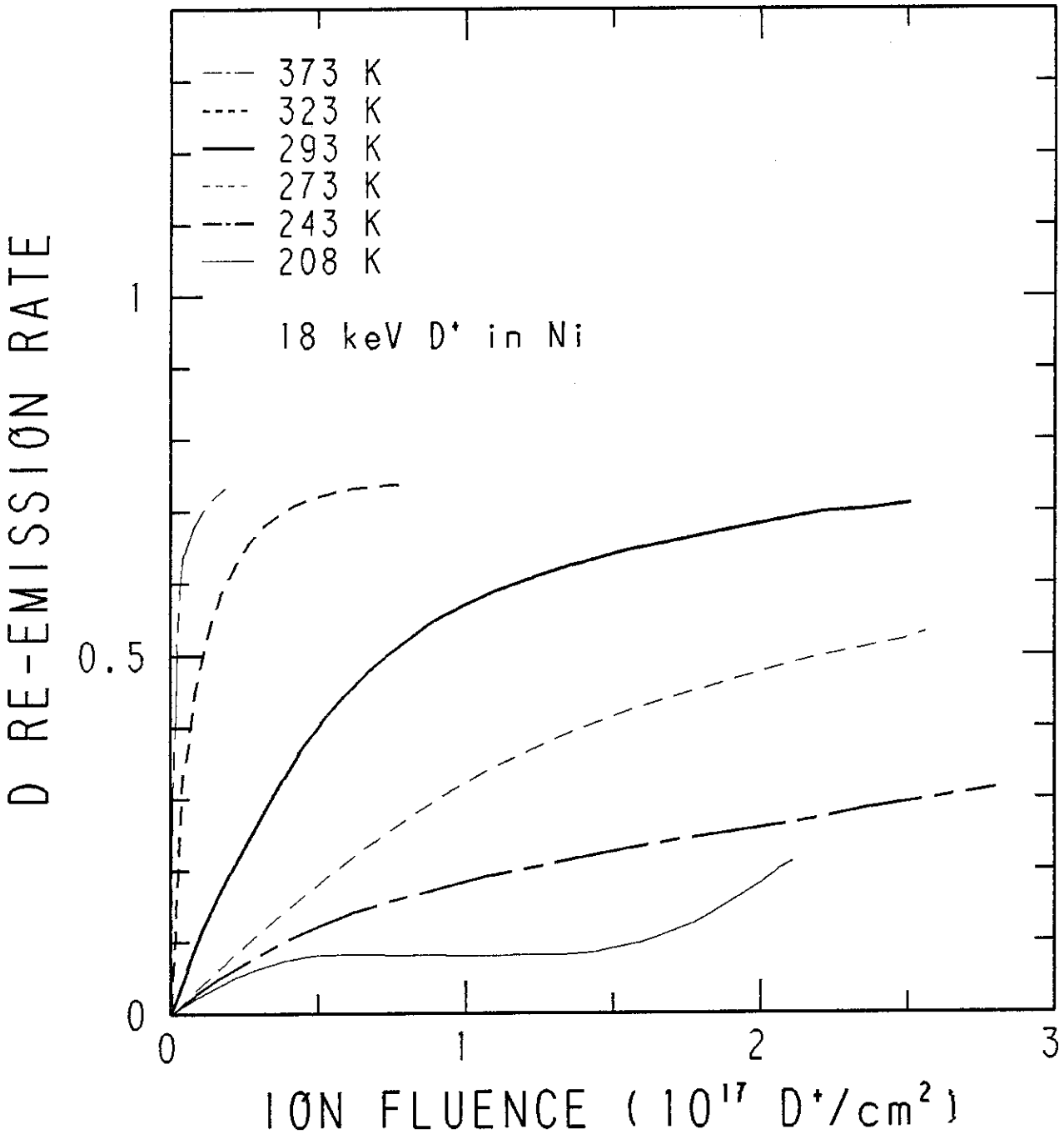

Fig. A-10 Fraction of beam re-emitted from Ni as a function of ion fluence of 18 keV D^+ ions at different target temperatures. (ref. 3)

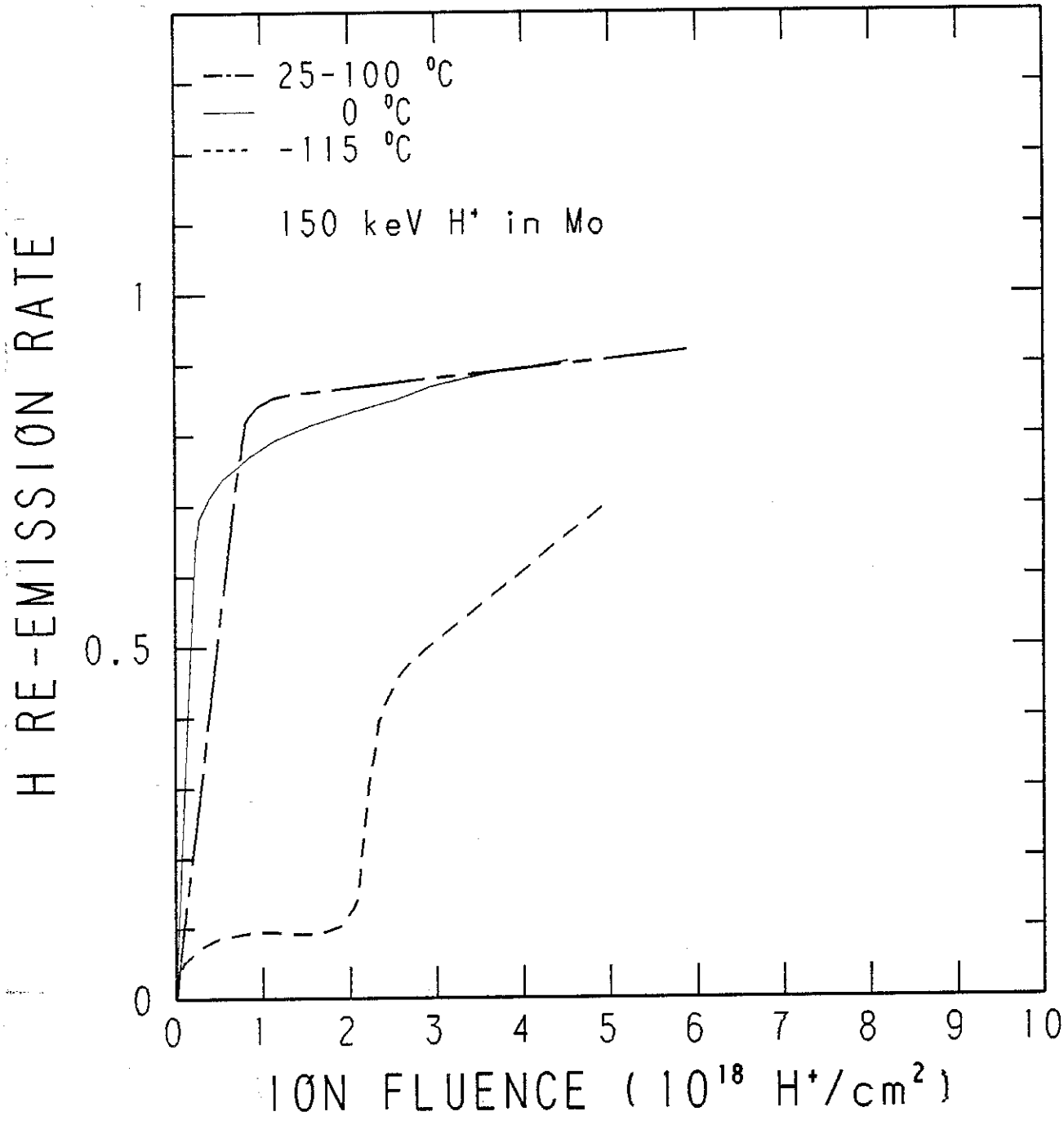

Fig. A-11 Hydrogen re-emission during 150 keV H^+ implantation as a function of fluence in Mo at three different implantation temperatures. The particle flux was 1.25×10^{15} ions/cm^2·sec. (ref. 9)

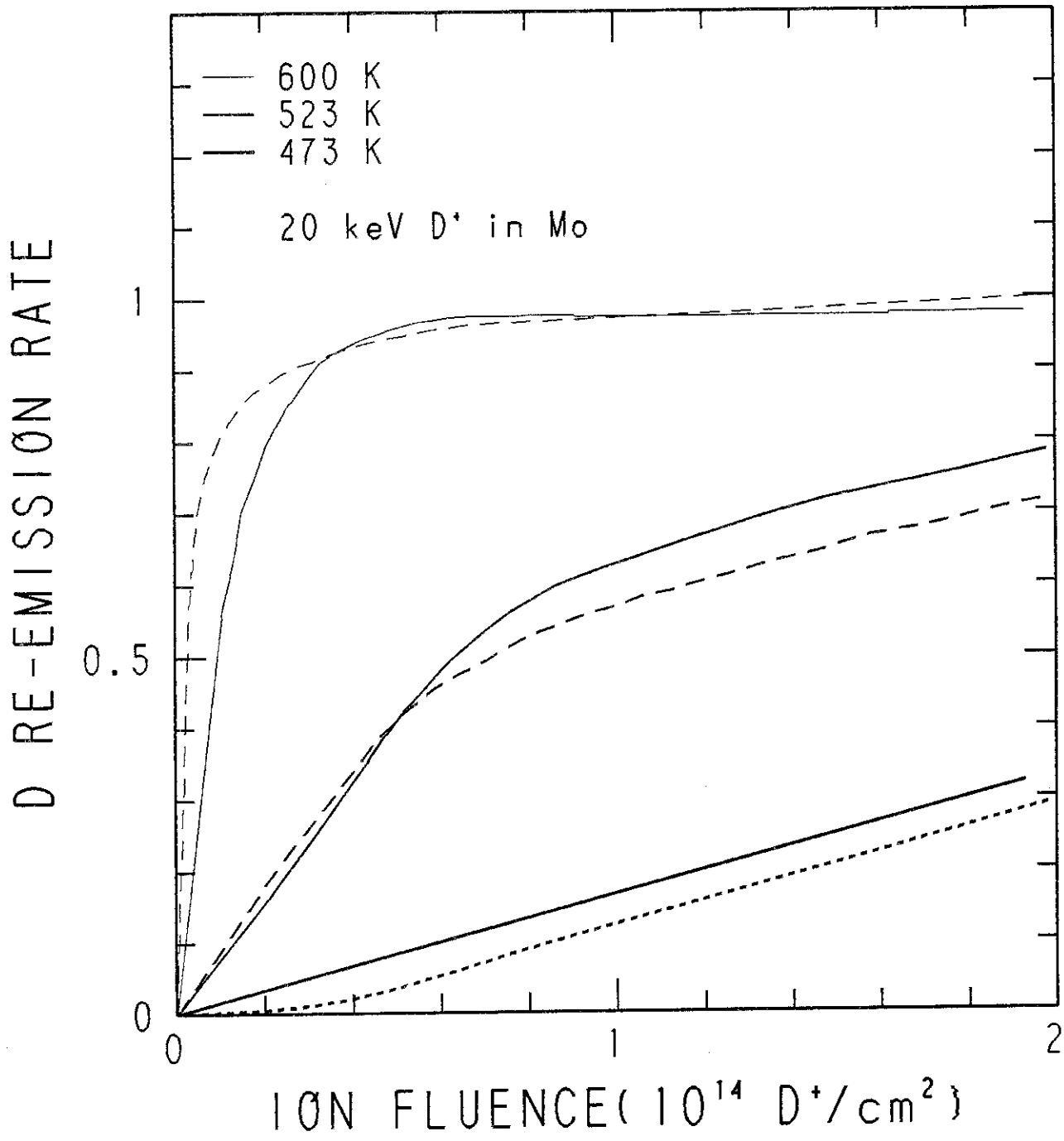

Fig. A-12 Deuterium re-emission rate from annealed Mo during bombardment by 20 keV D^+ ions. The fluence is converted from the time of bombardment, where the beam current is 2.5 μA and the beam diameter 3 mm. Theoretical curves are shown by slashed and dotted curves. They are calculated by the use of different values of diffusion coefficient D.

$D = 1 \times 10^{-8}$ cm^2 sec^{-1} (600 K)

$D = 2.8 \times 10^{-10}$ cm^2 sec^{-1} (523 K)

$D = 4.4 \times 10^{-11}$ cm^2 sec^{-1} (473 K) (ref. 10)

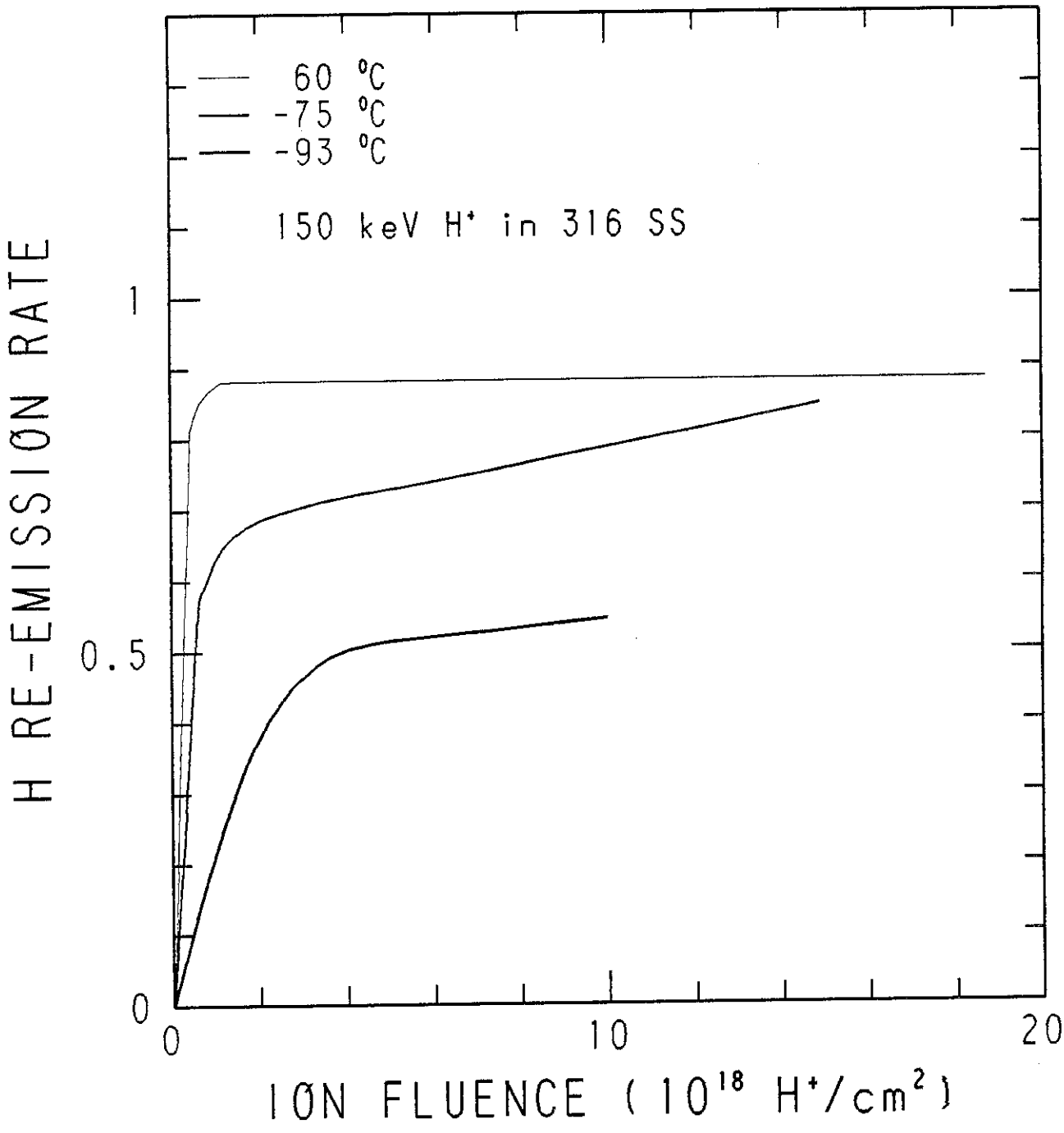

Fig. A-13 Hydrogen re-emission during 150 keV H^+ implantation as a function of fluence in 316 SS at three different implantation temperatures. Ion flux was 1.25×10^{15} $H^+/cm^2 \cdot sec$. (ref. 9)

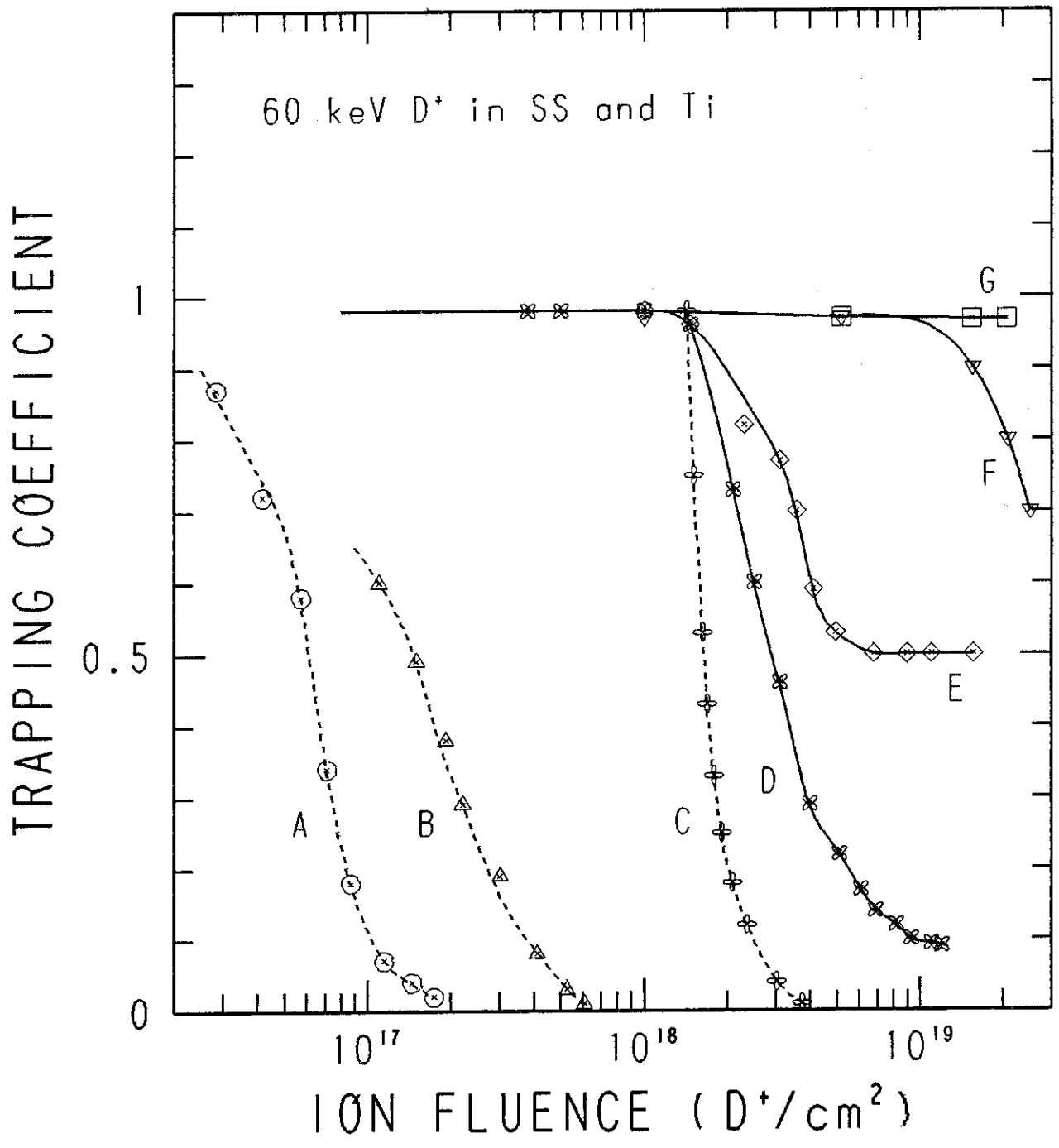

Fig. A-14 Trapping coefficient against for 60 keV D^+ ion fluence on stainless steel at 390°K(A), 300°K(B) and 173°K(C), and on titanium at 180°K(D), 630°K(E), 330°K(F) and 400°K(G). (ref. 1)

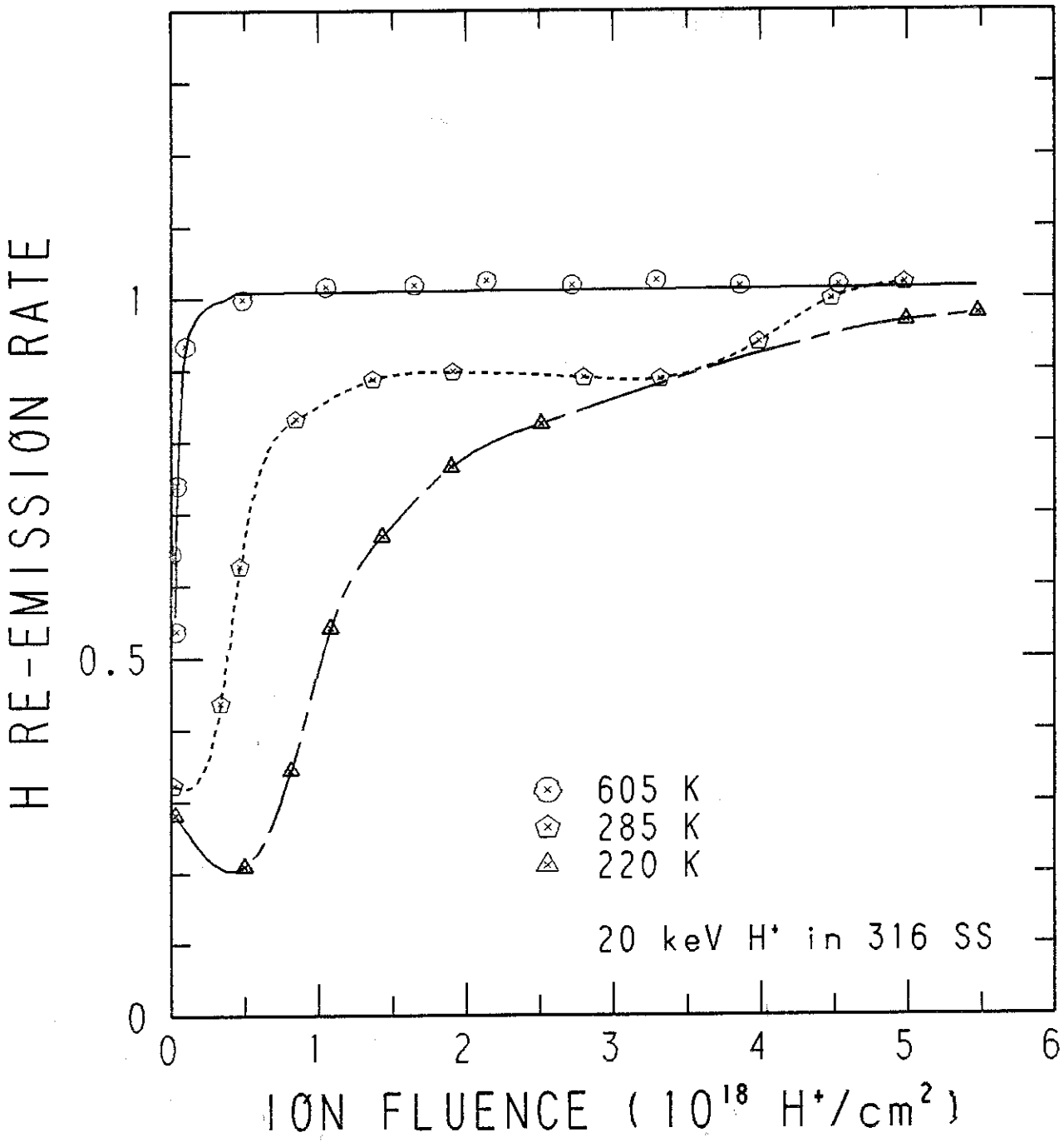

Fig. A-15 Dependence of the hydrogen re-emission rate on the fluence of 20 keV H^+ onto stainless steel at different implantation temperatures. (ref. 27)

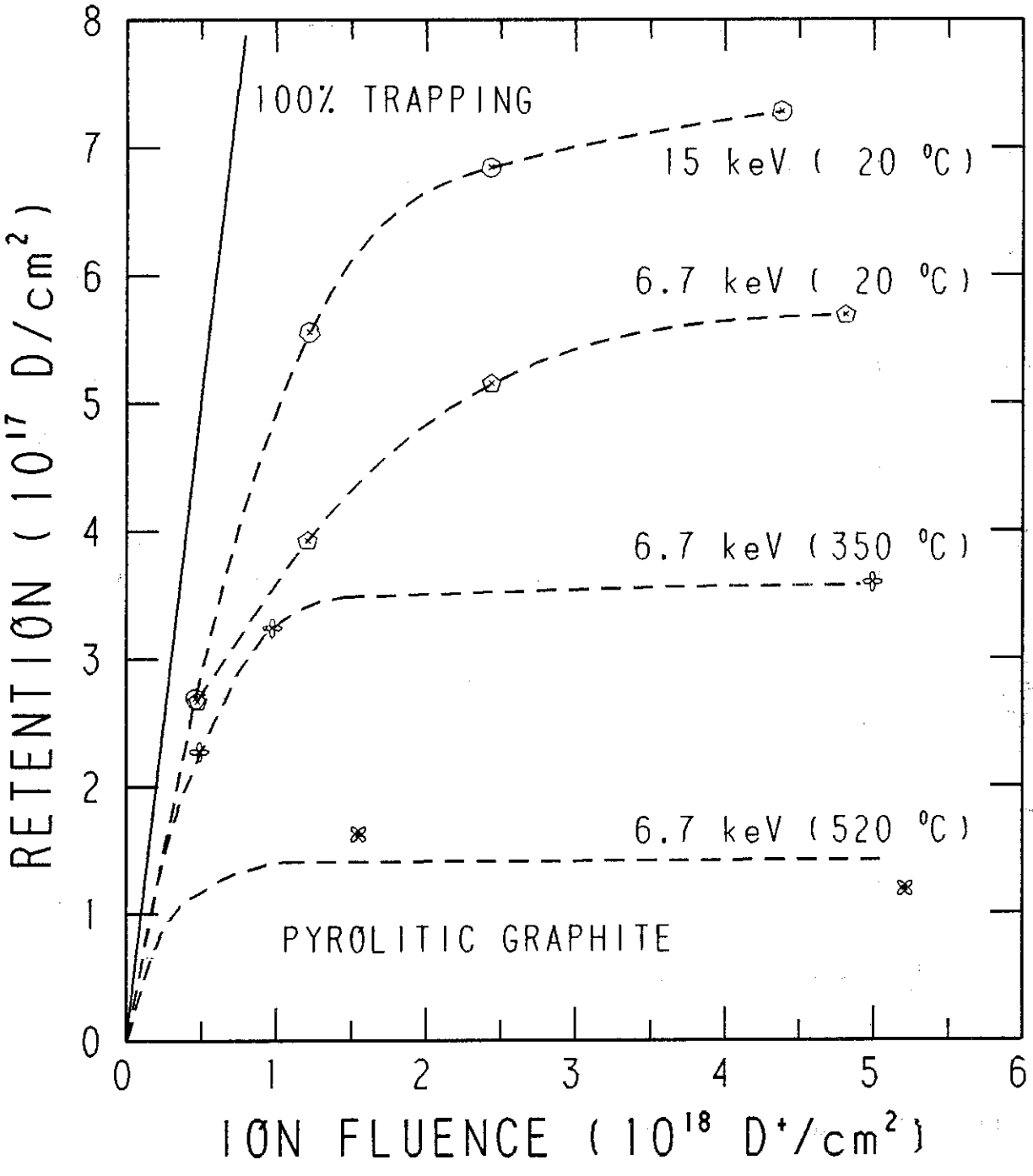

Fig. A-16 Amount of deuterium trapped in a surface layer of ∿400 nm of pyrolytic graphite (range of sensitivity for the nuclear reaction) at different target temperatures as a function of primary ion fluence. (ref. 14)

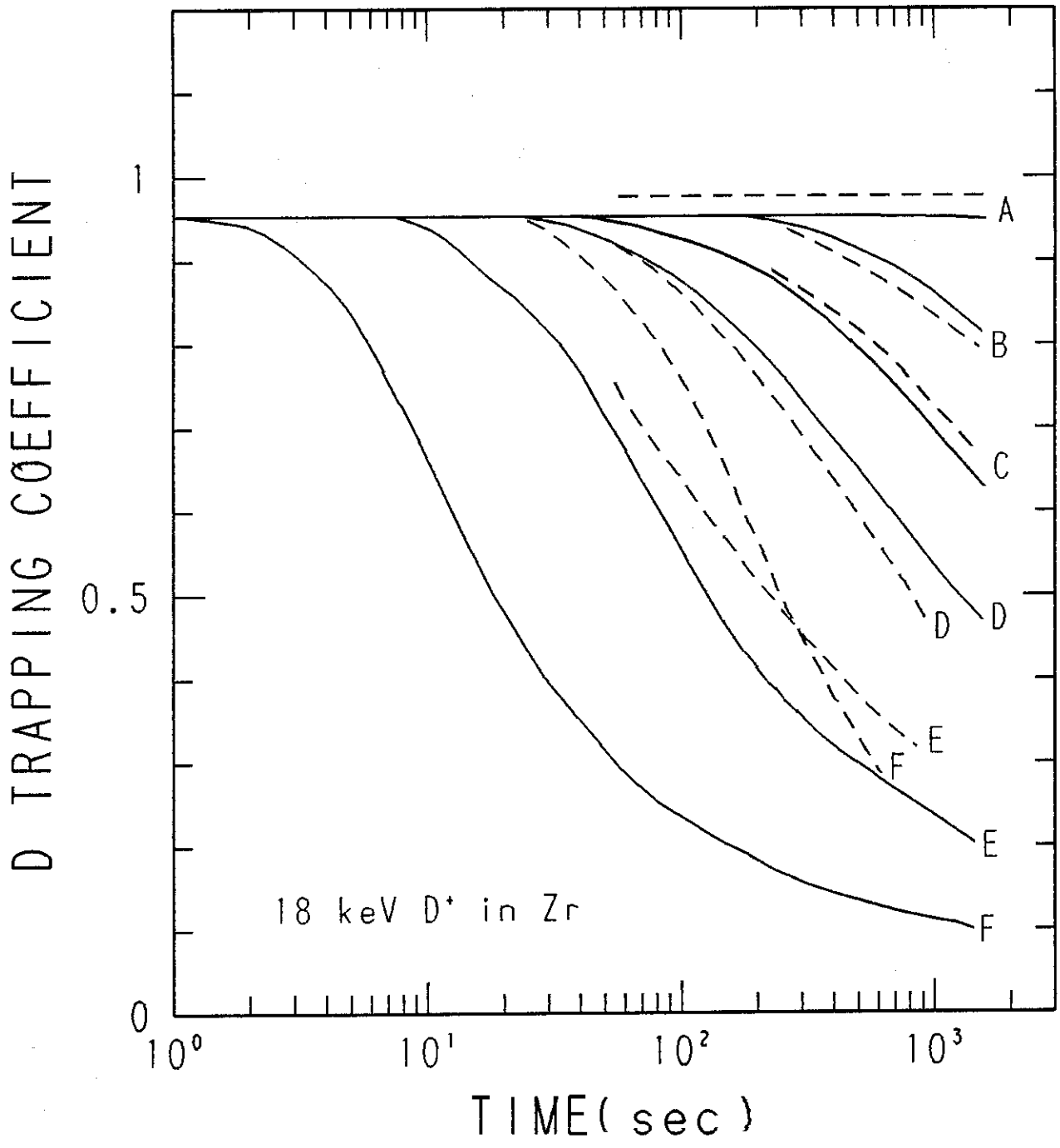

Fig. A-17 Trapping coefficient as a function of time for Zr target bombarded with 18 keV D^+. Broken lines are experimental results, solid lines are predictions of theory; a fraction of 0.06 of the incident beam is assumed to be backscattered. The target area bombarded was 0.07 cm^2. The activation energy for diffusion, is assumed to be 8250 cal/mol.

	A	B	C	D	E	F
I_b (μA)	54	52	47	47	59	49
T (K)	477	598	653	699	812	988

(ref. 29)

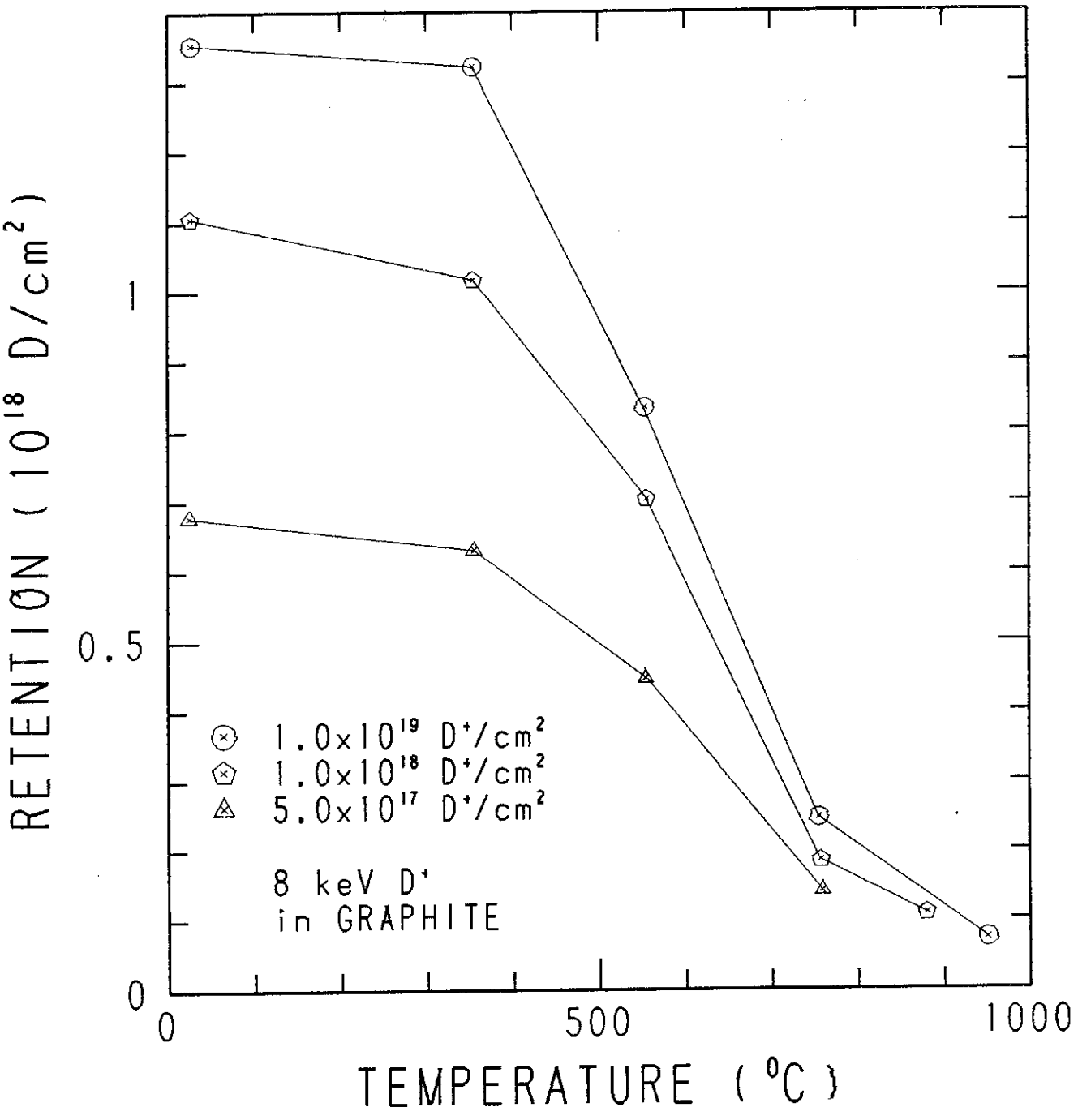

Fig. A-18 Amount of 8 keV D^+ implant trapped in the near surface of graphite as functions of anneal temperature for different fluences. (ref. 37)

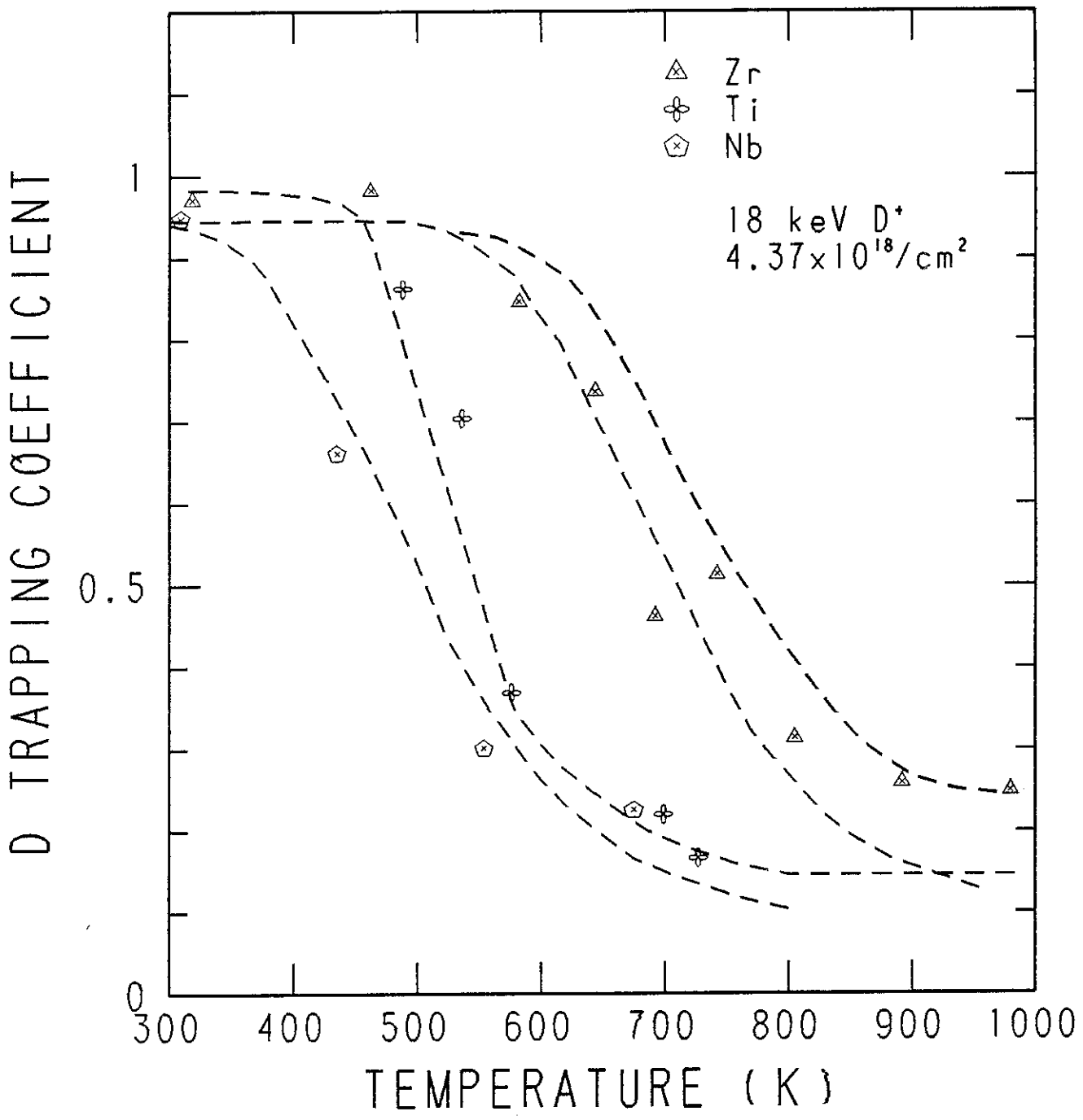

Fig. A-19 Trapping coefficient for Nb, Zr and Ti targets bombarded with a 50 μA beam of 18 keV D^+ for 1000 s as a function of temperature. The lower curve for Zr is for a value of the activation energy, Q=8250 cal/mol and upper curve for Q=6940 cal/mol. (ref. 29)

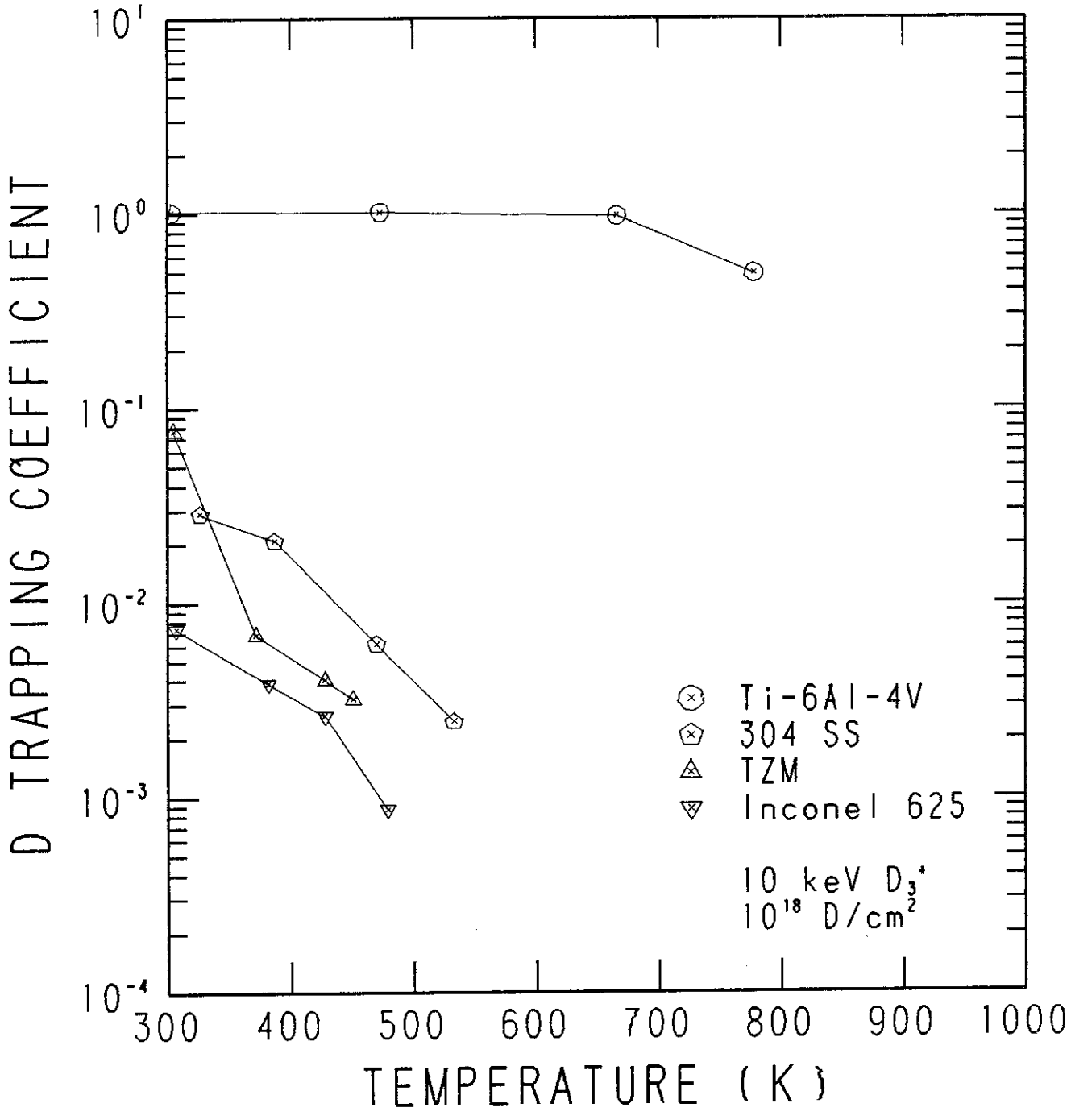

Fig. A-20 The fraction of the deuterium fluence retained in four alloys as a function of implantation temperatures. Standard fluence: 10^{18} D^+/cm^2 of 10 keV D_3^+. (ref. 53)

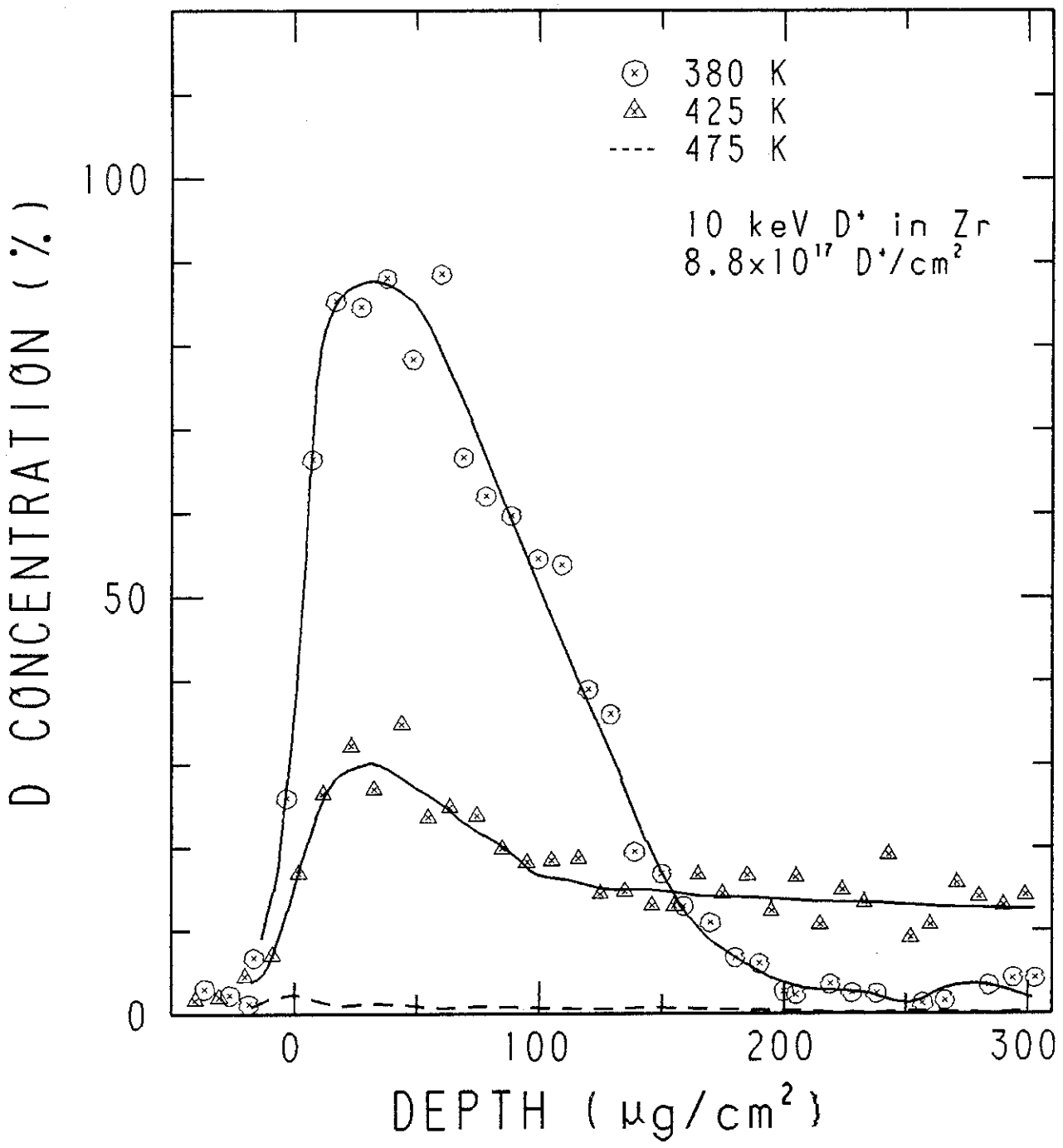

Fig. A-21 Depth profiles for 10 keV D^+ implanted into Zr, kept at different temperature, fluence = 8.8×10^{17} D^+/cm^2. (ref. 39)

A - V Incident Energy Dependence

The energy dependence of the re-emission rate in stainless steel is shown in Figs. A-22 and A-23. It will be seen in these figures that the re-emission rate increases with decreasing the incident ion energy. This is reasonable if the release mechanism of atoms from the trapping site is essentially thermal one. Because, the penetration range of the ions decreases with decreasing the ion energy.

The trapping of ions in targets, of course, only is applicable if the incident ion slows down in the target and is not backscattered. Thus, the contribution of backscattering must be corrected for the evaluation of trapping coefficient. Apart from the effect of backscattering, the probability of trapping in reactive metals as Ti and Zr seems to be independent of the incident ion energy as seen in Figs. A-6 and A-24.

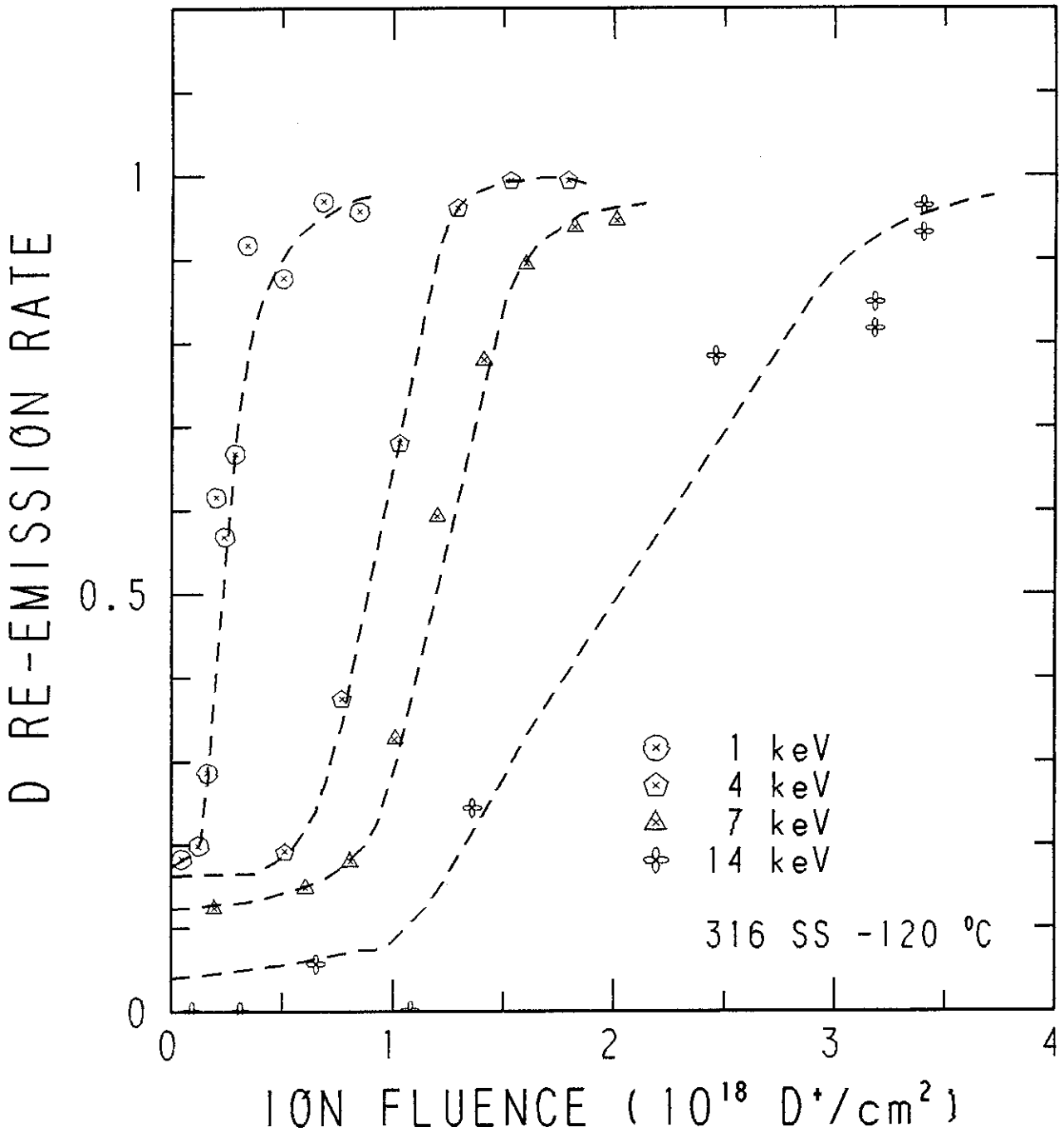

Fig. A-22 Deuterium re-emission from 316 SS during bombardment by deuterons of various energies as a function of fluence. Target temperature -120°C. (ref. 34)

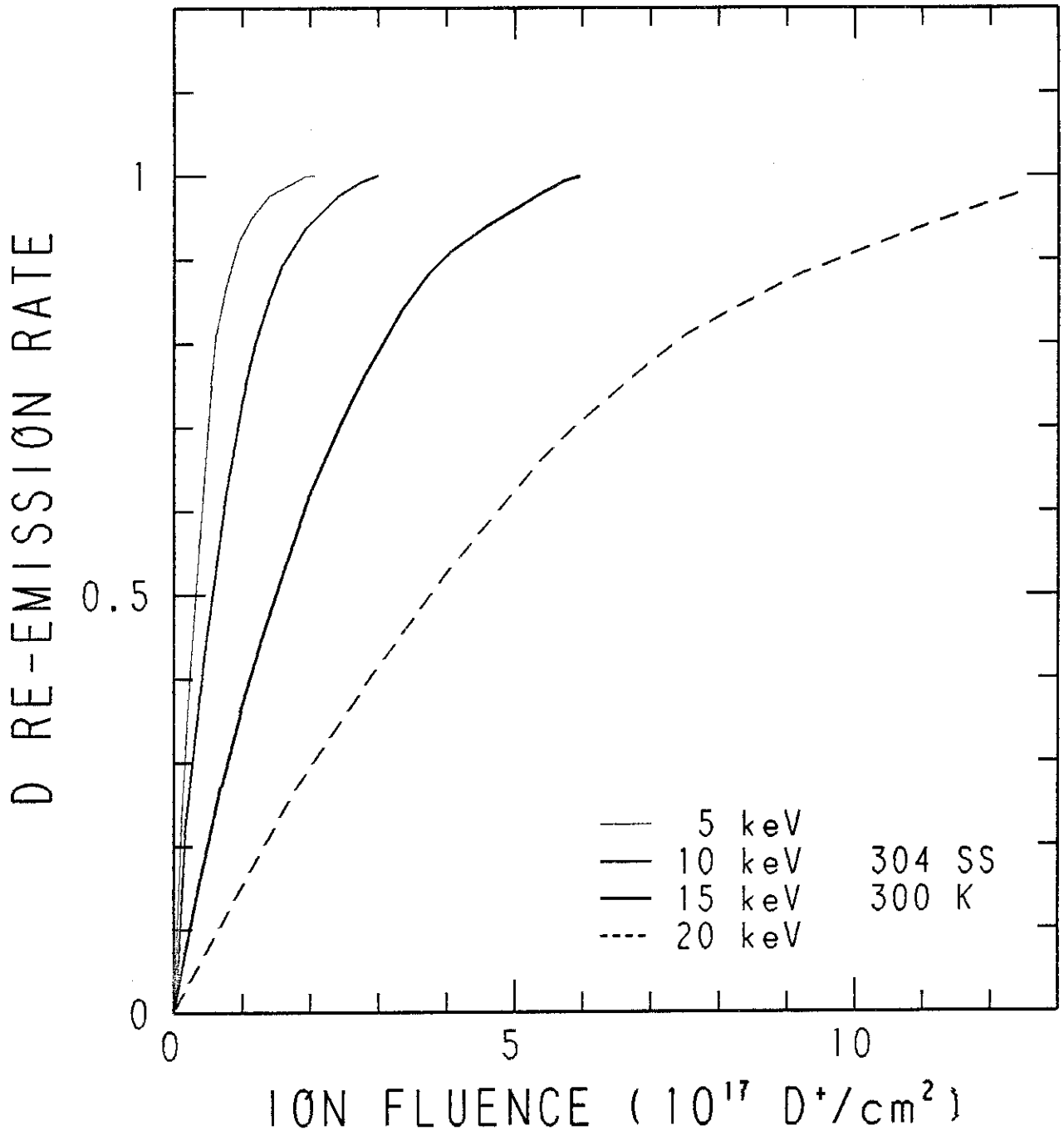

Fig. A-23 Release of D_2 from 304 SS during bombardment by deuterons of various energies. Target temperature 300 K. (ref. 33)

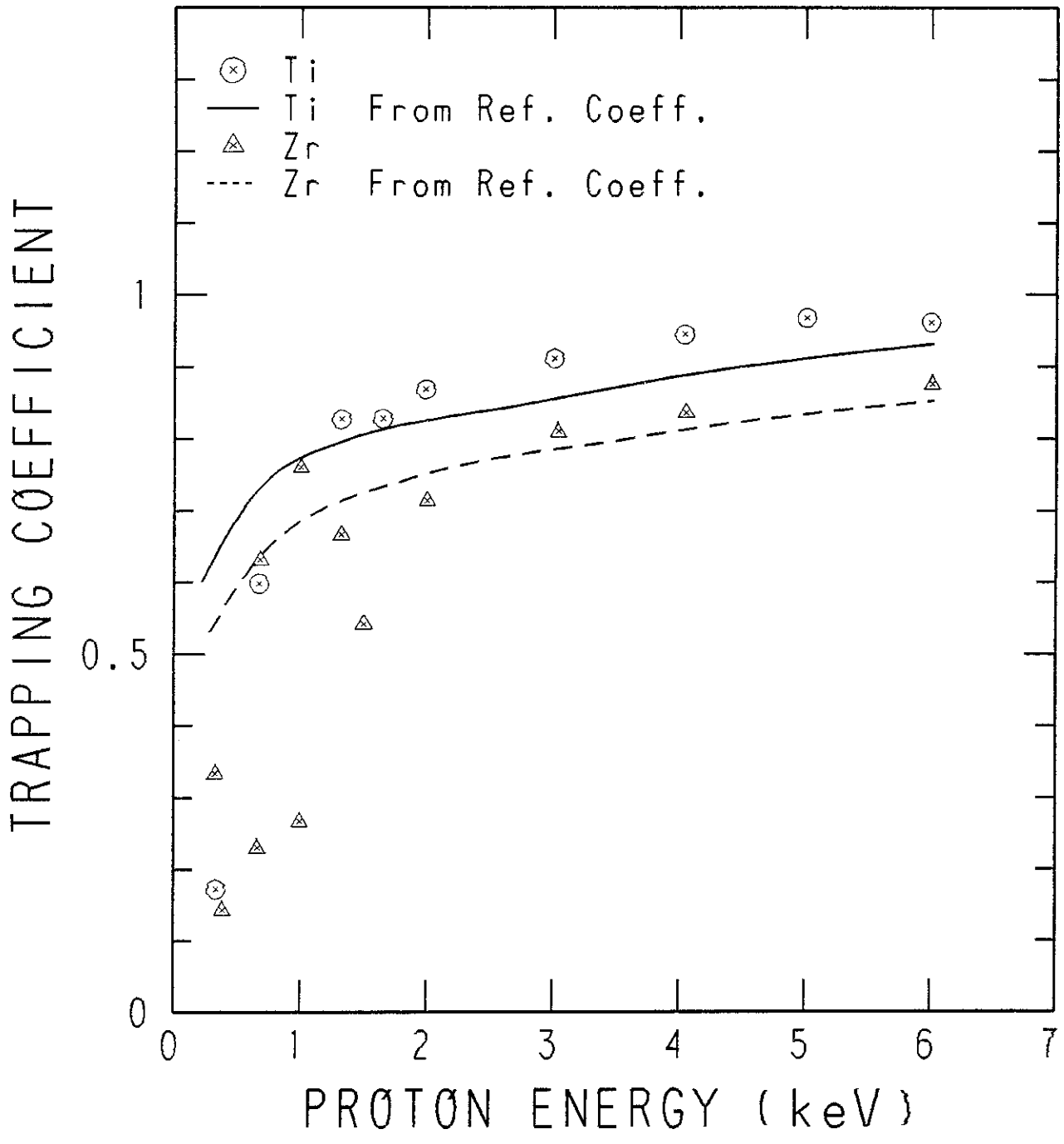

Fig. A-24 Experimental values of hydrogen trapping in Zr and Ti compared with calculated reflection coefficients. (ref. 16 and 17)

A - VI Damage Effects

Various experiments such as re-emission measurements (Fig. A-25), nuclear reaction analysis (Figs. A-26, A-27, A-28) and thermal desorption spectroscopy (A-29) revealed that the trapping of hydrogen depends strongly on the extent of lattice damage in the target. Increase in trapping efficiency with lattice damage is shown by damaging the target deliberately with heavy ions i.e. He, Ne and Ar before bombarding the surface with hydrogen. Profile measurements of the hydrogen isotopes as shown in Fig. A-30, A-31 and A-32 provide the evidence for the trapping of the diffusing atoms at the radiation damage generated by ion beam; the hydrogen atoms segregate in the damaged region. Calculations based on the thermal desorption spectroscopy (A-29) and nuclear reaction analysis (A-33) indicate that there are some radiation damage traps with different binding energies (measured with respect to the interstitial hydrogen energy) of 0.1 $\sim$ 0.3 eV, those are much larger than the energy for hydrogen diffusion.

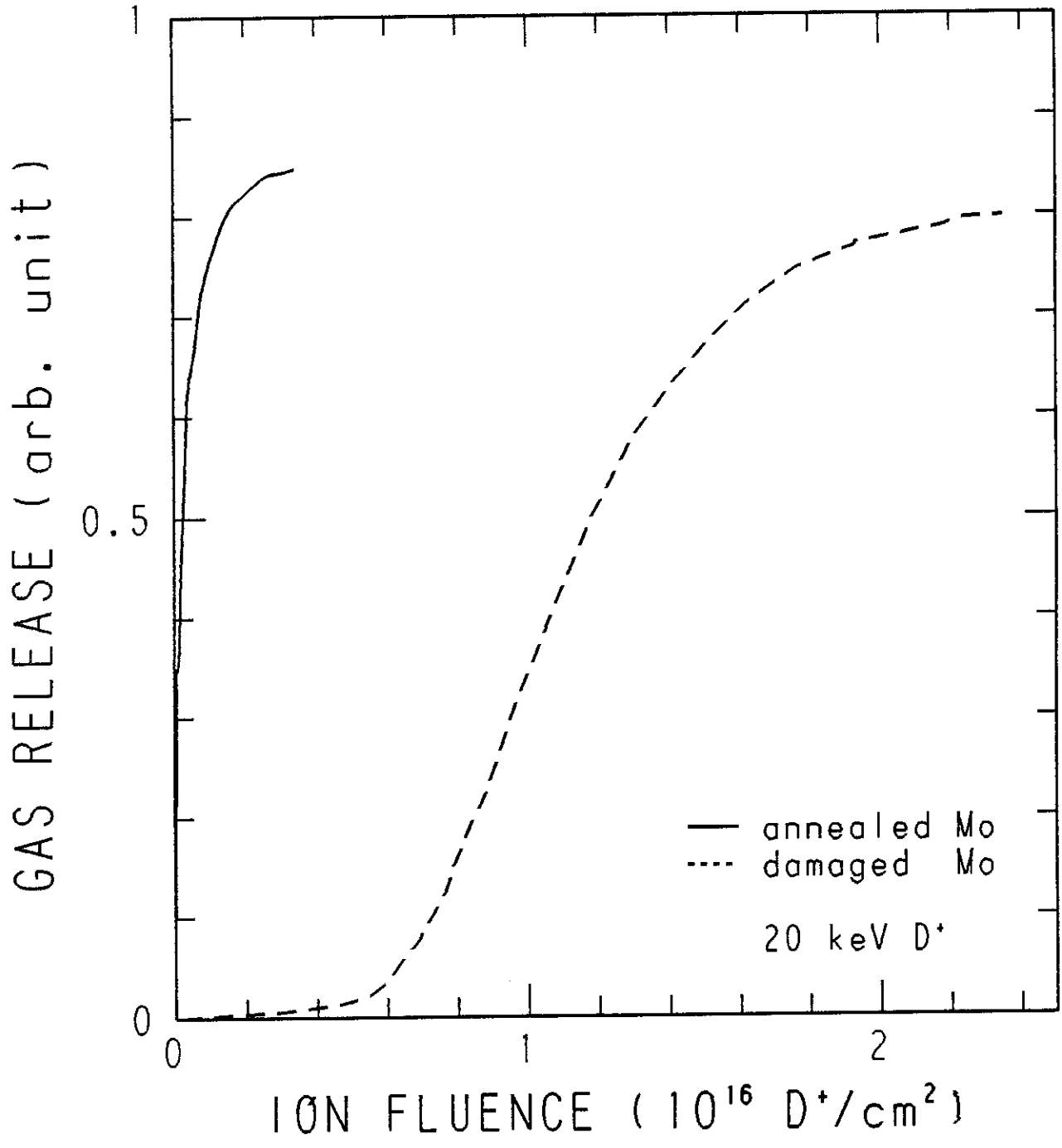

Fig. A-25 Gas release during 20 keV D^+ implantation of damaged and annealed Mo. The fluence is converted from the time of bombardment, where the beam current is 2.5 μA and the beam diameter 3 mm. (ref. 10)

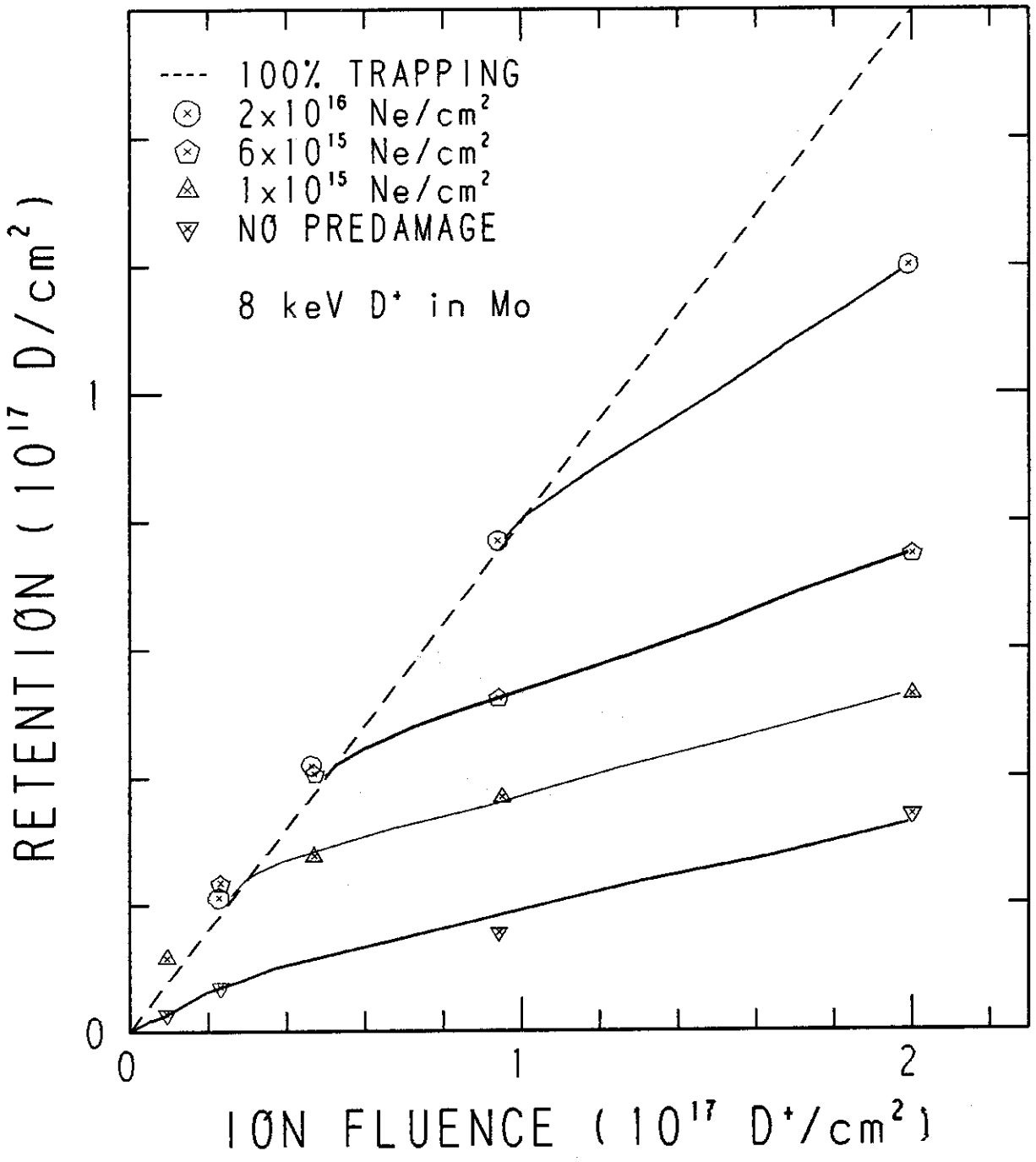

Fig. A-26 Total D retained in the near-surface region of Mo predamaged with 55-keV Ne^+, plotted as a function of 8-keV D^+ ion fluence for Ne^+ predamage fluences indicated. Dashed line corresponds to 100 % trapping after kinematic reflection is taken into account. (ref. 28)

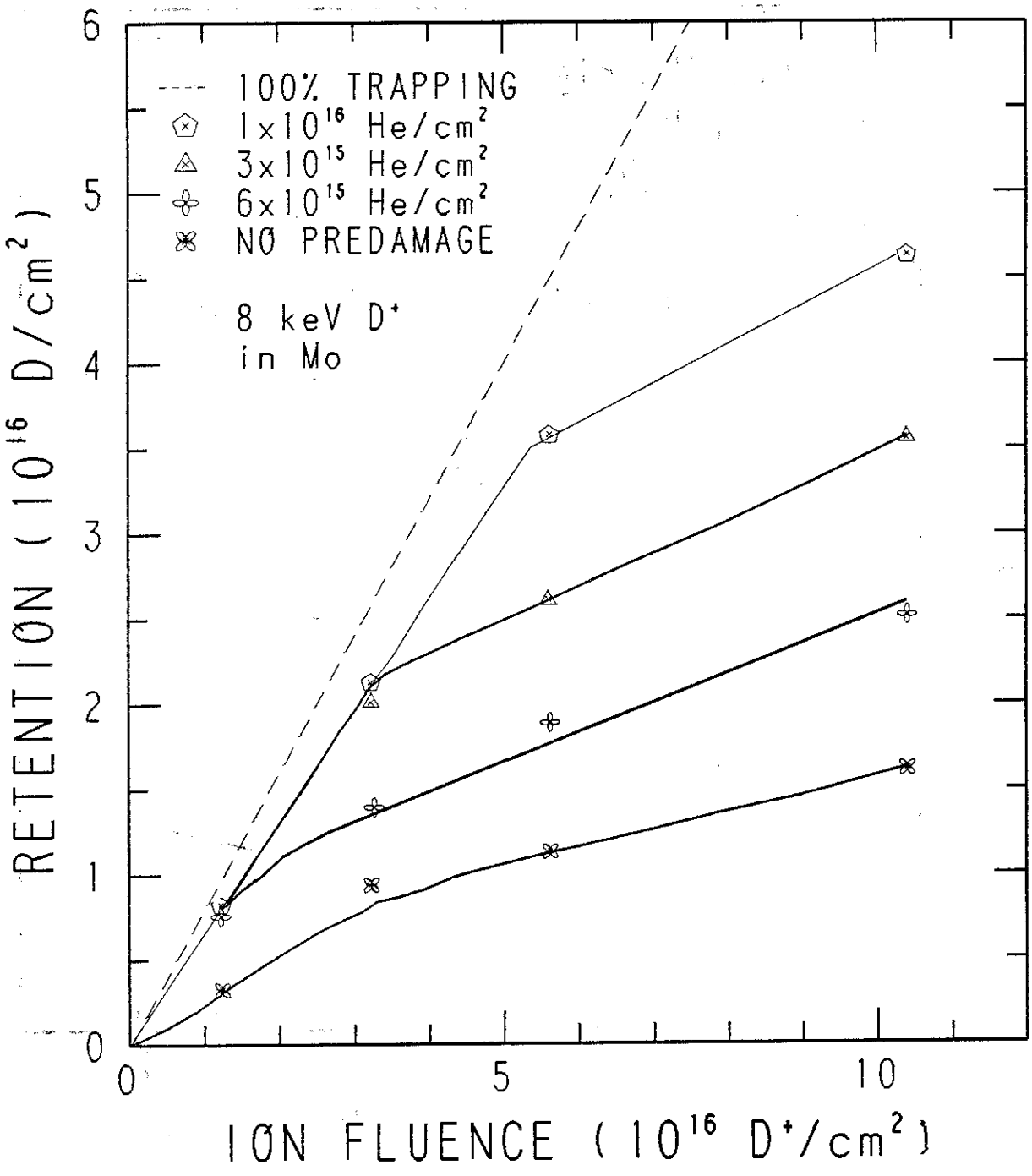

Fig. A-27 Total D retained in the near-surface region of Mo predamaged with 11-keV He^+, plotted as a function of 8-keV D^+ ion fluence for He^+ predamage fluences indicated after kinematic reflection is taken into account. (ref. 28)

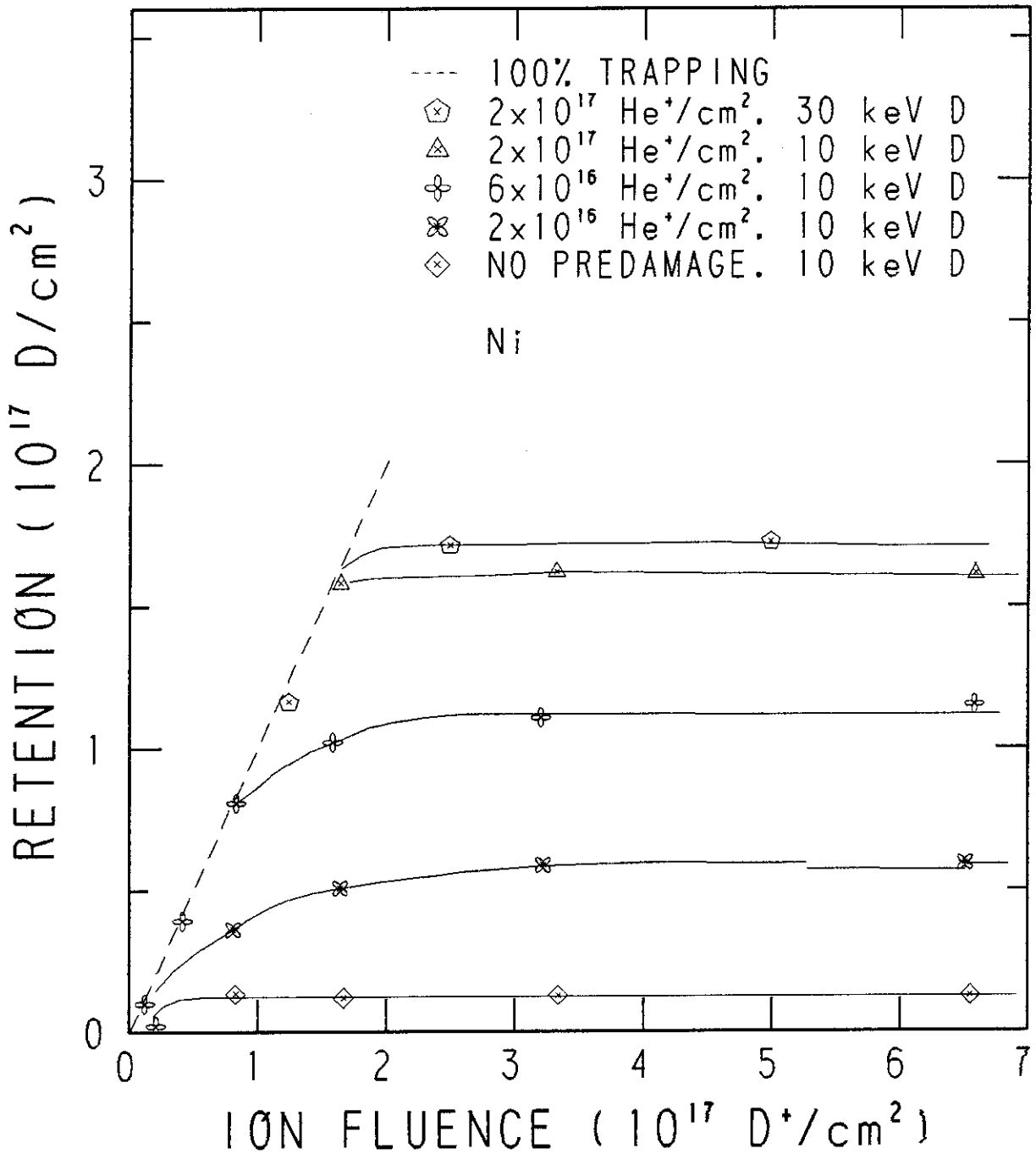

Fig. A-28 The total amount of D retained in the near-surface region of Ni as a function of D^+ fluence for 20 keV He^+ implantation with different fluences. All measurements performed at room temperature. (ref. 54)

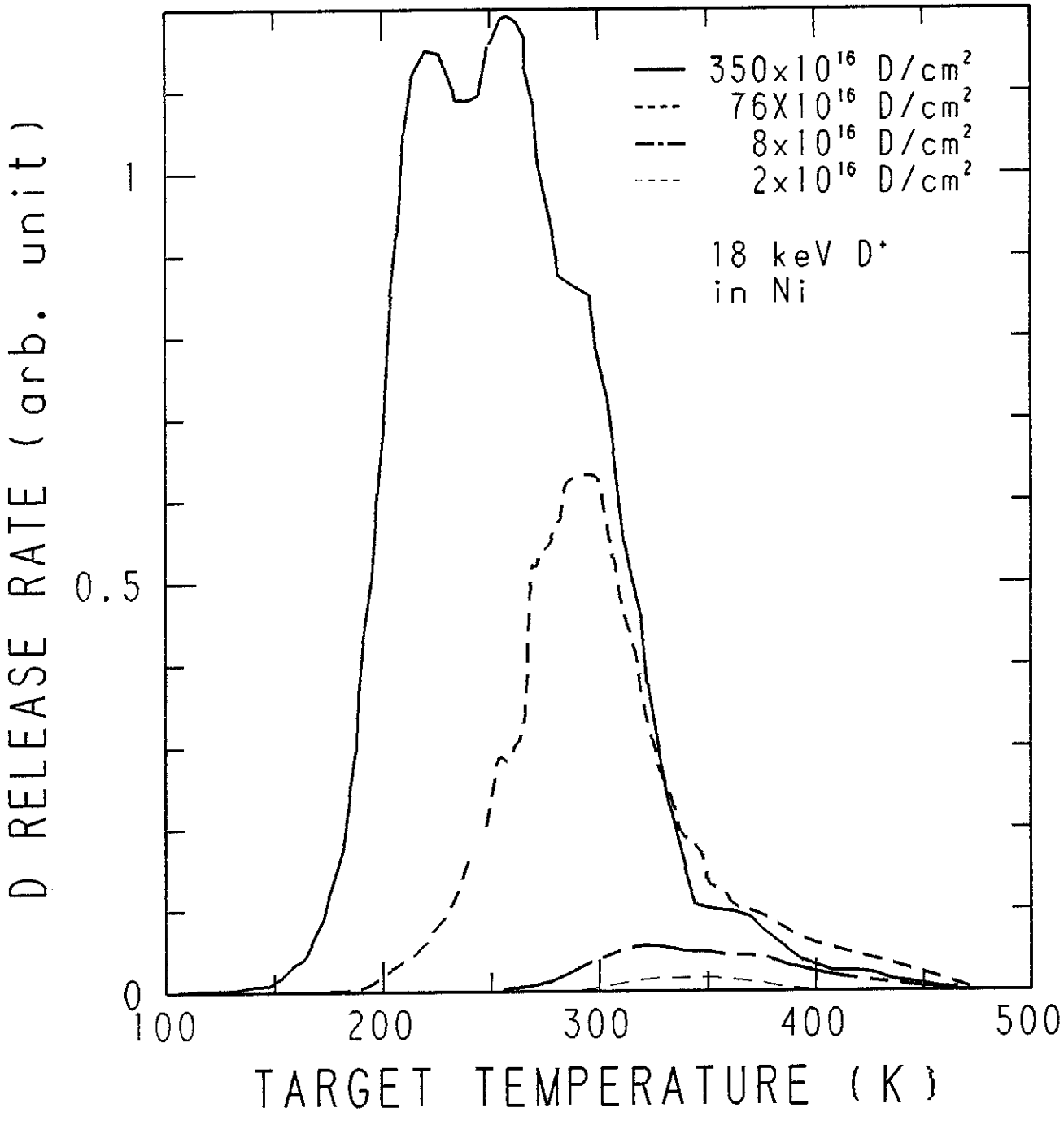

Fig. A-29 Gas release spectra of deuterium from Ni for various 18 keV D^+ ion fluences. (ref. 3)

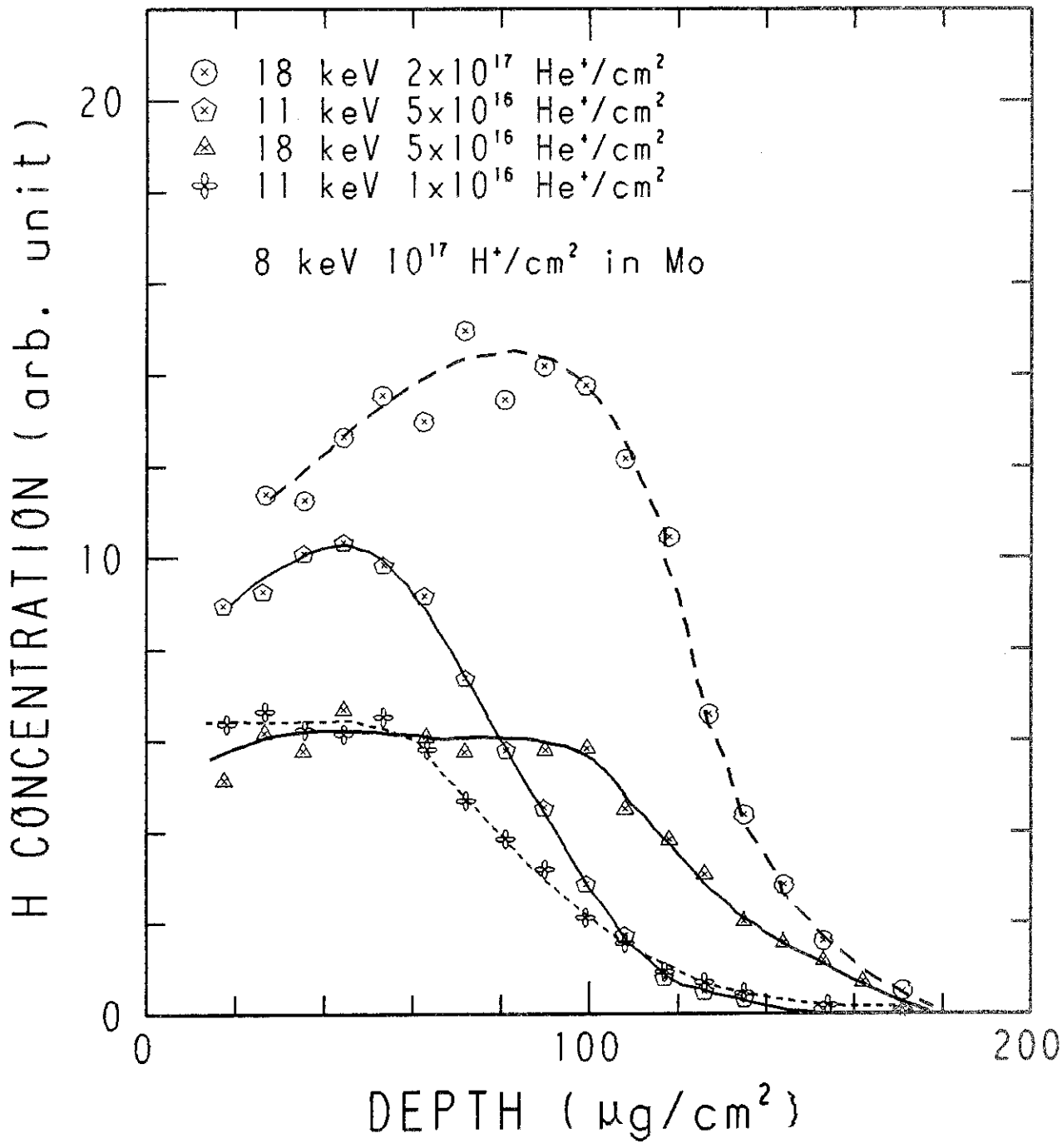

Fig. A-30 H profiles in Mo measured after He^+ predamage and subsequent 8-keV H^+ bombardment. The ion fluence was 10^{17} H^+/cm^2. (ref. 28)

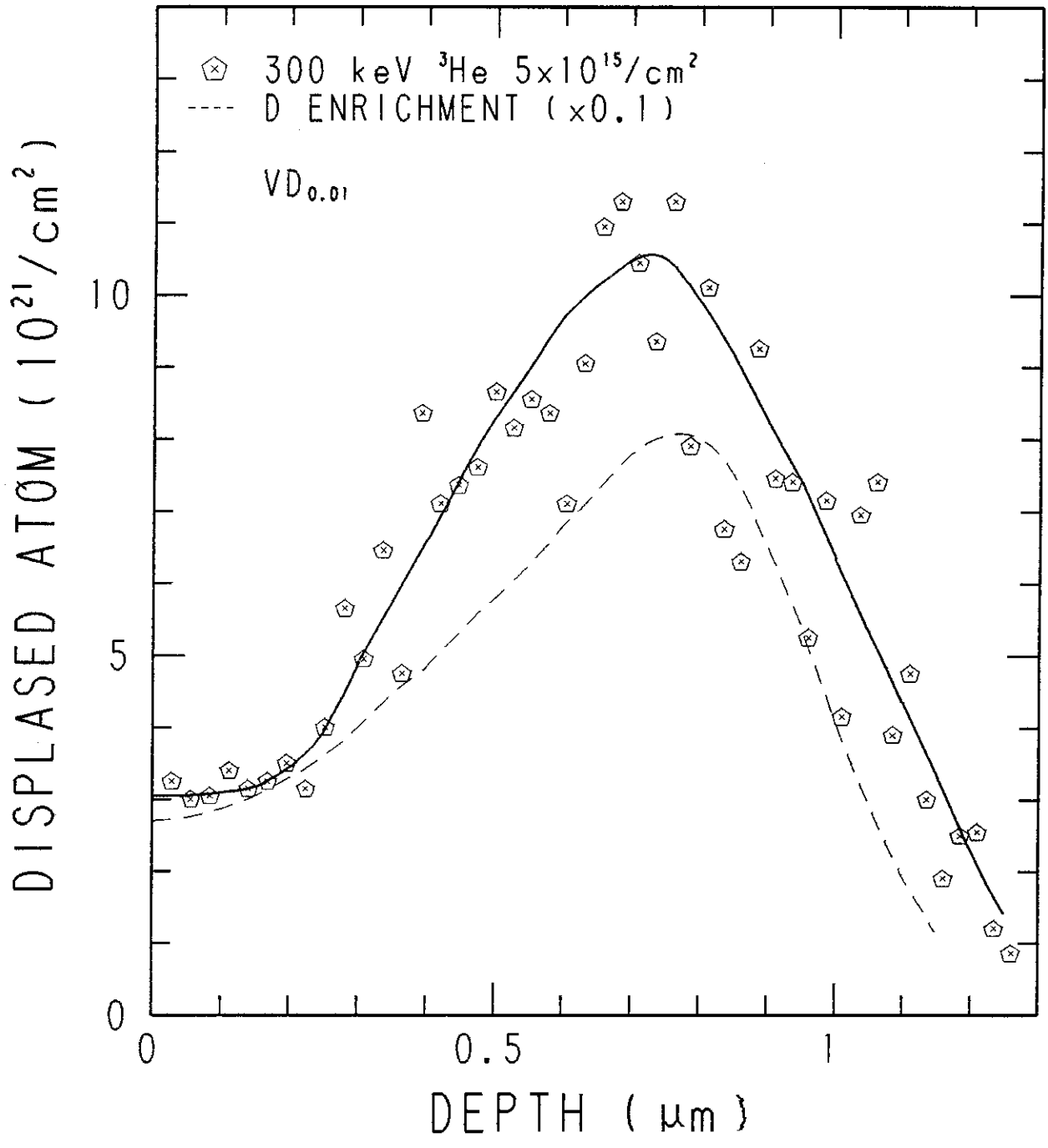

Fig. A-31 Distribution of displaced atoms and enrichment of deuterium concentration in $VD_{0.01}$ after bombardment of 5×10^{15} $^3He^+/cm^2$ at 300 keV. The ordinate scale for enrichment deuterium concentration should be reduced by a factor 0.1 of displacement atom. (ref. 75)

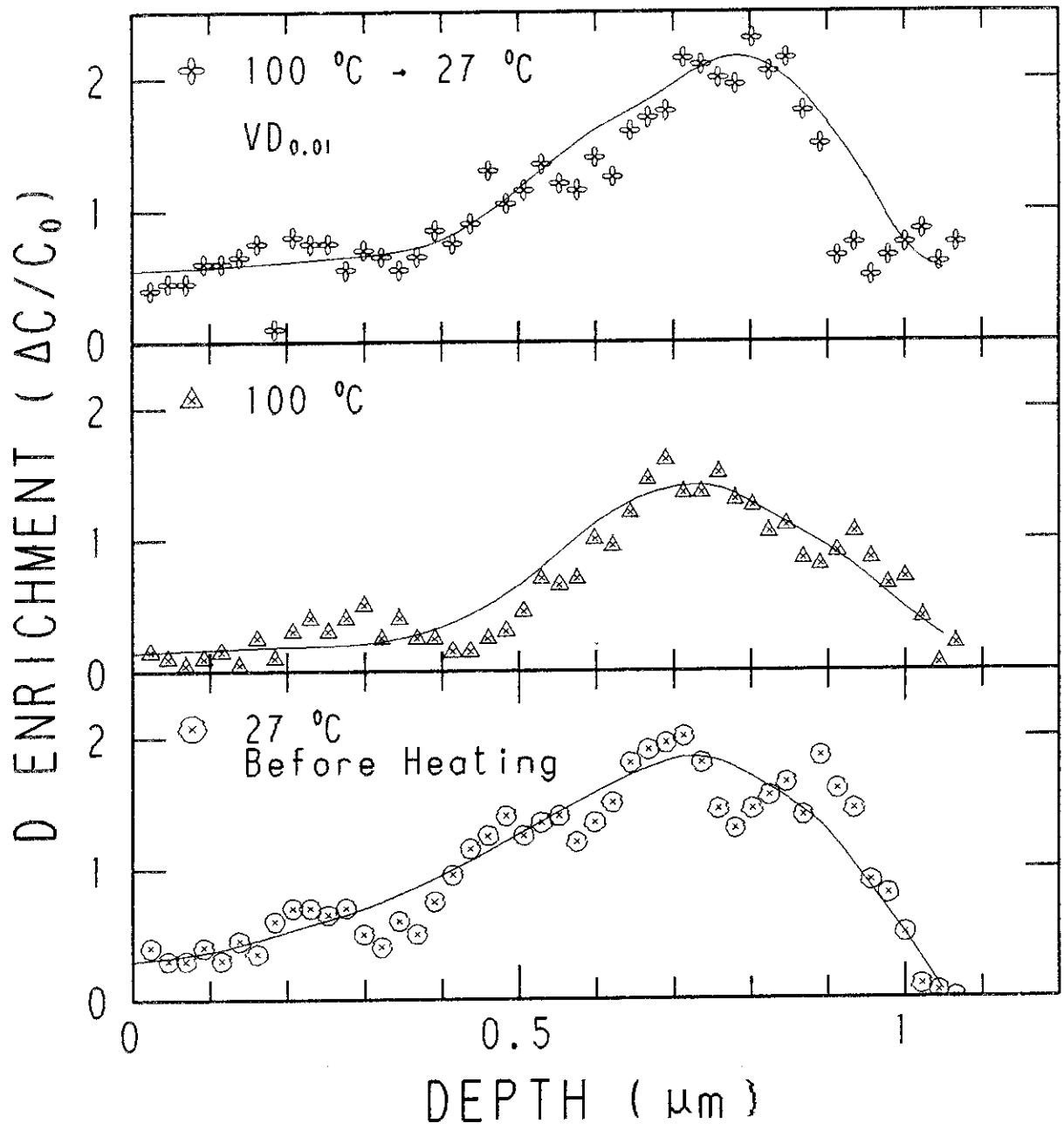

Fig. A-32 Temperature dependence of deuterium depth profiles in $VD_{0.01}$ after bombardment of 6×10^{15} $^3He^+/cm^2$ at 300 keV. (ref. 76)

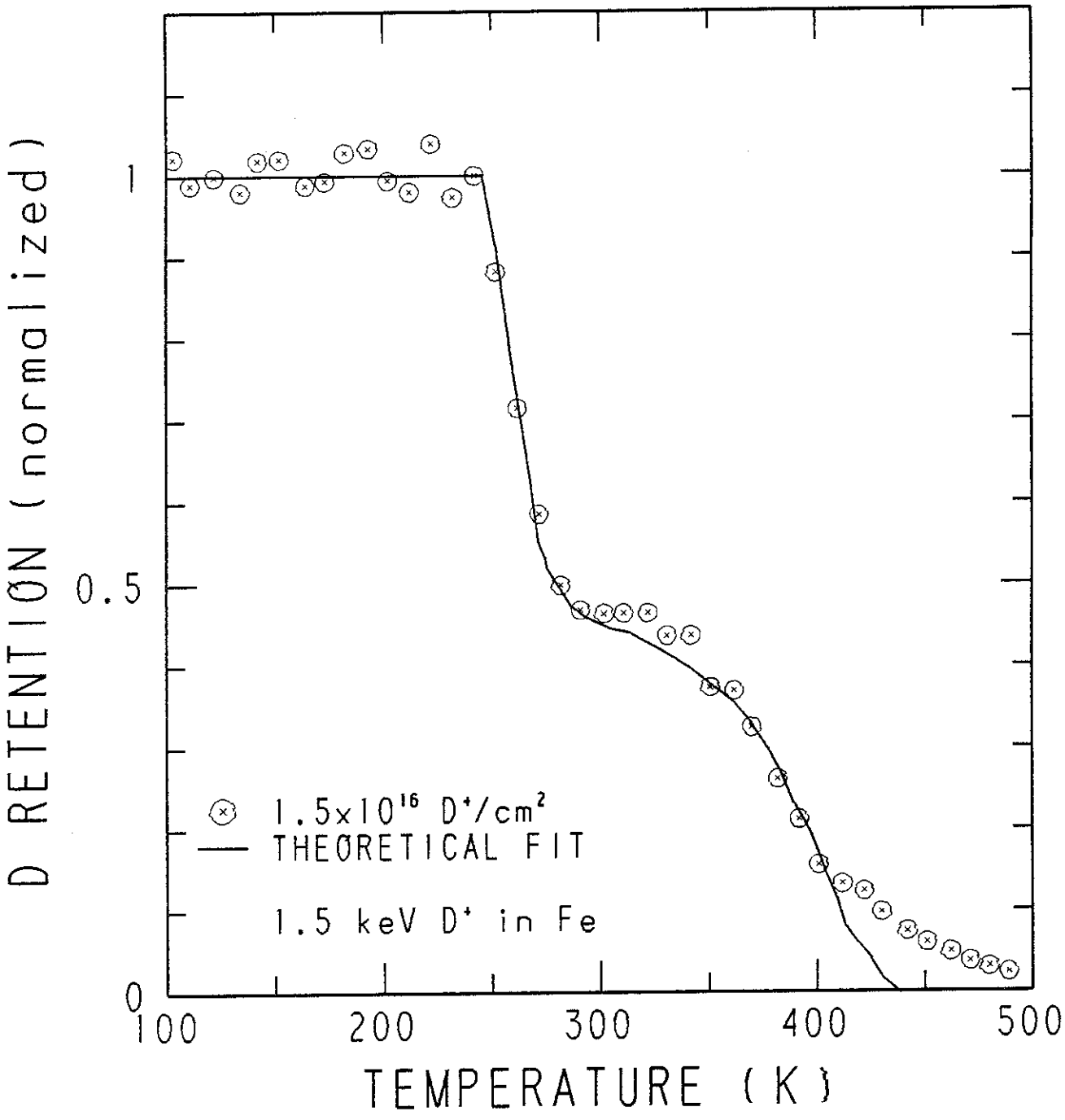

Fig. A-33 Deuterium release during linear ramping of temperature (2 K/min) from Fe implanted 1.5×10^{16} D^+/cm^2. (ref. 48)

A - VII Ion-Induced Release

As seen in Fig. A-22, a maximum hydrogen concentration (saturation) is reached even at low temperature where thermal detrapping is negligible. It is probable that this saturation is due to ion-induced release.

These effects are most easily observed in isotope exchange measurement conducted at low temperatures where thermal diffusion is negligible. In this process, an incident ion desorbs an atom previously trapped in the solid lattice. Consequently, the deuterium retention is observed to decrease when the implanting ion is switched to proton as shown in Fig. A-34. Details of the mechanism are not properly understood, but in practice the probability of detrapping can be quite well described by a cross-section. Release cross sections for deuterium as a function of incident proton energy are shown in Fig. A-36, those are evaluated from release rate measurements as shown in Fig. A-35 assuming the exponential decay. The variation of cross section with energy at 77 K is similar to that obtained at room temperature, but the absolute values are about an order magnitude lower. For low-temperature situation, thermal migration is suppressed and the detrapping may be related to the replacement of implanted atoms by later arrivals; in the higher temperature ($\sim$300 K), both replacement and thermal diffusion will be operative.

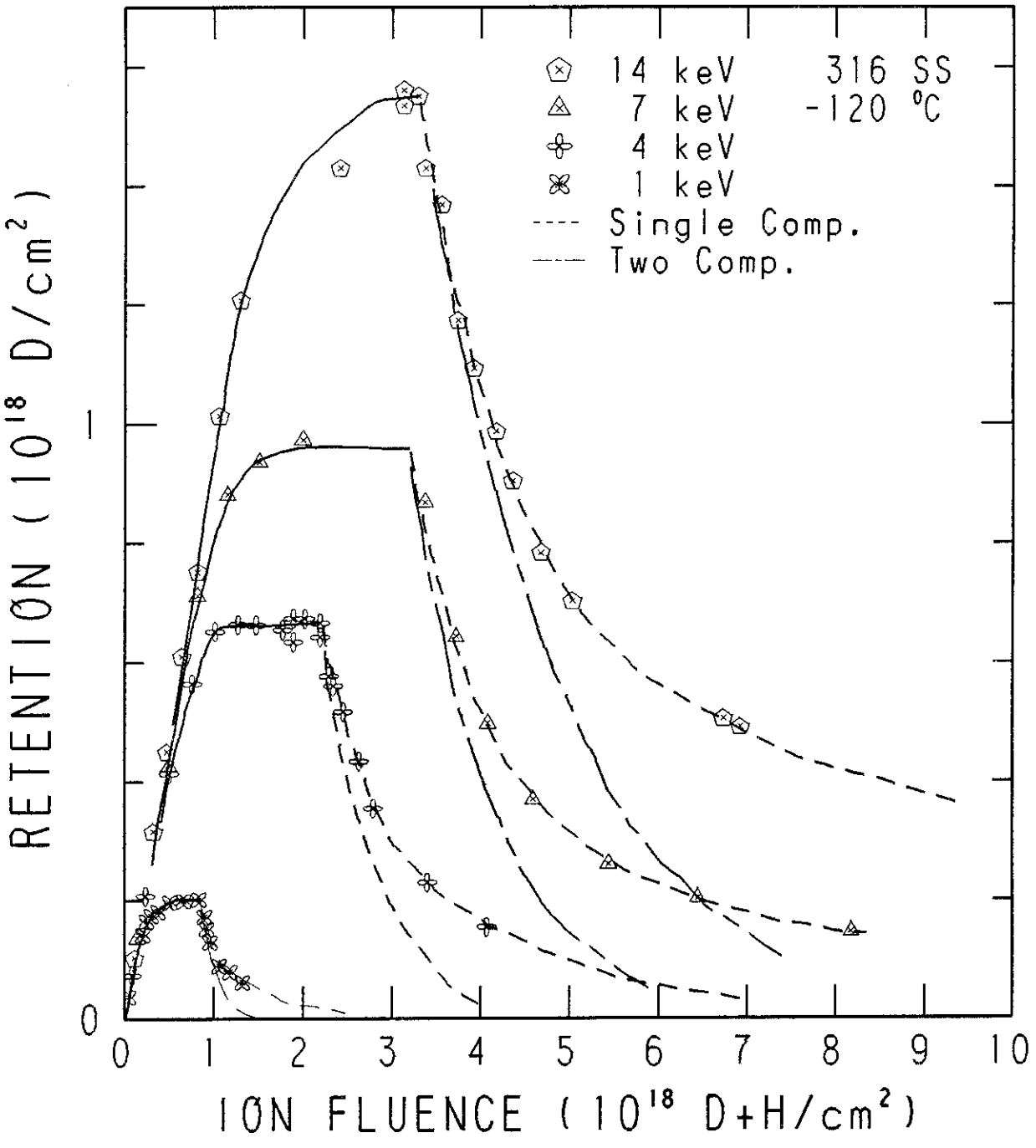

Fig. A-34 Trapping and replacement behavior of deuterium implanted 316 SS at 150 K as a function of fluence. The thin dashed lines in the linear portion of the trapping curves represent 100 % trapping after kinematic reflection is taken into account. The break in the 7 keV curve at saturation corresponds to an additional fluence of 2×10^{18} D^+/cm^2. (ref. 34)

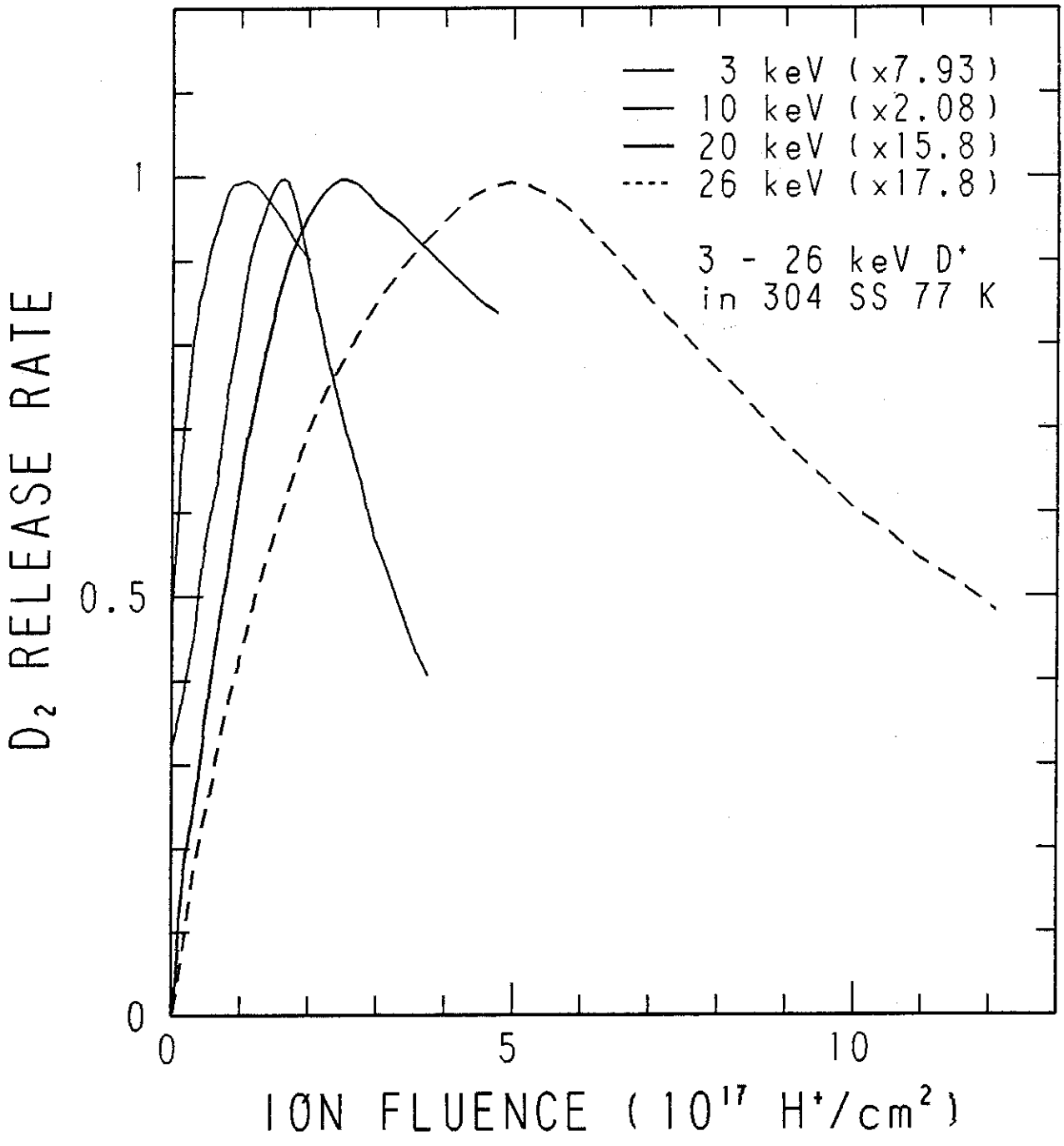

Fig. A-35 Release of D_2 from 304 SS during bombardment by protons after prior implantation with deuterons. The energy of protons and deuterons used was the same for each run and target temperature was 77 K. Incident proton current densities for 3, 10, 20 and 26 keV were 9.66×10^{13}, 2.74×10^{14}, 2.2×10^{14} and 4.58×10^{14} $H^+/cm^2 \cdot s$, respectively. The yields have been normalized to 1 atom/ion at the maximum yield. (ref. 33)

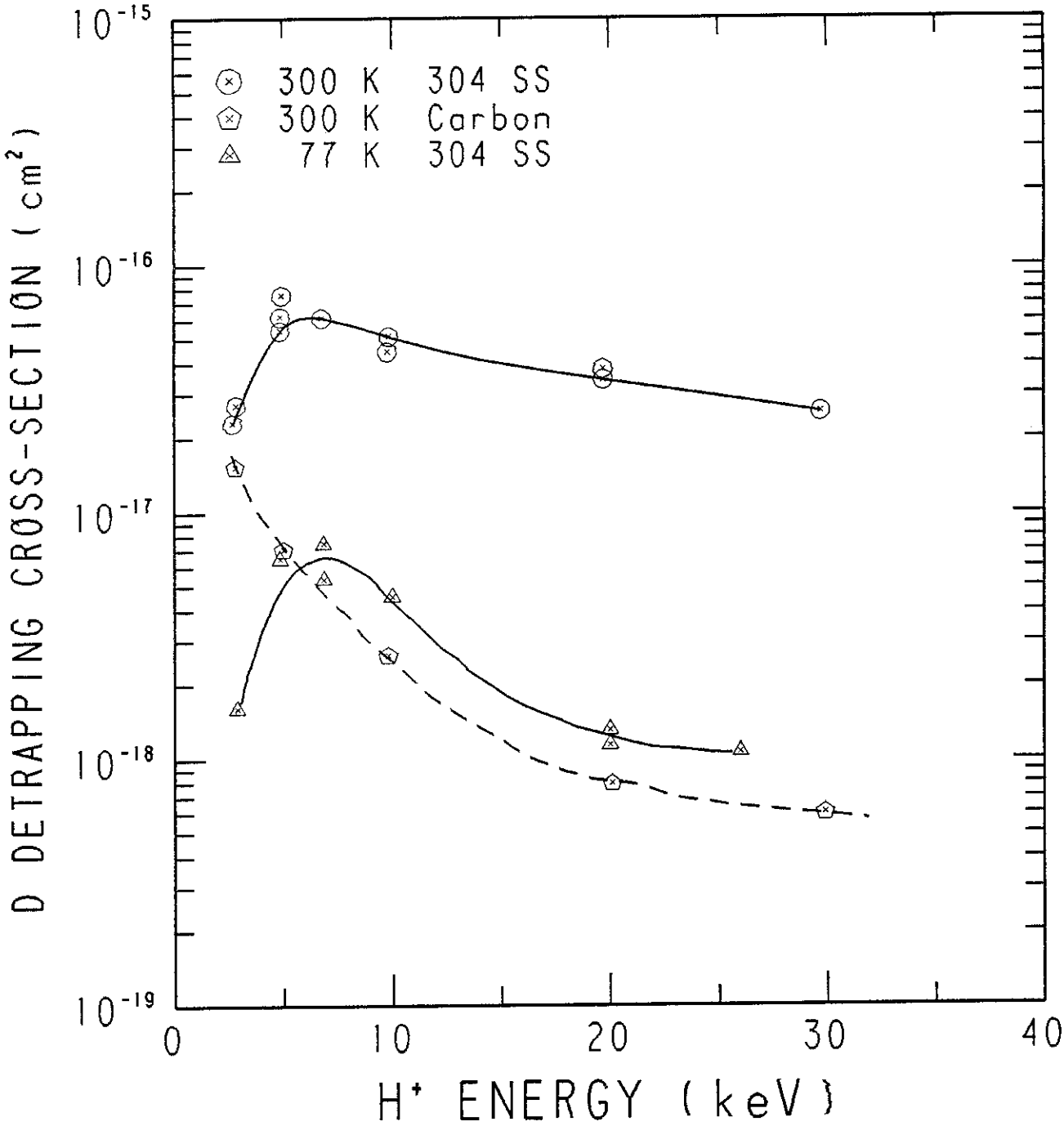

Fig. A-36 Cross section for the release of deuterium from 304 SS at 300 and 77°K by incident protons as a function of incident energy. (ref. 33)

3. SECTION B: HELIUM

B - I Target Temperature Dependence

Helium re-emission after high-energy helium implantation at various temperatures has been studied in a wide variety of metals such as aluminum (Figs. B-1, B-2), SAP (Fig. B-3), molybdenum (Fig. B-4), 316 SS (Fig. B-5), vanadium (Fig. B-6) and niobium (Fig. B-7). From these experiments a basic pattern of behavior has emerged. Three distinct temperature dependent modes of the helium release are exhibited.

At a very low temperature ($\sim$0.1 T_m, where T_m is melting temperature), the re-emission data show a period of high gas retention until a critical dose ($10^{17}\sim10^{18}$ ions/cm^2) was achieved, followed by a steady rise in the re-emission rate. The intermediate temperature regime (0.2 $\sim$ 0.4 T_m) was characterized by sudden bursts of helium. At high temperature (>0.5 T_m) the third type of gas re-emission is found. The helium release becomes a steady and smooth curve and approaches more rapidly to a steady-state release rate compared to the low temperature release. The period of high gas retention shows a dependence on material and temperature.

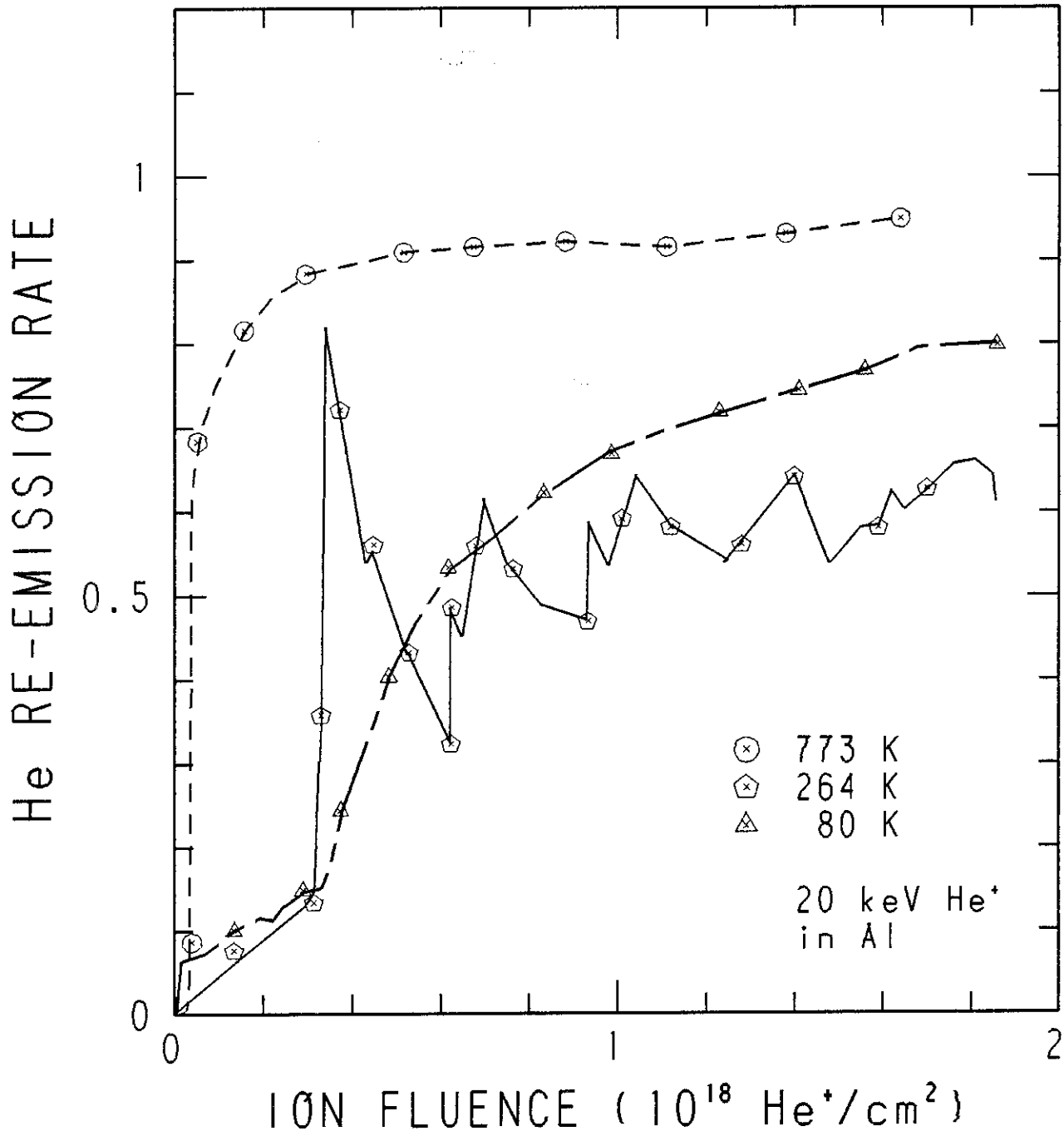

Fig. B-1 The re-emission rate (percent of incident flux) as a function of fluence for annealed Al implanted with 20 keV He^+ at 6.2×10^{14} $He^+/cm^2 \cdot sec$. The data for three implantation temperatures are shown. (ref. 26)

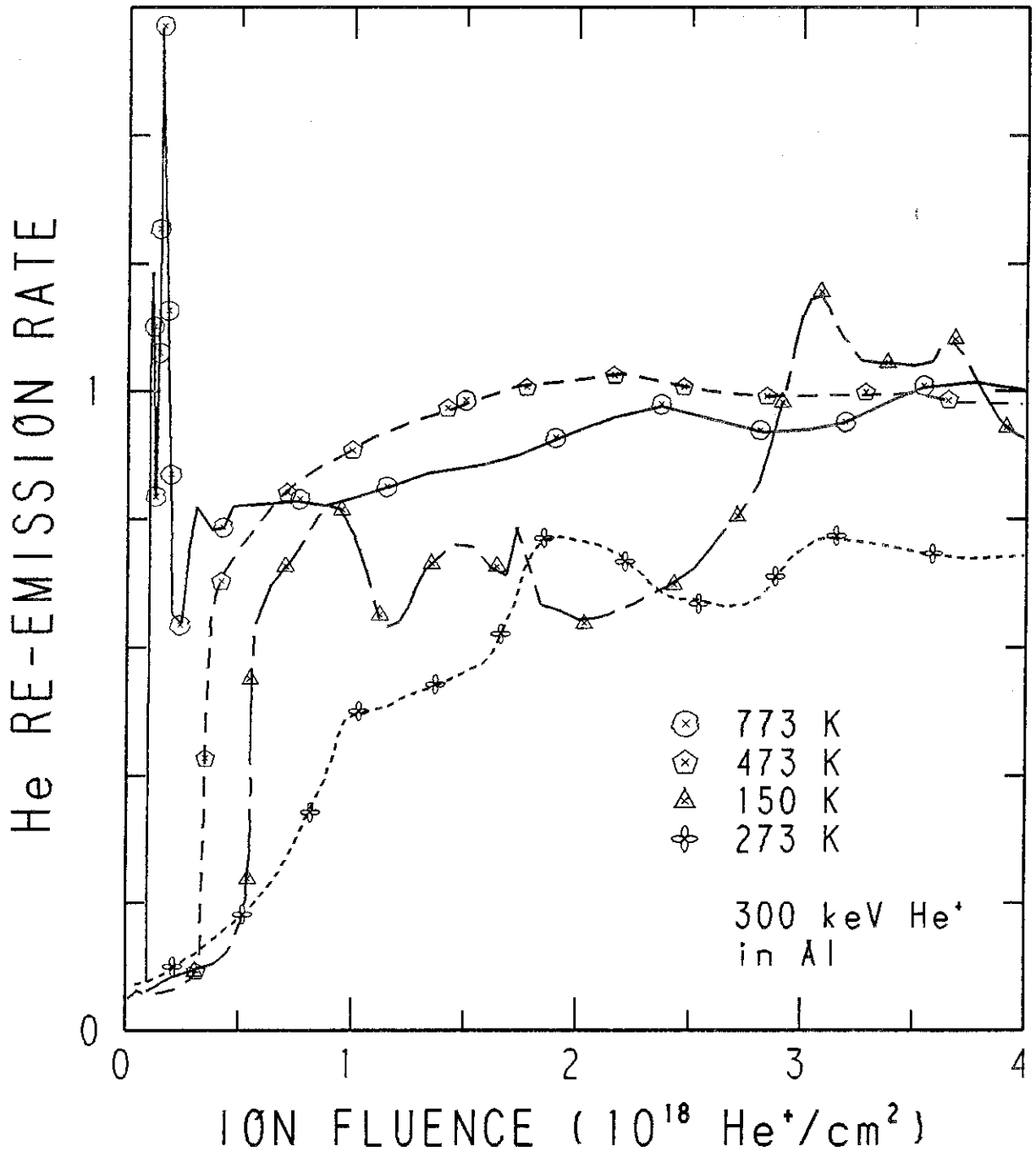

Fig. B-2 Helium re-emission during 300 keV He^+ implantation of Al as a function of fluence at four different implantation temperatures. (ref. 15)

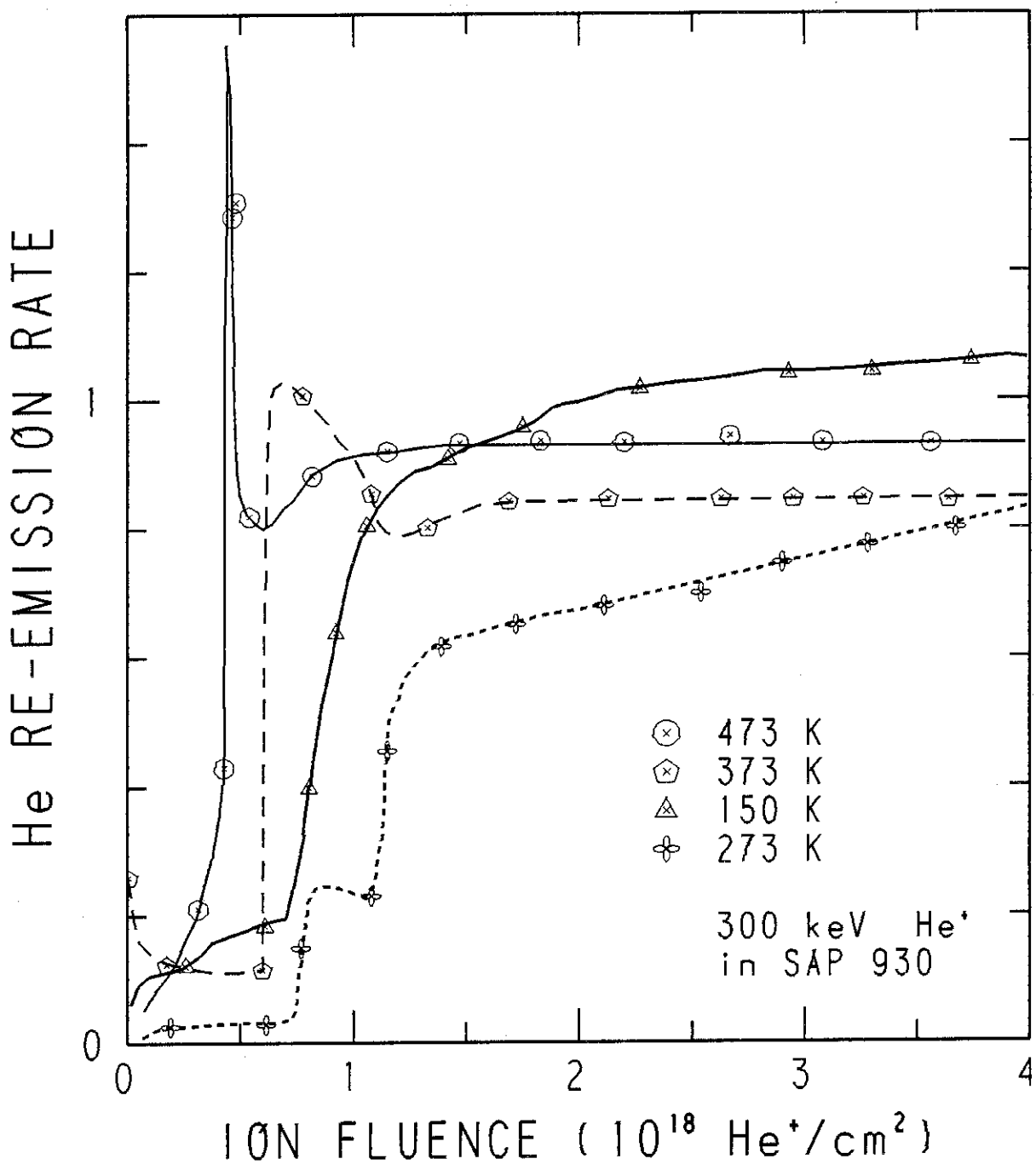

Fig. B-3 Helium re-emission during 300 keV He^+ implantation of SAP as a function of fluence at four different temperatures. (ref. 15)

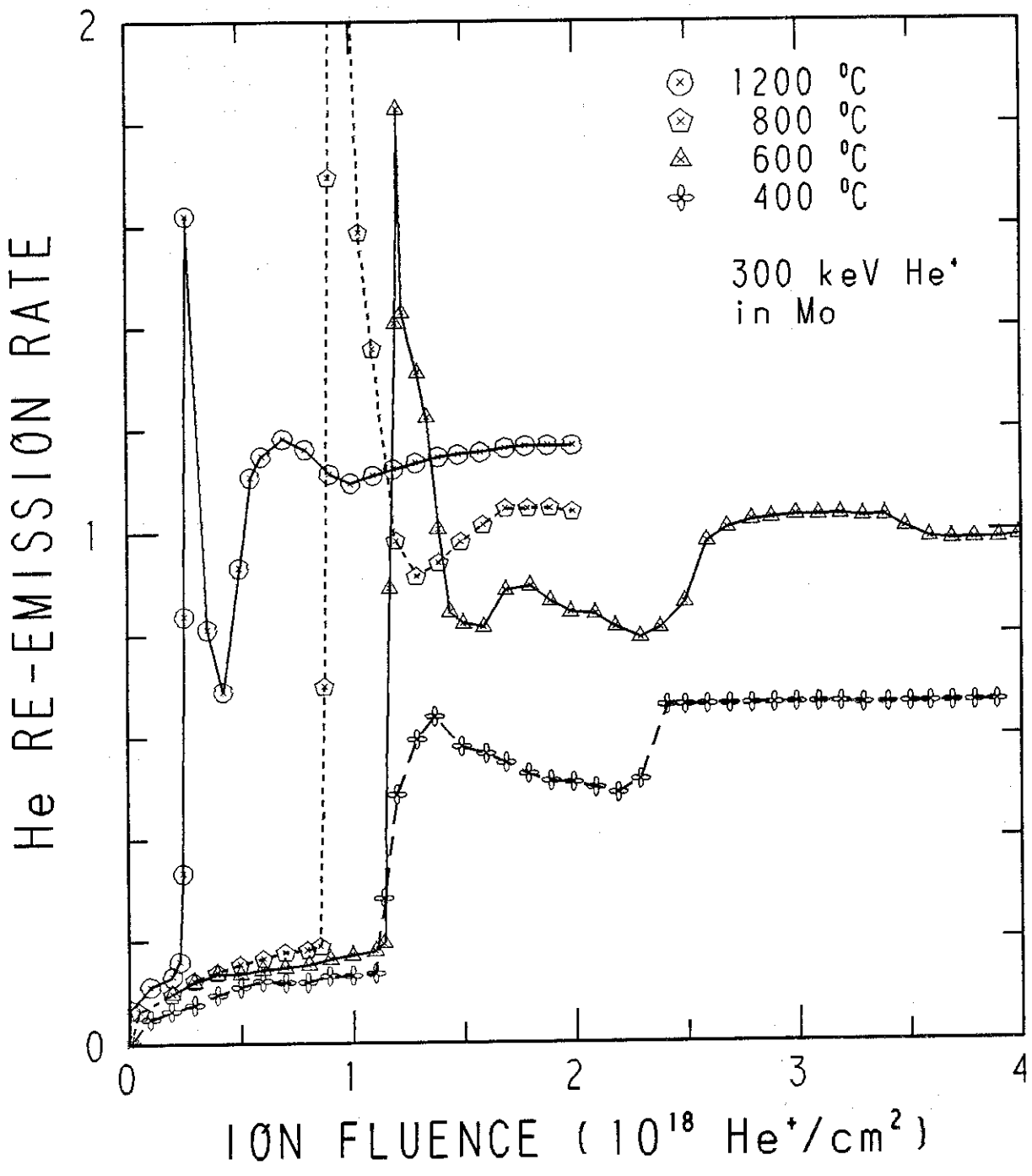

Fig. B-4 Helium re-emission during 300 keV He^+ implantation as a function of fluence at four different implantation temperatures in Mo. (ref. 9)

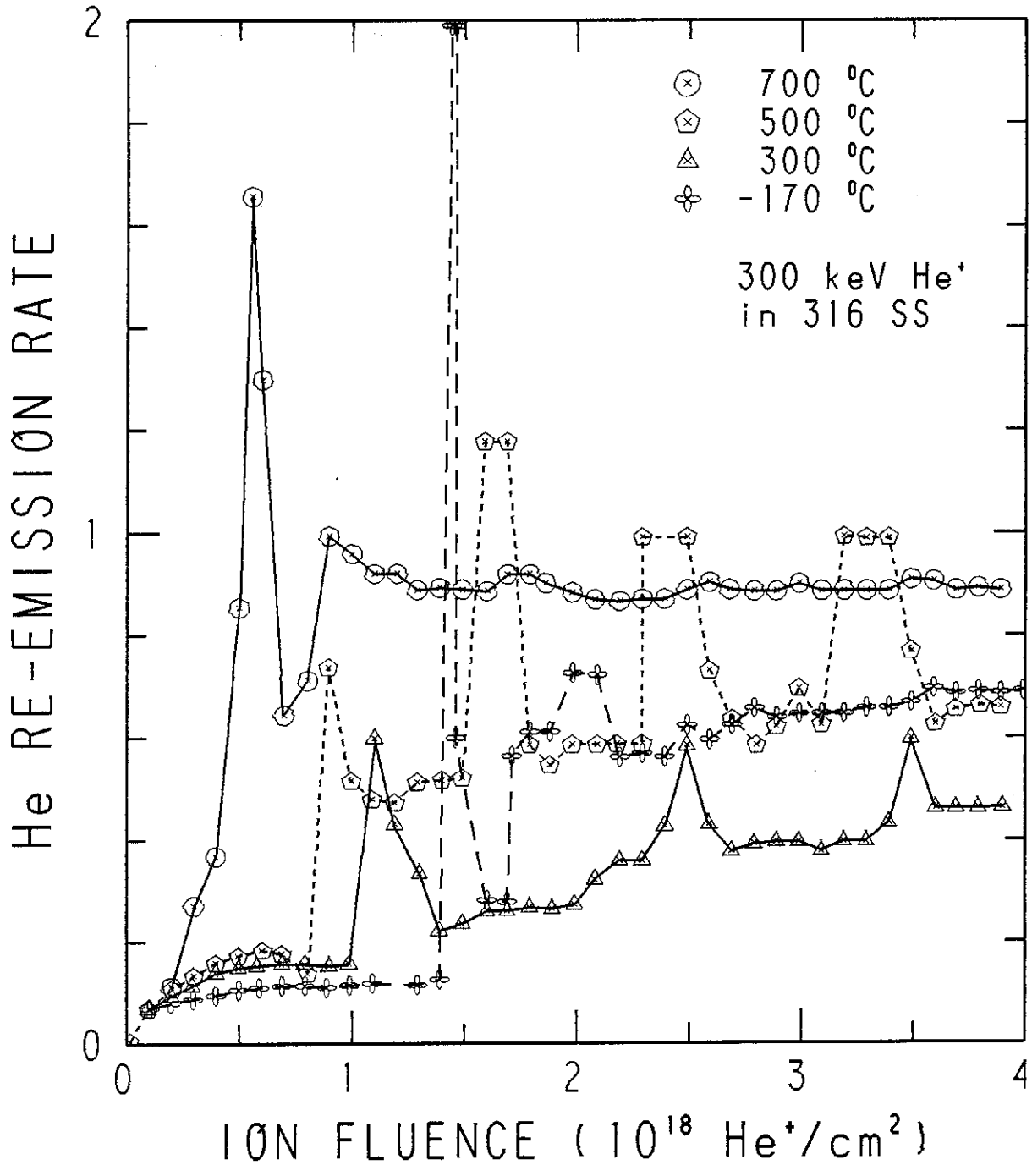

Fig. B-5 Helium re-emission during 300 keV He^+ implantation as a function of fluence in 316 SS at four different implantation temperatures. (ref. 7)

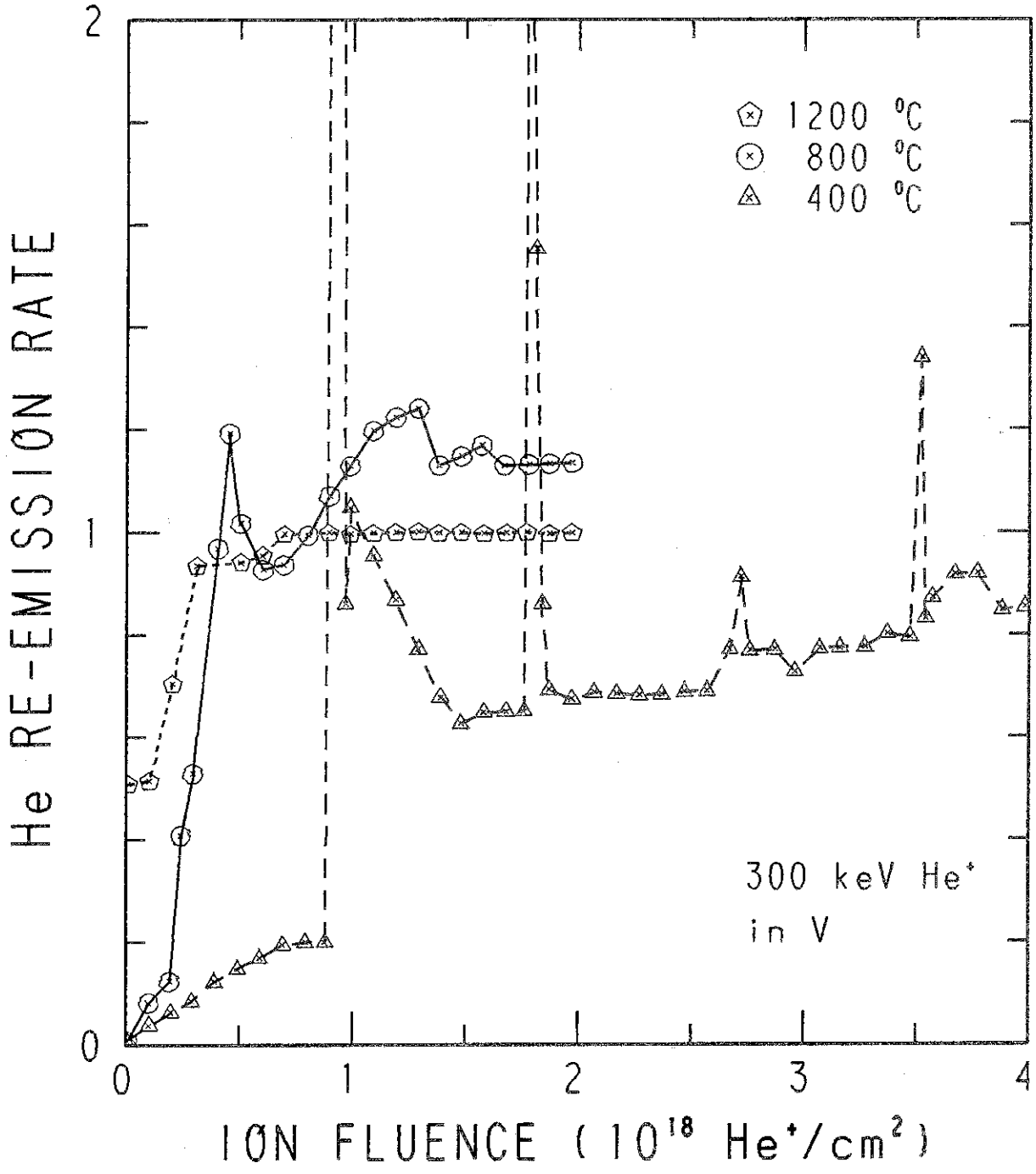

Fig. B-6 Helium re-emission during 300 keV He^+ implantation as a function of fluence in V at three different temperatures. (ref. 9, 11)

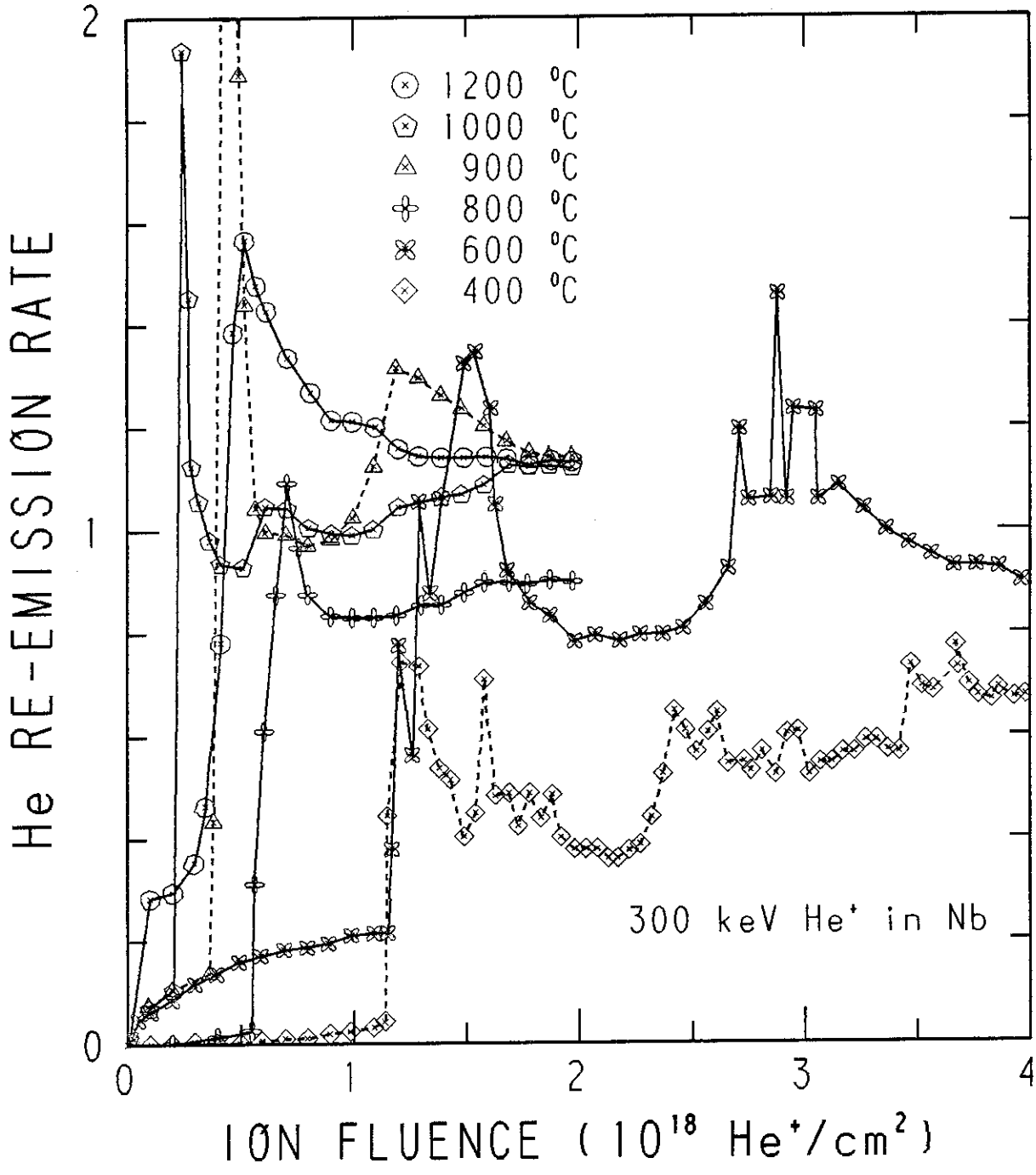

Fig. B-7 Helium re-emission during 300 keV He^+ implantation as a function of fluence in Nb at six different temperatures. (ref. 11)

B - II Incident Energy Dependence

In Fig. B-8, the amount of trapped helium is shown as a function of bombardment dose at different incident energy. At very low doses the trapping efficiency is close to unity. As the dose received by the surface is increased the target becomes saturated and eventually the retention becomes constant. The saturation concentration decreases with decreasing of incident energy, similar to that for hydrogen.

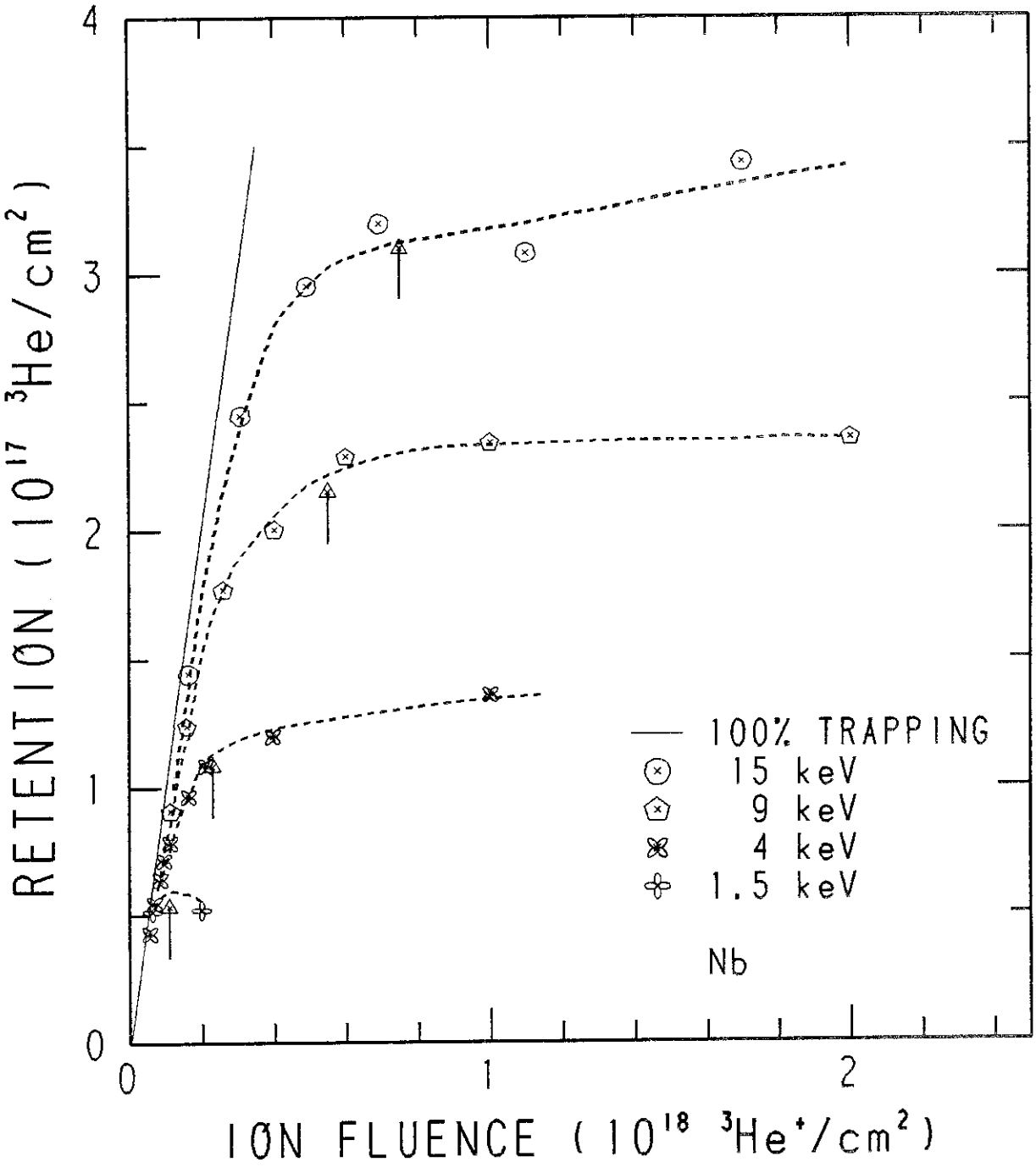

Fig. B-8 Trapping of $^{3}He^{+}$ ions in a Nb single crystal for different energies implanted to different fluences in a random direction. The ↑ marks give the critical doses for blistering as measured with ^{4}He at the same energy. (ref. 13)

B - III Microstructure Dependence

Helium re-emission in the intermediate temperature regime (270 ∿ 400 K) is strongly dependent on microstructure of the target. In Fig. B-9, He re-emission data from Al samples implanted under the same condition are shown; the re-emission of the annealed sample consists of a periodic series of He bursts with small re-emission between them.

That the trapping of helium depended strongly on the extent of lattice damage in the target has been shown by the observation of thermal desorption spectra. Two distinct regions of gas release being apparent in Fig. B-10 have been interpreted as being due to two types of trapping site related to the different helium defect configurations.

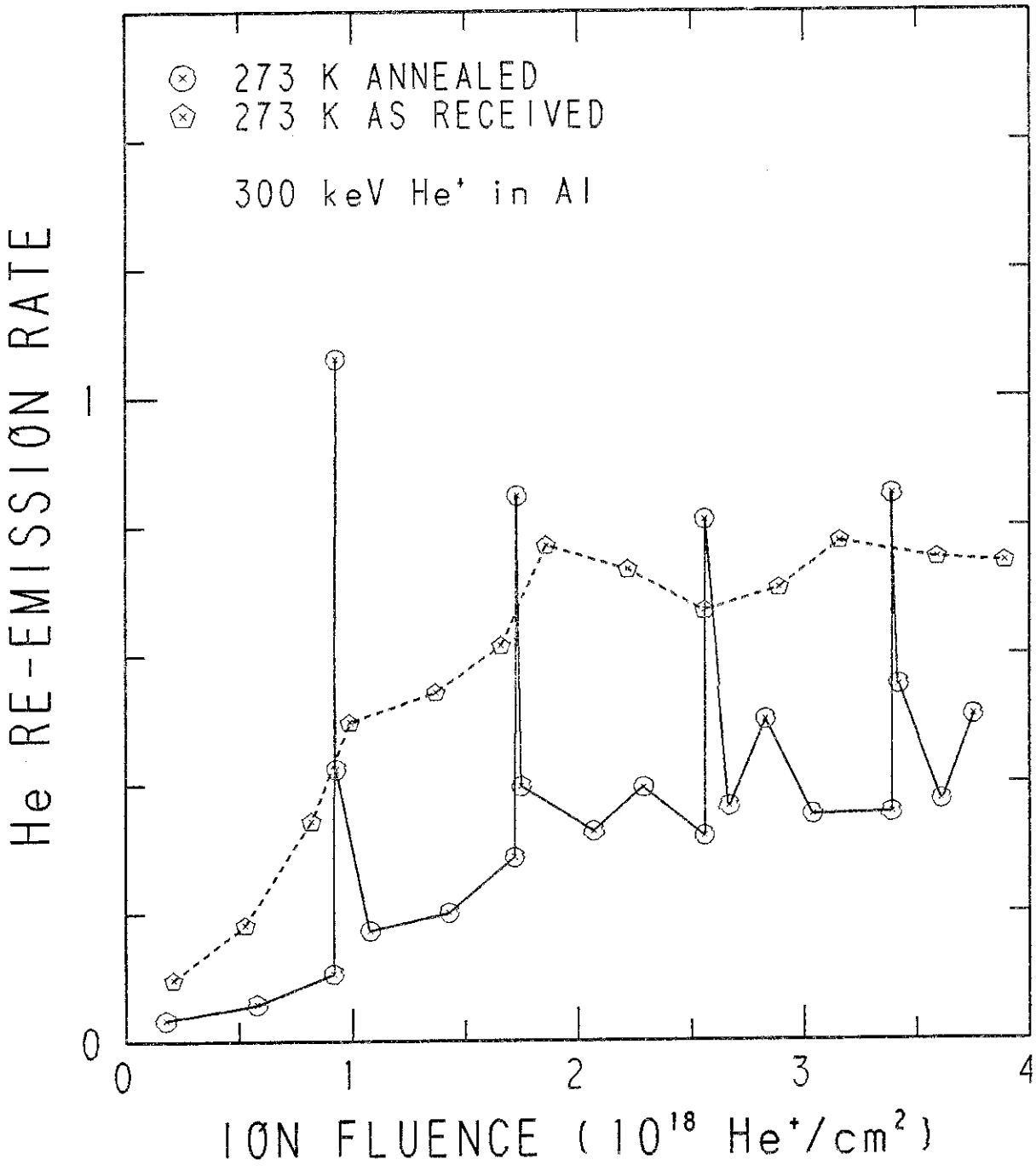

Fig. B-9 Helium re-emission during 300 keV He^+ implantation of annealed and as-received Al as a function of fluence at 273 K. (ref. 15)

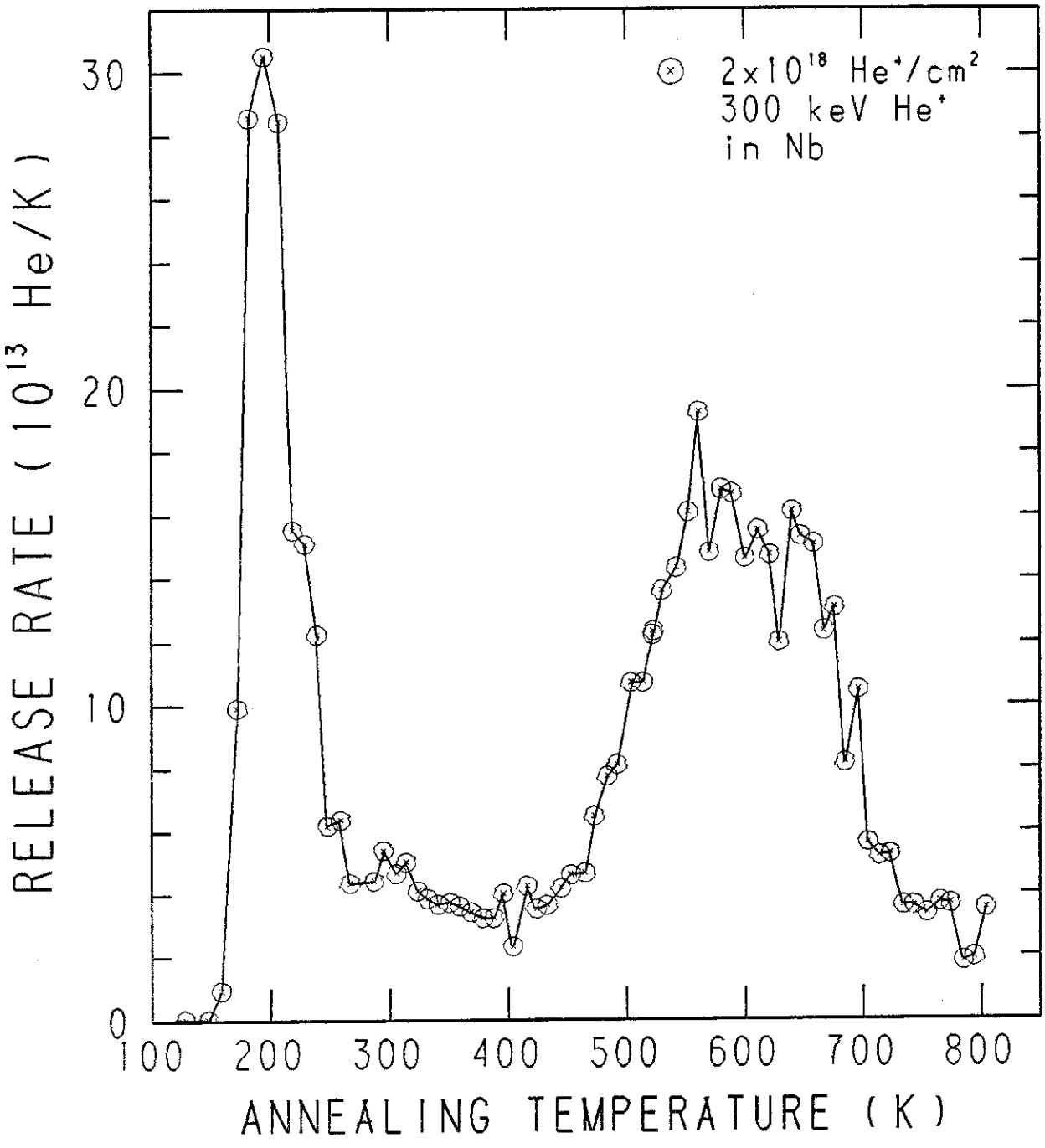

Fig. B-10 Helium release rate in Nb for a linear heat-up rate (∿10 K/min) after implantation near 173 K to a dose of 2×10^{18} He^{+}/cm^{2}. (ref. 5)

4. Table of Trapping and Re-emission Data

Specimens (Temp.)	Projectiles Species	Energies	Techniques	Remarks	Ref.
SS, Ti (173 - 740 K)	D^+	60 keV	GR	Dose and Target Temperature Dependences	1)
Mo, Ti, Ta, Zr (300 - 2000 K)	H^+, D^+	3 - 30 keV	GR, TDS	Ion Dose and Energy Dependences	2)
Ni (77 - 570 K)	D^+	18 keV	GR, TDS	Dose Dependence, Damage Effects	3)
Ni (77 - 900 K)	D^+	18 keV	GR, TDS	Damage Effects	4)
Nb (100 - 973 K)	He^+	300 keV	GR, TDS	Target Temperature and Microstructure Dependences	5)
W (300 - 2400 K)	He^+	250 keV	GR	Damage Effects	6)
316 SS (100 - 973 K)	He^+	300 keV	GR	Target Temperature Dependence, Blister Formation	7)
Mo (600 - 2000 K)	He^+	7 - 80 keV	GR	Ion Dose Dependence, Blister Formation	8)
Mo, V, 316 SS (100 - 1473 K)	He^+ ‡ H^+	300 keV 150 keV	GR	Target Temperature Dependence	9)
Mo (RT - 750 K)	D^+	5 - 35 keV	GR, TDS	Target Temperature Dependence, Damage Effects	10)
V, Nb (673 - 1473 K)	He^+	300 keV	GR	Target Temperature Dependence, Blister Formation	11)
Nb, Pd	He^+	10 - 300 keV	Theory	Re-emission Rate as a Function of Dose, Ion Energy Dependence	12)
Nb (RT)	$^3He^+$	1.5 - 15 keV	NRA	Ion Energy Dependence, Depth Profiling	13)

Specimens (Temp.)	Projectiles Species	Energies	Techniques	Remarks	Ref.
C (300 - 800 K)	D^+	6 - 15 keV	NRA	Ion Energy Dependence, Depth Profiling	14)
Al, SAP 930 (150 - 773 K)	He^+	300 keV	GR	Target Temperature and Microstructure Dependences, Blistering	15)
Ti (RT - 523 K)	H^+	0.3 - 8 keV	Weight Change	Ion Energy Dependence	16)
Zr (423 K)	D^+	0.3 - 6 keV	Weight Change	Ion Energy Dependence	17)
Mo (250 K)	D_2^+	100 eV - 2 keV	GR, TDS	Ion Dose and Energy Dependences	18)
Al (33 - 350 K)	H^+, D^+	5 - 10 keV	NRA	Target Temperature Dependence, Depth Profiling	19)
C (300 - 1900 K)	H^+, D^+	1 - 5 keV	Weight Change	Ion Energy Dependence	20)
C, SiC (293 - 1973 K)	D^+	20 keV	GR, TDS	Target Temperature Dependence	21)
Si (RT - 1073 K)	H^+, He^+	150 - 300 keV	GR	Ion Dose Dependence, Damage Effects	22)
Nb (293 - 723 K)	D^+	8 - 16 keV	NRA	Damage Effects, Depth Profiling	23)
Mo (RT)	H^+	8 keV	NRA	Damage Effects, Depth Profiling	24)
Nb (293 - 1273 K)	$^3He^+$	9 - 15 keV	NRA	Target Temperature Dependence, Depth Profiling	25)
Al (353 - 958 K)	He^+	20 keV	GR	Target Temperature Dependence, Blister Formation	26)

Specimens (Temp.)	Projectiles Species	Energies	Techniques	Remarks	Ref.
316 SS, 302 SS (100 - 605 K)	H^+	20 keV	TDS	Target Temperature and Microstructure Dependences	27)
Mo, Nb (RT)	H^+, D^+	8 keV	NRA	Damage Effects, Depth Profiling	28)
Nb, Zr, Ti, Pd (230 - 1000 K)	D^+	18 keV	GR	Target Temperature Dependence	29)
316 SS (RT)	D^+	7 keV	NRA	Time Dependence, Depth Profiling	30)
316 SS (153 - 313 K)	D^+	7 keV	NRA	Ion Dose and Temperature Dependences, Depth Profiling	31)
C (300 - 1050 K)	D^+ H^+	5 - 30 keV	GR, TDS	Radiation Induced Release, Methane Production	32)
304 SS (77 - 1000 K)	H^+, D^+	5 - 30 keV	GR	Ion Energy Dependence, Ion-Induced Release	33)
316 SS (150 K)	H^+, D^+	1 - 14 keV	NRA	Ion-Induced Release	34)
314 SS, 304 SS (RT - 1200 K)	D^+	15 - 750 eV	TDS	Ion Dose and Energy Dependences	35)
V, Nb, Ta, Ti, Zr, Li	Hydrogen Isotopes		Theory	Ion Dose and Temperature Dependences	36)
Graphite (RT - 1223 K)	D^+, He^+	8 keV	TDA, RBS	Ion Dose and Temperature Dependences	37)
Al, Mg (30 - 300 K)	H^+, D^+	5 - 20 keV	NRA	Damage Effects, Depth Profiling	38)
Zr (50 - 500 K)	D^+	10 - 30 keV	NRA	Target Temperature Dependence, Depth Profiling	39)

Specimens (Temp.)	Projectiles Species	Energies	Techniques	Remarks	Ref.
Nb (RT)	$^3He^+$, $^4He^+$	30 - 50 keV	NRA	Ion-Induced Release, Ion Energy Dependence	40)
316 SS 90 - 600 K)	D^+	0.33 - 1 keV	TDS	Ion Dose and Microstructure Dependences	41)
316 SS (297 - 700 K)	D^+	1 - 10 keV	TDS	Ion-Induced Release, Depth Profiling	42)
Ni, Cu, Ag, Au, Pt, Be, Zr, Fe, Nb, Mo (273 - 1473 K)	$^3He^+$	0.2 - 340 keV	NRA	Depth Profiling, Ion Energy and Temperature Dependences	43)
C, Si (RT)	D^+	20 - 7000 eV	Theory	Incident Energy Dependence, Depth Profiling	44)
TiB_2 (RT - 873 K)	H^+	60 - 210 keV	NRA	Damage Effects, Depth Profiling	45)
Be (RT)	D_2^+, He^+	5 keV	IBA	Dose Dependence, Depth Profiling Radiation Enhanced Oxidation	46)
316 SS, Ti (RT)	D^+, T^+	60 - 200 eV	Theory	Retained Hydrogen Concentration	47)
Fe (70 - 500 K)	D^+	15 keV	NRA	Damage Effects, Depth Profiling	48)
Ti, Ti-6Al, Ti-6Al-4V (RT - 423 K)	D^+	3.3 keV	NRA, SIMS	Depth Profiling, Time and Temperature Dependences	49)
BeO, Al_2O_3 (140 - 470 K)	D^+	5 keV	NRA	Ion Induced Release	50)
C, Si (RT)	D^+	50 - 1000 eV	NRA, GR, TDS	Incident Energy Dependence	51)
Si, C (RT)	H^+, D^+	40 eV - 400 keV	NRA, SIMS	Depth Profiling, Energy Dependence	52)

Specimens (Temp.)	Projectiles Species	Energies	Techniques	Remarks	Ref.
304 SS, Inconel 625 TZM, Ti-6Al-4V (RT - 423 K)	D^+	3.3 keV	GR, TDS, NRA	Target Temperature Dependence	53)
Ni (30 - 500 K)	D^+	10 keV	NRA	Damage Effects, Depth Profiling	54)
304 SS (295 - 375 K)	D^+	2 keV	TDS, NRA	Time and Temperature Dependences	55)
VB_2, TiC, TiB_2, B, 316 SS (153 K, RT)	D^+, H^+	1 - 14 keV	NRA, GR	Radiation Induced Release, Incident Energy Dependence	56)
TiC, TiB_2, VB_2, B_4C, B, Si, C (RT)	H^+, D^+	1.5 keV	NRA	Dose Dependence, Ion-Induced Release	57)
Graphite (RT)	H^+, D^+	1 keV	GR	Energy Dependence, Ion-Induced Release	58)
C (RT)	D^+	8 keV	Theory	Ion Dose Dependence, Damage Effects	59)
Al, Pt, BeO, Al_2O_3 (RT)	$^3He^+$, $^4He^+$	10 - 40 keV	GR	Energy and Incident angle Dependences	60)
SS (<150 K)	D^+, H^+	1 - 14 keV	Theory	Radiation Induced Release	61)
Graphite (295 - 900 K)	H^+	0.3 keV	GR	Dose and Temperature Dependences	62)
Ni, Pd, Mo, Ta (33 - 38 K)	D^+	10 keV	NRA	Dose Dependence, Blistering	63)
Zr (70 - 500 K)	D^+	10 keV	NRA	Depth Profiling, Time and Temperature Dependences	64)

Specimens (Temp.)	Projectiles Species	Energies	Techniques	Remarks	Ref.
Inconel 600, Nimonic PE16, Hastelloy B, 316L SS (77, 300 K)	D^+	33, 36 keV	GR	Dose Dependence, Blistering	65)
TiC, 304 SS Graphite	D^+ $^3He^+$	0.5, 1.5 keV 3 keV	NRA	Depth profiling, Electron Beam Annealing, Temperature Dependence	66)
Ni, Be (300 - 975 K)	H^+ He^+	2 keV 4 keV	GR	Re-emission for various H/He Flux Ratio	67)
Ti (140 - 500 K)	D^+	6.7 keV	NRA	Depth Profiling, Temperature Dependence	68)
Graphite (RT)	D^+	1 - 8 keV	IBA (NRA,ERD,RBS)	Ion-Induced Release, Depth Profiling	69)
Mo (160 K)	D^+ $^3He^+$	4 - 8 keV 4 - 16 keV	NRA	Ion-Induced Release, Depth Profiling	70)
Mo (160 K)	D^+ $^3He^+$	8 keV 4 keV	NRA	Ion-Induced Release, Depth Profiling	71)
304 SS (90 - 500 K)	D^+	0.125 - 1 keV	GR, TDS	Energy and Temperature Dependences, Ion-Induced Release	72)
C (RT)	H^+, D^+	10 - 30 keV	GR	Ion Energy Dependence, Ion-Induced Release	73)
Ti, TiB_2, TiC (375 - 775 K)	D^+	3.3 keV	GR, TDS, NRA	Temperature Dependence, Depth Profiling	74)
V (RT - 373 K)	$^3He^+$	300 - 750 keV	NRA	Damage Effects, Depth Profiling	75)
V, Nb, Ta (RT - 373 K)	$^3He^+$	250 - 730 keV	NRA	Damage Effects, Depth Profiling, Temperature Dependence	76)

References

1) Freeman, N.J., Latimer, I.D. and Daly, N.R.: "Burial of 60 keV deuterium ions in stainless steel and titanium", Nature, 212, 1346 (1966).

2) McCracken, G.M. and Maple, J.H.C.: "The trapping of hydrogen ions in molybdenum, titanium, tantalum and zirconium", Brit. J. Appl. Phys., 18, 919 (1967).

3) Erents, S.K. and McCracken, G.M.: "Trapping and re-emission of fast deuterium ions from nickel", Brit. J. Appl. Phys. (J. Phys. D), 2, 1397 (1969).

4) Erents, S.K. and McCracken, G.M.: "Trapping and re-emission of fast deuterium ions from nickel II", Radiat. Effects, 3, 123 (1970).

5) Bauer, W. and Morse, D.: "Helium implantation and re-emission from niobium at elevated temperatures", J. Nucl. Mater., 44, 337 (1972).

6) Kornelson, E.V.: "The interaction of injected helium with lattice defects in a tungsten crystal", Radiat. Effects, 13, 227 (1972).

7) Bauer, W. and Thomas, G.J.: "Helium re-emission and surface deformation in 316 stainless steel during -170°C to 700°C implantation", J. Nucl. Mater., 47, 241 (1973).

8) Erents, S.K. and McCracken, G.M.: "Blistering of molybdenum under helium ion bombardment", Radiat. Effects, 18, 191 (1973).

9) Bauer, W. and Thomas, G.J.: "Helium and hydrogen re-emission during implantation of molybdenum, vanadium and stainless steel", J. Nucl. Mater., 53, 127 (1974).

10) McCracken, G.J. and Erents, S.K.: "Radiation damage and gas diffusion in molybdenum under deuteron bombardment", Application of ion beam to metals. (Plenum, New York, 1974) P. 585.

11) Thomas, G.J. and Bauer, W.: "Helium implantation effects in vanadium and niobium", Application of ion beam to Metals. (Plenum, New York, 1974) P. 533.

12) Wilson, W.D., Bisson, C.L. and Amos, D.E.: "Particle re-emission during irradiation", J. Nucl. Mater., 53, 154 (1974).

13) Behrisch, R., Bøttiger, J., Eckstein, W., Roth, J. and Scherzer, B.M.U.: "Trapping of Low-energy helium ions in niobium", J. Nucl. Mater., 56, 365 (1975).

14) Scherzer, B.M.U., Behrisch, R., Eckstein, W., Littmark, U., Roth, J. and Sinha, M.K.: "Temperature dependence of trapping and depth profiles of 6 to 15 keV deuterium in carbon", J. Nucl. Mater., 63, 100 (1976).

15) Bauer, W. and Thomas, G.J.: "Helium implantation effects in SAP and aluminum", J. Nucl. Mater., 63, 299 (1976).

16) Bohdansky, J., Roth, J., Sinha, M.K. and Ottenberger, W.: "Trapping coefficients of energetic hydrogen (0.3 - 8 keV) in Ti at high doses", J. Nucl. Mater., 63, 115 (1976).

17) Bohdansky, J., Roth, J., and Poschenrieder, W.P.: "The trapping of hydrogen ions in zirconium for ion energies between 0.3 and 6 keV", Applications of Ion Beams to Materials. (The Institute of Physics, London, 1976) P. 307.

18) Bragnza, C., Carter, G. and Farrell, G.: "Backscattering, trapping and post-bombardment thermal release of 100 eV to 2 KeV D_2^+ ions at a Mo surface", Nucl. Instrum. Methods, 132, 679 (1976).

19) Bugeat, J.P., Chami, A.C. and Ligeon, E.: "A study of hydrogen implanted in alminium", Phys. Lett., 58A, 127 (1976).

20) Erents, S.K., Braganza, C.M. and McCracken, G.M.: "Methane formation during the interaction of energetic proton and deuterons with carbon", J. Nucl. Mater., 63, 399 (1976).

21) Erents, S.K.: "Gas release from low-Z materials under hydrogen bombardment", Application of Ion Beams to Materials. (The Institute of Physics, London, 1976) P. 318.

22) Mattern, P.L., Thomas, G.J. and Bauer, W.: "Hydrogen and helium implantation in vitreous silica", J. Vac. Sci. Technol., 13, 430 (1976).

23) Picraux, S.T., Bøttiger, J. and Rud, N.: "Enhanced hydrogen trapping due to He ion damage", J. Nucl. Mater. 63, 110 (1976).

24) Picraux, S.T., Bøttiger, J. and Rud, N.: "Profile studies of hydrogen trapping in metals due to ion damage", Appl. Phys. Lett., 28, 179 (1976).

25) Roth, J., Picraux, S.T., Eckstein, W., Bøttiger, J. and Behrisch, R.: "Temperature dependence of He trapping in niobium", J. Nucl. Mater., 63, 120 (1976).

26) Wilson, K.L. and Thomas, G.J.: "Low-energy helium implantation of aluminum", J. Nucl. Mater., 63, 266 (1976).

27) Wilson, K.L., Thomas, G.J. and Bauer, W.: "Low energy proton implantation of stainless steel", Nucl. Technol., 29, 322 (1976).

28) Bøttiger, J., Picraux, S.T., Rud, N. and Laursen, T.: "Trapping of hydrogen isotopes in molybdenum and niobium predamaged by ion implantation", J. Appl. Phys., 48, 920 (1977).

29) Hotston, E.S. and McCracken, G.M.: "Trapping of energetic hydrogen ions in reactive metals", J. Nucl. Mater., 68, 277 (1977).

30) Altstetter, C.J., Behrisch, R., Bøttiger, J., Pohl, F. and Scherzer, B.M.U.: "Depth profiling of deuterium implanted into stainless steel at room temperature", Nucl. Instrum. Methods, 149, 59 (1978).

31) Altstetter, C.J., Behrisch, R. and Scherzer, B.M.U.: "Trapping of deuterium implanted into stainless steel at low temperatures", J. Vac. Sci. Technol., 15, 706 (1978).

32) Braganza, C.M., Erents, S.K. and McCracken, G.M.: "Interaction of 5 - 30 keV deuterons with a carbon surface", J. Nucl. Mater., 75, 220 (1978).

33) Braganza, C.M., Erents, S.K., Hotston, E.S. and McCracken, G.M.: "Ion-induced release of deuterium trapped in stainless steel", J. Nucl. Mater., 76 & 77, 298 (1978).

34) Blewer, R.S., Behrisch, R., Scherzer, B.M.U. and Schulz, R.: "Trapping and replacement of 1-14 keV hydrogen and deuterium in 316 stainless steel", J. Nucl. Mater., 76 & 77, 305 (1978).

35) Farrell, G. and Donnelly, S.E.: "Thermal desorption and bombardment-induced release of deuterium into stainless steels at low energy", J. Nucl. Mater., 76 & 77, 322 (1978).

36) Hotston, E.S.: "The choice of materials for divertor targets", J. Nucl. Mater., 76 & 77, 536 (1978).

37) Langley, R.A., Blewer, R.S. and Roth, J.: "Behavior of implanted D and He in pyrolytic graphite", J. Nucl. Mater., 76 & 77, 313 (1978).

38) Ligeon, E., Bugeat, J.P. and Chami, A.C.: "The use of hydrogen and deuterium implantation to investigate some aspects of defect-impurity interactions in metals", Nucl. Instrum. Methods, 149, 99 (1978).

39) Möller, W., Børgesen, P. and Bøttiger, J.: "Temperature dependent depth profiles of deuterons implanted into zirconium", J. Nucl. Mater., 76 & 77, 287 (1978).

40) Roth, J., Scherzer, B.M.U., Behrisch, R. and Børgesen, P.: "The replacement of ^{3}He implanted in Nb by subsequent ^{4}He bombardment and vice versa", Nucl. Instrum. Methods, 149, 53 (1978).

41) Wilson, K.L. and Baskes, M.I.: "Thermal desorption of deuterium implanted stainless steel", J. Nucl. Mater., 74, 179 (1978).

42) Wilson, K.L. and Baskes, M.I.: "Deuterium trapping in irradiated 316 stainless steel", J. Nucl. Mater., 76 & 77, 291 (1978).

43) Biersack, J.P., Fink, D., Henkelmann, R.A. and Müller, K.: "Range profiles and thermal release of helium implanted into various metals", J. Nucl. Mater., 85 & 86, 1165 (1979).

44) Cohen, S.A. and McCracken, G.M.: "A model for hydrogen isotope backscattering, trapping and depth profiles in carbon and amorphous silicon", J. Nucl. Mater., 84, 157 (1979).

45) Doyle, B.L. and Vook, F.L.: "Hydrogen trapping and re-emission in TiB_2 coating for Tokamaks upon thermal, pulsed electron and laser annealing", J. Nucl. Mater., 85 & 86, 1019 (1979).

46) Langley, R.A.: "Interaction of implanted deuterium and helium with berylliums: Radiation enhanced oxidation", J. Nucl. Mater., 85 & 86, 1123 (1979).

47) Look, G.W. and Baskes, M.I.: "Hydrogen profiles in TOKAMAK fission reactor first walls", J. Nucl. Mater., 85 & 86, 995 (1979).

48) Myers, S.M., Picraux, S.T. and Stoltz, R.E.: "Defect trapping of ion-implanted deuterium in Fe", J. Appl. Phys., 50, 5710 (1979).

49) Pontau, A.E., Haggmark, L.G., Wilson, K.L., Bastasz, R., Malinowski, M.E., Dawson, D.B. and Baner, W.: "Deuterium profiles in titanium and alloy", J. Nucl. Mater., 85 & 86, 1013 (1979).

50) Scherzer, B.M.U., Blewer, R.S., Behrisch, R., Schulz, R., Roth, J., Borders, J. and Langley, R.A.: "Radiation induced detrapping of implanted deuterium in BeO by high energy ^3He and proton irradiation", J. Nucl. Mater., 85 & 86, 1025 (1979).

51) Staudenmaier, G., Roth, J., Behrisch, R., Bohdansky, J., Eckstein, W., Staib, P., Matteson, S. and Erents, S.K.: "Trapping of deuterium implanted in carbon and silicon: A calibration for

particle-energy measurements in the plasma boundary of tokamaks", J. Nucl. Mater., 84, 149 (1979).

52) Wampler, W.R., Picraux, S.T., Cohen, S.A., Dylla, H.F., McCracken, G.M., Rossnagel, S.M. and Magee, C.W.: "Hydrogen isotope trapping in materials exposed in PLT", J. Nucl, Mater., 85 & 86, 983 (1979).

53) Wilson, K.L. and Pontau, A.E.: "The temperature dependence of deuterium trapping in fusion reactor materials", J. Nucl. Mater., 85 & 86, 989 (1979).

54) Besenbacher, F., Bøttiger, J., Laursen, T. and Möller, W.: "Hydrogen trapping in ion-implanted nickel", J. Nucl. Mater., 93 & 94, 617 (1980).

55) Bohdansky, J., Wilson, K.L., Pontau, A.E., Haggmark, L.G. and Baskes, M.I.: "Combined depth profiling and thermal desorption of implanted deuterium in 304 LN stainless steel", J. Nucl. Mater., 93 & 94, 594 (1980).

56) Doyle, B.L., Brice, D.K. and Wampler, W.R.: "A local mixing model for deuterium replacement in solids", Radiat. Effects Lett. 57, 81 (1980).

57) Doyle, B.L., Wampler, W.R., Brice, D.K. and Picraux, S.T.: "Saturation and isotopic replacement of deuterium in low-Z materials", J. Nucl. Mater., 93 & 94, 551 (1980).

58) Erents, S.K.: "Low energy proton induced re-emission of deuterium from carbon", Nucl. Instrum. Methods, 170, 455 (1980).

59) Erents, S.K. and Hotston, E.S.: " A simple model for the trapping of deuterons in a carbon target", Nucl. Instrum. Methods, 170, 449 (1980).

60) Filleux, C., Morgeli, M., Stettler, W., Eberhardt, P. and Geiss, J.: "Trapping of low energy helium ions in polycrystalline Al and Pt and

in BeO and anodic Al_2O_3 films at room temperature", Radiat. Effects, 46, 1 (1980).

61) Hotston, E.S.: "A current induced diffusion model of gas sputtering", J. Nucl. Mater., 88, 279 (1980).

62) Hucks, P., Flaskamp, K. and Vietzke, E.: "The trapping of thermal atomic hydrogen on pyrolytic graphite", J. Nucl. Mater., 93 & 94, 558 (1980).

63) Möller, W., Besenbacher, F. and Laursen, T.: "The correlation between ion retention and surface deformation in deuterium-implanted metals", J. Nucl. Mater., 93 & 94, 750 (1980).

64) Möller, W. and Bøttiger, J.: "Retention and precipitation of 10 keV deuterons implanted into zirconium", J. Nucl. Mater., 88, 95 (1980).

65) Navinšek, B., Peternel, M., Žabkar, A. and Erents, S.K.: "Blistering and deuterium trapping induced by D^+ ion bombardment in metal alloys", J. Nucl. Mater., 93 & 94, 739 (1980)

66) Picraux, S.T. and Wampler, W.R.: "Release of H and He from TiC, stainless steel and graphite by pulsed electron and furnace heating", J. Nucl. Mater., 93 & 94, 853 (1980).

67) Pontau, A.E., Bauer, W. and Conn, R.W.: He pumping in the presence of an H beam", J. Nucl. Mater., 93 & 94, 564 (1980).

68) Roth, J., Eckstein, W. and Bohdansky, J.: "Depth profiling of D implanted into Ti at different temperatures", Radiat. Effects, 48, 231 (1980).

69) Roth, J., Scherzer, B.M.U., Blewer, R.S., Brice, D.K., Picraux, S.T. and Wampler, W.R.: "Trapping, detrapping and replacement of keV hydrogen implanted into graphite", J. Nucl. Mater., 93 & 94, 601 (1980).

70) Schulz, R., Behrisch, R. and Scherzer, B.M.U.: "Trapping and mutual release of D and ^{3}He in molybdenum", J. Nucl. Mater., 93 & 94, 608 (1980).

71) Schulz, R., Behrisch, R. and Scherzer, B.M.U.: "D and ^{3}He trapping and mutual replacement in molybdenum", Nucl. Instrum. Methods, 168, 295 (1980).

72) Thomas, E.W.: "Retention and re-emission of 0.125 - 1 keV deuterium in stainless steel", J. Appl. Phys., 51, 1176 (1980).

73) Underwood, M.C., Erents, S.K. and Hotston, E.S.: "Experimental measurements of hydrogen isotope exchange in carbon surface under ion bombardment", J. Nucl. Mater., 93 & 94, 575 (1980).

74) Wilson, K.L. and Pontau, A.F.: "Deuterium trapping and release in titanium-based coatings for TFTR", J. Nucl. Mater., 93 & 94, 569 (1980).

75) Yamaguchi, S., Ozawa, K., Yoshinari, O., Koiwa, M. and Hirabayashi, M.: "Deuterium enrichment during ion bombardment in $VD_{0.01}$ alloys", Nucl. Instrum. Methods, 168, 301 (1980).

76) Yamaguchi, S., Yoshinari, O., Takahashi, J., Fujino, Y., Ozawa, K., Naramoto, H., Koiwa, M. and Hirabayashi, M.: "Deuterium trapping by radiation induced defects in V, Nb and Ta", Proc. JIMIS-2, Hydrogen in Metals, 249 (1980).